

Chapter 9

Composites



Tatyana Ageyeva, Tamás Bárány and József Karger-Kocsis

Contents

9.1	Introduction.....	484
9.2	Nanocomposites.....	486
9.2.1	Preparation.....	487
9.2.2	Structure Development and Characterization.....	492
9.2.3	Properties and Their Prediction.....	493
9.2.4	Processing and Applications.....	499
9.3	Discontinuous Fiber-Reinforced Composites.....	499
9.3.1	Manufacturing.....	500
9.3.2	Structure Development and Characterization.....	502
9.3.3	Properties and Their Prediction.....	505
9.3.4	Processing and Applications.....	515
9.4	Mat-Reinforced Composites.....	516
9.4.1	Manufacturing.....	518
9.4.2	Structure Development and Characterization.....	519
9.4.3	Properties and Their Prediction.....	522
9.4.4	Applications.....	526
9.5	Fabric-Reinforced Composites.....	527
9.5.1	Manufacturing.....	528
9.5.2	Structure Development and Characterization.....	532
9.5.3	Properties and Their Prediction.....	534
9.5.4	Processing and Applications.....	544
9.6	Laminate Composites.....	545
9.6.1	Manufacturing.....	546
9.6.2	Structure Development and Characterization.....	549

József Karger-Kocsis is deceased

T. Ageyeva · T. Bárány (✉) · J. Karger-Kocsis
Department of Polymer Engineering, Faculty of Mechanical Engineering, Budapest
University of Technology and Economics, Műegyetem rkp. 3, Budapest 1111, Hungary
e-mail: barany@pt.bme.hu

T. Ageyeva
Bauman Moscow State Technical University, 2nd Baumanskaya Str., 5, 105005 Moscow,
Russia

9.6.3 Properties and Their Prediction.....	553
9.6.4 Processing and Applications	556
9.7 Conclusion and Outlook.....	556
References	557

Abstract The current chapter is dedicated to polypropylene (PP) based composites. The material grouping and presentation in the chapter follows the logic of the reinforcement length gain and covers the areas from nano- to macro-composites. Thus, separate sections are devoted to PP-nanocomposites, discontinuous fiber-reinforced, mat-reinforced, fabric-reinforced and aligned fiber-reinforced composites. Each section describes the aspects of manufacturing techniques, structure development, properties characterization as well as processing and application of the related composites. As PP matrix belongs to the family of fairly unexpensive high-volume thermoplastics and related composites are feasible for semi-structural and structural applications, the chapter is mostly concentrated in PP-composites for automotive application.

Abbreviations and Designations

0D	Zero-dimensional
1D	One-dimensional
2D	Two-dimensional
3D	Three-dimensional
ACN	Addressable conducting network
AFM	Atomic force microscopy
C	Central layers
CAD	Computer aided design
CEC	Cation exchange capacity
CF	Carbon fiber
CMT	Carbon fiber mat thermoplastic
CNT	Carbon nanotubes
CT	Compact tension
DBP	Double-belt press
D-LFT	Directly produced long fiber reinforced thermoplastics
DMTA	Dynamic-mechanical thermal analysis
EMI	Electromagnetic interference
ETC	Extreme temperature conditions
EFW	Essential work of fracture
FCP	Fatigue crack propagation
FDM	Fused deposition modelling
FE	Finite element
FR-PP	Fabric reinforced polypropylene
FTIR	Fourier-transform infrared
GF	Glass fiber

GMT	Glass mat-reinforced thermoplastics
GMT-C	Continuous fiber GMT
GMT-D	Discrete fiber GMT
GO	Graphene oxide
GR	Graphene
HDT	Heat distortion temperature
HDT-B	Heat distortion temperature tested by B-method
HPSC	High pressure stiffness conditions
HRR	Heat release rate
IFR	Intumescent flame retardant
L	Longitudinal
LEFM	Linear elastic fracture mechanics
LGF	Long glass fiber
LOI	Limiting oxygen index
LPSC	Low pressure stamping conditions
LTCE	Linear thermal coefficient of expansion
LWRT	Lightweight reinforced thermoplastics
MAO	Methylaluminoxane
MFD	Mold filling direction
MMT	Sodium montmorillonite
MRT	Mat-reinforced thermoplastics
MWCNT	Multiwall carbon nanotube
NF	Natural fibers
NMT	Natural mat thermoplastic
PA	Polyamide
POSS	Polyhedral oligomeric silsesquioxane
PP-g-MA	Maleic anhydride grafted PP
PP-g-MAA	PP grafted with maleic acid
PYFM	Post-yield fracture mechanics
RC	Reference forming conditions
RT	Room temperature
S	Surface layers
SCC	Slow cooling conditions
SCF	Short carbon fiber
SEM	Scanning electron microscopy
SGF	Short glass fiber
SMC	Sheet molding compound
SR-PP	Self-reinforced PP
T	Transverse
TC	Transcrystalline
TEM	Transmission electron microscopy
TGA	Thermogravimetric analysis
TTSP	Time-temperature superposition principle
UD	Unidirectional

XRD	X-ray diffraction
ZN	Ziegler-Natta
ε	Strain
E	Flexural modulus
E_f	Flexural modulus of the fibers
E_m	Flexural modulus of the matrix
K_Q	Fracture toughness
R	Reinforcing effectiveness term
T_g	Glass transition temperature
T_m	Melting temperature
V_f	Fiber volume fraction
V_m	Matrix volume fraction
ρ	Density
σ	Normal stress
τ	Shear stress
μ	Dynamic viscosity of the resin

9.1 Introduction

Composites are defined as materials consisting of two or more distinct phases (matrix and reinforcing phases) separated by a recognizable interphase. Earlier definition emphasizes that the two phases should be chemically and physically different. This is, however, no more a stringent criterion because the two phases may be of the same polymer, as this is the case with single-polymer composites possessing ultimate recyclability. The polypropylene (PP)-based single-phase composites are termed as to “all-PP” or self-reinforced polypropylene composites, as well. Composite materials exhibit such structural and functional properties which cannot be attained by any of their constituents alone. The reinforcing phase is much stronger and stiffer than that of the matrix. The role of the matrix is to keep in position and protect the reinforcement from environmental attack. For the stress (shear and transverse types) transfer from the “weak” matrix to the “strong” reinforcement, the finite thickness interphase is responsible. The reinforcing (disperse) phase is usually anisometric and thus exhibits a rather large length-to-thickness (aspect) ratio. The length of the reinforcement varies in an extreme large range from nanoscale to practically infinite (in case of endless or continuous fiber reinforcement). The variation in their thickness is more restricted and usually remains under few millimeters. Note that the thickness of carbon (CF) and glass fibers (GF) is in the ranges of 5–10 μm and 10–25 μm , respectively. It is worth of noting that isometric nanoparticles (i.e. having an aspect ratio of 1) may meet the criteria of reinforcement albeit such particles, at least in microscale, belong to the category of fillers. Major effect of fillers is cost-reduction along with some improvements in the non-structural properties.

Composites are classified differently. Considering the matrix phase, the usual classification is ceramic-, metal- and polymer-matrix based systems. Depending on the actual size of the reinforcement, one can speak about nano-, micro- and macrocomposites. From the viewpoint of the reinforcing structures possible categories are for example discontinuous/continuous fiber-reinforced materials, composites with textile architectures, laminate composites. Because of the embedded fiber reinforcements, the composites can be made anisotropic in that their mechanical response depends on the loading direction. This feature is highly desirable and beneficial because during design and manufacturing the composite’s structure can be tailored upon the expected loading condition. Polymer composites are very popular due to their low cost and easy fabrication methods. This note especially holds for PP-based ones as PP belongs to the family of the rather inexpensive high-volume thermoplastics. The PP matrix can be combined with the reinforcement in different ways to prepare a great variety of preforms, semi-finished products, textile fabrics, etc. Their structure and appearance determine the processing alternative to convert them into the final parts. Figure 9.1 shows an overview of the manufacturing alternatives of thermoplastic composites.

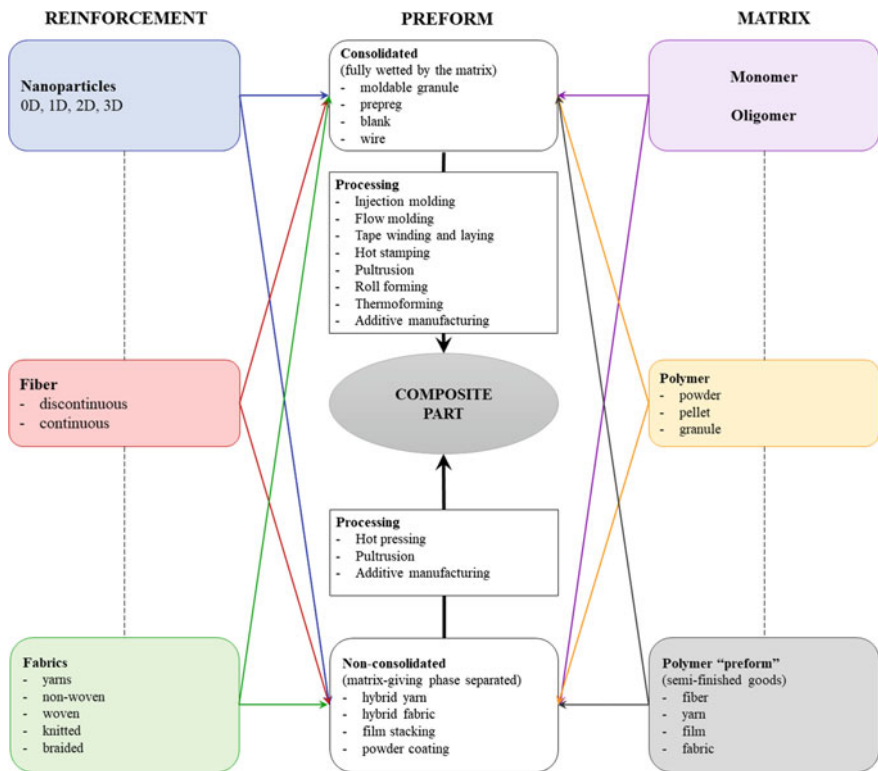


Fig. 9.1 Overview of possible manufacturing routes for thermoplastic matrix-based composite products

Note that the chart in Fig. 9.1 is of general character and valid for all thermoplastic polymer-based composites. In this diagram, consolidated and non-consolidated “preforms” were differentiated. The basic difference between them is whether the reinforcement is fully wetted by the matrix or no intimate contact exist between reinforcement and matrix. In the latter case, the matrix-yielding phase is available in separate forms, usually as fiber or film.

Moreover, Fig. 9.1 serves as guide-line for the present chapter on PP composites. Accordingly, next we shall introduce the structure-property relationships of PP-nanocomposites, discontinuous fiber-reinforced composites, mat-reinforced composites, fabric-reinforced composites and aligned fiber-reinforced laminate composites. Splitting between mat- and fabric-reinforced PP composites, irrespective of the fact that they are listed under “fabrics” in Fig. 9.1, is reasoned by the broad application of mat-reinforced PP composites.

The mechanical properties of PP based composites depend on the numerous factors, such as, reinforcement nature, volume fraction and architecture, quality of impregnation, amount of various defects and fiber-matrix interface quality. Nevertheless, reinforcement architecture plays a crucial role in mechanical response. Thus, mat and short fiber reinforced PPs demonstrates lowest values of strength and modulus, while unidirectional (UD) shows the highest level of mechanical response but only in longitudinal direction (Fig. 9.2).

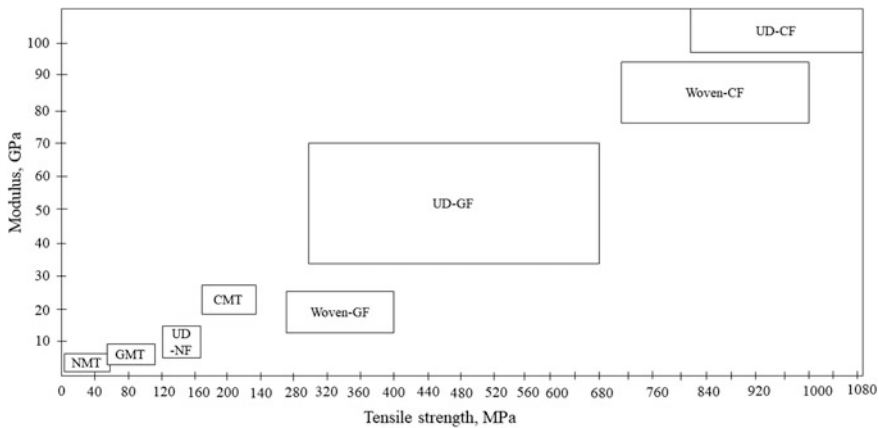


Fig. 9.2 Mechanical properties of different types of PP based composites. Designations: NMT—Natural fiber mat-reinforced thermoplastic; GMT—glass mat thermoplastic; CMT—carbon-mat thermoplastic; NF—natural fibers; woven—woven textile. Note, the matrix materials of the mentioned composites is always PP

9.2 Nanocomposites

Nanoparticle-modified polymer composites (also termed polymeric nanocomposites, inorganic/organic hybrid materials) have attracted great scientific and technological interest owing to their exceptional physico-mechanical, thermal and other

properties achieved at very low nanoparticle content (<5 wt% or <2–3 vol%). Nanoparticle means that the size of the related inorganic or organic filler—at least in one dimension—is on nanometre scale. Although the term nanocomposite sounds as a current one, nanocomposites have been produced industrially more than half century ago. In this respect attention should be drawn to the reinforcement of rubbers by nanometer scale carbon black. In addition, many natural and artificial products can be considered as nanocomposites based on their structural build-up.

Major specific feature of nanofillers and -reinforcements is their huge interfacial surface area, which may be as high as 1000 m²/g. As a consequence, the interphase properties may become the controlling parameters of the macroscopic response of polymer nanocomposites. Unlike the two-dimensional (2D) interface, the interphase (3D) concept considers that the molecular mobility changes from the particle's surface toward the bulk in the range of several nanometers.

A further aspect is that with decreasing mean particle size the average distance between the nanoparticles also decreases when keeping the volume fraction of the filler constant. This may activate filler-filler interactions and result in a peculiar physical network structure.

Nanoparticles may be grouped upon their shape in 0D (spheroid), 1D (e.g. tube, fiber, whisker), 2D (platelet, disk) and 3D (framework). The anisometric nature of fillers is usually characterized by the aspect ratio (length/thickness or length/diameter ratio).

Polymer nanocomposites, including the PP-based ones, are very promising materials for various applications due to improved and novel properties, as shown later.

9.2.1 Preparation

There are numerous ways to produce nanocomposites. In this chapter a distinction between preformed and in situ generated nanoparticles will be made. The corresponding nanocomposites can be produced by different techniques which are usually listed in three major groups: (i) in situ polymerization, (ii) solvent-assisted techniques (including aqueous dispersions) and (iii) melt compounding. There are, however, some other methods, such as a combination of the above methods (e.g. water-assisted melt compounding [1]), ball milling (dry or wet), sol-gel chemistry implemented in one of the above listed techniques, etc.

Among the in situ techniques we may consider also the polymer intercalation in 2D layered structures and 3D frameworks because microscopic particles (>10 μm) are introduced into the polymer or monomer in which the particles disintegrate in nanoscale during processing or polymerization.

To incorporate micron-size preformed inorganic particles into a polymer matrix is a well-known method for improving the modulus, heat distortion temperature (HDT) and to reduce the shrinkage of such composites. This is associated, however, with a pronounced reduction in ductility. By diminishing the particle size (nanoscale) or by enhancing the particle volume fraction, the flexural and the tensile

strength can be enhanced. On the other hand, the fracture toughness and modulus remain fairly independent of the particle size, even when going down to the nanoscale. An increase of the glass transition temperature (T_g) of polymers owing to addition of various preformed nanoparticles reflect a restricted motion of the polymer chains, and thus a good bonding between the particles and the matrix.

9.2.1.1 In Situ Polymerization

In this case the nanofiller is dispersed or swollen in the monomer or oligomer in the presence or absence of additional solvent. A very promising way is to render the surface of the particle catalytic for the subsequent polymerization. In case of 0D particles the related method is termed as polymerization filling, whereas for 2D and 3D additives as intercalative polymerization. The in situ polymerization was explored to produce PP nanocomposites with different fillers with and without catalytic activities for the propylene polymerization. Basic advantage of the in situ polymerization that thermodynamic and kinetic limitations, which are controlling parameters of melt compounding, and partly also for solution blending, are “bypassed”. The polymer grows from the fillers’ surface thereby hampering the agglomeration of 0D particles and causing intergallery expansion (intercalation) or full delamination (exfoliation) in 2D-type nanoreinforcements. Attention should be paid, however, to the fact, that subsequent melt processing of such in situ polymerized PP nanocomposites may result in a pronounced agglomeration, deintercalation phenomena. Zapata and Quijada [2] compared the properties of PP/silica (0D) nanocomposites produced with and without catalytic activity of the silica in metallocene polymerization of propylene. The authors found that the dispersion of the silica nanospheres is better when their surface is catalytically active. PP/fumed silica nanocomposites were prepared by Azinfar et al. [3] using a “bisupported” Ziegler-Natta (ZN) catalyst in which magnesium ethoxide and silica served as conjugate support of the catalyst. In majority of the polymerization works, however, 2D fillers were preferentially used being more suited for catalyst support and offering larger property improvements than 0D versions. Among the 2D nanofillers clays and graphene (GR) versions were tried. Ramazani et al. [4] used pristine clay (sodium montmorillonite, MMT), whereas Cardoso et al. [5] an organophilic clay as ZN catalyst supports for the preparation of PP/clay nanocomposites. In both cases the clay was intercalated and partly exfoliated after the polymerization. Using organophilic clay (introduced later), however, is beneficial with respect of further melt processing for which the in situ polymerized PP/clay nanocomposite may serve as adequate “masterbatch”. GR nanosheets (up to 20 wt %) were successfully dispersed in PP via in situ polymerization using a metallocene complex with methylaluminumoxane (MAO) cocatalyst. GR increased the crystallization and degradation temperatures and resulted in balanced stiffness/ductility performance [6]. Funck and Kaminsky [7] demonstrated that oxidized multiwall carbon nanotube (MWCNT) can be incorporated into PP through polymerization of propylene with a metallocene/MAO catalyst and in situ coating. Huang et al. [8] followed a

similar way and prepared PP/graphene oxide (GO) nanocomposites through in situ ZN polymerization. In this work the surface functional groups ($-OH$ and $-COOH$) of GO were converted into Mg/Ti catalyst species prior to polymerization. This work demonstrated that using a GO-supported ZN catalysts even a polar GO can well be dispersed in apolar PP. Unlike 2D layered structures which can be delaminated (exfoliated, intercalated) during polymerization, the 3D frameworks (natural zeolites, synthetic molecular sieves and mesoporous glasses) are stable and thus have to be added as nanofillers.

With respect to the catalysts and in situ propylene polymerization methods in absence and presence of nanofillers, the interested reader is addressed to the book of Kaminsky [9].

9.2.1.2 Solvent-Assisted Techniques

Preparation of nanocomposites via solution dispersion is mostly of academic interest (to study selected structure-property relationships) and especially adapted for polymers soluble only in organic solvents. On the other hand, the properties of polymer nanocomposites prepared by solution mixing can serve as benchmarking for melt compounded ones, as they exhibit the highest available values. That is the reason why works often compared the properties of solution and melt blending produced PP nanocomposites, such those with GR [10]. Solvent-assisted dispersion of clay [11] and cellulose nanowhisker [12] in PP were also topics of investigations.

Considering the fact that some nanoparticles are water-swellaible (e.g. clays) and dispersible (e.g. boehmites [13], oxidized carbonaceous nanofillers), they can be incorporated in their aqueous slurry into the molten polymer during compounding. The beauty of this method is that nanofillers without surface treatment can be used instead of their more expensive organophilic versions. This was explored in different polymers [1], including PP/boehmite [13], and PP/clay [14] nanocomposites. A further advent of this water-mediated method is that rubber latices can also be used and thus rubber-toughened PP nanocomposites can also be produced in line. Note that the mean size of the rubber in the latex matches very well with the size requirements for thermoplastics [15]. PP latex is also available and thus can be combined with water dispersible nanofillers, such as GO, through latex compounding. In a follow-up procedure the GO-containing “masterbatch” (eventually after reduction of GO to GR) can be dispersed in molten PP [16].

9.2.1.3 Melt Compounding

The vast majority of works was dealing with the preparation of PP nanocomposites through melt compounding. This note holds for all types of nanofillers. 0D-type nanoparticles, e.g. SiO_2 [17, 18], TiO_2 [19], $CaCO_3$ [20], alumina (Al_2O_3 [21], boehmite [13]), polyhedral oligomeric silsesquioxane (POSS) [22] are frequently incorporated into PP by melt compounding techniques. Note that many

nanoparticles are commercially available with and without surface treatments. Among the 1D fillers halloysite [23], carbon nanotube (CNT) variants [24–26], cellulose nanofibers and whiskers [27, 28] should be mentioned.

The commonly used 2D reinforcements are 2:1 layered silicates (phyllosilicates) of natural (e.g. bentonite, MMT—often termed clays) and artificial (e.g. fluorohectorite) origin. They contain two tetrahedral silicate sheets fused to an edge-shared octahedral one resulting in an overall thickness of ca. 1 nm. The lateral dimension of the layered silicates varies in a very broad range from several ten nanometres to several micrometres yielding an aspect ratio of up to 6000 for synthetic versions [29]. Isomorphic substitution of higher valence cations (Al^{3+} and Mg^{2+}) in the silicate framework by lower valence ones (Fe^{2+} , Mg^{2+} and Li^+ , respectively) generated negative charges on the layers, which are counterbalanced usually by alkaline cations (Na^+ , Ca^{2+} —generally in hydrated forms). As a consequence, such layered silicates exhibit a cation exchange capacity (CEC) and the inter-gallery cations can be replaced by suitable organic cationic surfactants. For that ammonium salts are preferentially used. By this cation exchange the hydrophilic silicate is rendered organophilic and at the same time the interlayer spacing (basal or d spacing) increases. The latter is tuned by the chemical build-up of the onium intercalant (often containing a long alkyl chain) the further role of which may be to support the chemical interaction with the matrix [30]. Note that the interlayer spacing should be larger than ca. 1.5 nm in organophilic clay (i.e. the interlamellar distance > 0.5 nm). Since the price of the organophilic silicates is higher (more than threefold) than that of the purified pristine ones which was the driving force for the development of water-assisted techniques [1].

Though the overwhelming majority of the works done in the past were dealing with “cationic” layered silicates, layered silicates with anion exchange capacity (their layers have a positive surface charge which is compensated by intergallery anions) are also available. The corresponding hydrotalcites are incorporated in PP, especially to improve its fire resistance [31, 32]. An excellent review on synthetic layered nanoparticles, covering clays, layered double hydroxides and the like, was compiled by Utracki et al. [29].

Other recently explored 2D nanofillers are GR and its derivatives, such GO, differently reduced GOs. GR is a 2D one atom thick planar sheet composed of sp^2 hybridized C atoms exhibiting outstanding mechanical, thermal and electric properties. This carbon allotrope is the thinnest known material in the universe. Oxidation of GR results in the appearance of polar groups (hydroxyl, carboxyl, epoxy) rendering it more hydrophilic. Reduction of GO, by whatever means, restores in large extent the original sp^2 hybridization along with property improvements. Though GR can be produced via direct synthesis, most of the works followed a “top down” strategy using graphite. It is the right place to underline that the terms used for PP/GR(GO) nanocomposites are rather inconsistent. An excellent review on PP/GR nanocomposites, covering their preparation through in situ polymerization, solution-assisted techniques and melt compounding was published by Tripathi et al. [33].

Melt compounding is a very attractive way to produce commercial nanocomposites. This is owing to: (a) fast dispersion of the nanoparticles in the melt, (b) available industrial melt compounding capacities, and (c) environmental friendly preparation. Similar to solvent intercalation, melt intercalation is also governed by thermodynamic (compatibility) and kinetic (diffusivity) parameters. It is intuitive that polymer molecules densely adhering to 0D particle's surface, intercalating in 2D layers or penetrating in 3D frameworks lose their conformational freedom which is associated with entropy loss. The attributes "nano", "nanoscale" already suggest that the formation of polymer nanocomposites has many similarities with (im)miscible polymer blends and thus the related rules can also be adopted. So, in order to get molecular, i.e. nanoscale, dispersion, the Gibb's free energy must be negative. As entropy loss produces an adverse effect, it has to be "overcompensated". This may occur by entropy gain (e.g. interdiffusion between molecules of the organophilic modifier and PP molecules) and/or by energetically favored interactions (e.g. between molecules of "functionalized" PP and functional groups on the particles. Energetically favored interactions involve acid/base and chemical reactions, H-bonding etc., all of them affecting the term enthalpy of mixing. Effects of possible interactions and kinetics have to be considered when selecting the surface modification and compounding conditions [34, 35]. As far as kinetics of nanostructure formation concerns the effects of locally acting shear and elongational flow fields should be emphasized. As the majority of the experimental work was done by extrusion melt compounding, the related research focused on the effects of shear stresses varied by different ways [36, 37]. Effects of the elongational flow on the morphology development became under spot of interest only recently [38, 39]. Basic outcome of these studies was that the dispersion state of the nanoparticles is governed also by the shear/elongational flow and residence time (i.e. kinetics). It is worth of noting that the above thermodynamical interactions and kinetics (processing-related effects) are often interrelated especially due to the fact that compatibilizers are mostly used, as well.

As most nanoparticles are of polar nature, their incorporation into the apolar PP is a great challenge. Recall that traditional fillers are often "coated" by surfactants (tensides). Their role is to improve the compatibility between the filler and polymer via their long alkyl chains. The same philosophy can be followed for the dispersion of nanofillers. The related polymers, oligomers are called as compatibilizers. They are usually grafted copolymers due to economic reasons. Maleic anhydride grafted PP (PP-g-MA, grafting degree is at about 1 wt%) is the preferred compatibilizer (e.g. [40, 41]). It was reported that lower molecular mass PP-g-MA may favor the organoclay exfoliation in contrast to that of higher molecular mass version [42]. Generally, in the presence of compatibilizer a higher degree of dispersion (intercalation/exfoliation when appropriate) was found than in their absence. This was reflected in improved mechanical properties.

Using PP-containing blends attention should be drawn to the fact that the nanoparticle introduced may be preferentially embedded in one of the blend's components. Moreover, the nanofillers themselves may work for interphase modification, compatibilization [43].

9.2.2 Structure Development and Characterization

The structure of polymer nanocomposites is very complex as it covers the following domains: dispersion state of the nanoparticles, changes on molecular and supermolecular level in the matrix (bulk), interphase formation between the surface of the nanoparticles and bulk material. Moreover, there is a strong interrelation between the above characteristics. As a consequence, it is not an easy task to find those structural parameters which control a given property.

9.2.2.1 Particle Dispersion

It is obvious that nanoscale sensitive experimental techniques have to be used to detect the dispersion state of the nanoparticles. For that purpose, transmission electron microscopy (TEM) is preferred. It should be born in mind, however, that the view field at high magnifications may not represent that of the whole sample. Further, it is essential to describe the dispersion state. Albeit some trials were made to make use of image analysis codes, this issue is not yet solved properly. Another straightforward technique is the atomic force microscopy (AFM). Real breakthrough in the characterization of the dispersion of nanoparticles can be expected from tomographic methods, such as electron, X-ray microcomputed, focused ion beam [44] and optical coherence tomography methods [45].

Polymer intercalation in 2D silicate layers is usually evidenced by X-ray diffraction (XRD) performed at small diffraction angles (2Θ). In XRD pattern intercalation manifests in a shift towards lower scattering angles in the range $2\Theta = 1\text{--}10^\circ$. In contrast to the frequently quoted claim that missing peak in the XRD spectra represents exfoliation, it is not at all correct. In order to get a reliable picture on the silicate dispersion, XRD and TEM results should be compared, and even optical microscopy included (due to the presence of micronscale agglomerates).

9.2.2.2 Matrix Polymer (Bulk)

Changes in the matrix morphology owing to the presence of nanoparticles occur at different levels. Like some micro- and macroscopic fillers and reinforcements, nanoparticles also act as heterogeneous nucleation agents. High nucleation density on the filler surface may generate transcrystalline (TC) growth. TC is caused by dense nuclei on the heterogeneous surface due to which the spherulitic crystallization is laterally hindered. So, growth occurs in one direction, viz. perpendicular to the filler surface. It is believed that the TC layer supports the stress transfer from the weak matrix to the “strong” nano-reinforcement [46]. PP TC, being of epitaxial origin, was observed on the crystalline surfaces of CNT [47] and GR [48].

The heterogeneous nucleating effect of nanoparticles has been demonstrated for many semi-crystalline thermoplastics including PP. It is noteworthy that practically all of them support the crystallization in α -form. Studies devoted to the crystallization (isothermal, non-isothermal) behavior of various PP-based nanocomposites showed that the usual descriptions (Avrami, Ozawa etc.) are valid. Very interesting results were achieved by investigating PP/mesoporous silicate nanocomposites. It was shown that isotactic PP confined in the mesopores does not crystallize [49]. This fact explains the reason of a research trend dealing with the crystallization behavior of polymers under spatial constraints.

9.2.2.3 Interphase

To examine the interactions between nanoparticles and polymers various techniques can be used. Fourier-transform infrared (FTIR) spectroscopy, solid state nuclear magnetic resonance, calorimetry, thermogravimetric analysis (TGA), chromatographic and electrophoretic measurements, all can contribute to get a better insight in structure-property relationships and interphase properties [30]. A rather simple and informative method is the dynamic-mechanical thermal analysis (DMTA). Strong absorption of polymer molecules on nanoparticles possessing very high specific surface area yields a change in the T_g peak (shape alteration, intensity reduction, shift toward higher temperature). A direct evidence for changes in the interphase characteristics may deliver the AFM.

9.2.3 *Properties and Their Prediction*

It was shown before that the structure of nanocomposites is highly complex and partly of hierarchical nature. Therefore, it is of great challenge to trace those structural parameters which affect the desired property. In respect to the structure-property relationships the basic question we have to give an answer is: do these issues belong to polymer physics or continuum (composite) mechanics? In the former case the bulk and interphase, whereas in the latter reinforcement-related characteristics should govern the properties. Unfortunately, no definite answer can be given to the above question. In certain conditions, grouped in low frequency mechanical tests (creep, fatigue), aspects of polymer physics may dominate. In tests of high frequency loading (dynamic, impact) the use of composite analogies (i.e. continuum mechanics) seems to be straightforward. With other wording, composite rules are more promising to describe the elastic (linear elastic, linear mechanic), whereas polymer physics principles are more suited to assess the relations between structure and viscoelastic (non-linear elastic) properties.

9.2.3.1 Mechanical Response

Stiffness and ultimate tensile properties

The simplest way to predict stiffness (Young's or E -modulus) is to check whether or not the rule of mixtures holds. For macroscopically filled systems the Kerner equation is widely used. The disagreement between the Kerner's prediction and experimental results got for nanocomposites with 0D fillers forced the researchers to consider the interphase. It was treated as an immobilized layer which increased the effective filler volume fraction. Results suggested that the thickness of the immobilized layer may be much larger than the size of the particles [50]. For the prediction of the shear modulus of PP nanocomposites with 0D fillers the Einstein equation and its modifications (Guth, Cohan, Mooney) may work [51], which are well accepted predictions for rubbers. The strength of traditionally filled systems decays according to a power law function. This means that the strength of the composite is always below than that of the neat matrix polymer as the filler does not bear any part of the external load. In contrast, considerable strength increase was measured for nanoparticle reinforced thermoplastic systems. The related functions were treated by empirical models as listed in Ref. [50]. On the other hand, the reinforcing effect of nanoparticle is not fully understood. Behind the strength increase one may surmise some analogy with nanoparticle-reinforced rubbers.

Usual analytical descriptions of the stiffness of PP nanocomposites with 1D and 2D nanoparticles agree with those of conventional composites. Accordingly, the popular models are: Voigt upper bound—Reuss lower bound, Hashin and Shtrikman upper and lower bounds, Halpin-Tsai model, Mori-Tanaka theory, Hui-Shia model [52]. Interested reader may find several papers quoting why one of models was working better than the other(s). Kalaitzidou et al. [53] for example analyzed the flexural and tensile moduli of PP nano (graphite nanoplatelet, vapor-grown carbon nanofiber, carbon black, MMT) and microcomposites (CF) and found that the Halpin-Tsai and Tandon-Weng models worked best, however, only up to a given concentration of the reinforcements. Above a threshold filler loading the models overestimated the experimental values. It is noteworthy, that for modelling the mechanical (elastic) properties of polymer nanocomposites molecular dynamics [54, 55] and finite element (FE) simulations are becoming favored topics [52]. Among the latter multiscale representative volume element modelling seems to be the most promising way [56].

The scenario is far less so clear for the ultimate properties. Exfoliation of 2D nanoparticles raises the stiffness which is accompanied by reduced strain (ductility). So, the nanocomposites are becoming "harder" but more "fragile". The ultimate properties depend not only on the intercalation/exfoliation state, but also on characteristics of the interphase (wetting, adhesion) and the bulk (polymorphism, crystallinity, spherulite size).

Creep and fatigue behavior

Few papers were published on the yield, creep and fatigue behavior of nanocomposites. This is quite surprising as the above long duration tests are very sensitive to changes in the interphase and bulk properties. Studying the temperature

and strain rate sensitivity of the yield strength of organoclay modified polyamide-6 (PA-6) and PP nanocomposites, Mallick and Zhou [57] found that the Eyring equation works well also for these nanocomposites. Based on normalized stress-cycles (S-N) curves, derived from tension-tension fatigue, the authors concluded that the fatigue failure is initiated by re-agglomerated particles [57]. The creep failure of PP and its nanocomposites with and without PP-g-MA was found to occur at a critical strain independent of the stress level applied in the work of Lv et al. [58]. This peculiar critical strain is combined with a time-strain superposition method to predict the creep failure lifetime of PP nanocomposites. Researchers prefer to perform short term creep test at different temperatures and/or stress levels and generate master curves by time-temperature and time-strain superpositions [59]. Drozdov et al. [60] found that reinforcement of PP with 1 wt% of organoclay increased the time to failure by an order of magnitude. The cited authors proposed new constitutive equations considering the viscoelasticity and viscoplasticity of the investigated nanocomposites. Incorporation of clay in PP resulted in reduced fatigue crack growth rates [61]. Note that this is a universal feature of reinforcements [62]. The creep and fatigue performances of polymer nanocomposites were finely surveyed by Pegoretti [63].

Toughness

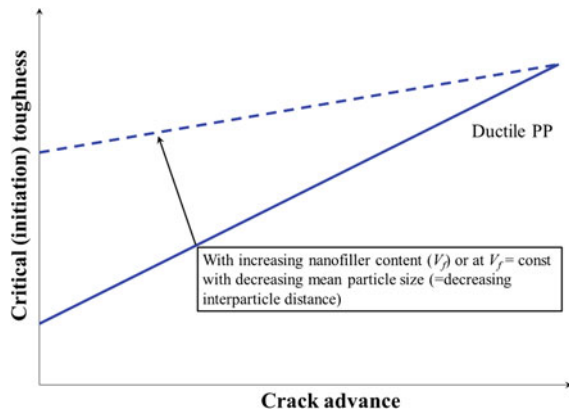
Toughness of nanocomposite deserves a separate treatise owing to highly contradictory findings in the open literature. Usually there is trade-off between stiffness, strength and toughness. Accordingly, nanoparticles with reinforcing effect should result in toughness reduction. In many cases, however, the opposite tendency was found [64]. It should be emphasized here that fracture mechanical studies on polymer composites, especially on PP-based ones are scarce [50, 65–67]. On the other hand, only fracture mechanical methods provide toughness values which can be collated being material parameters (e.g. [68]).

The usual thumb of rule is that at very low nanoparticle content (<2–3 wt%) the toughness does not alter compared to the matrix. At higher nanoparticle content, however, a strong decrease in the toughness can be observed. To explain the toughness improvement first the “percolation theory” of Wu was adopted [69]. It was soon recognized that this theory could not account for the toughness upgrade, as the matrix ligament between the particles is too large to create the necessary stress overlapping. To overcome this problem a double percolation model was proposed [50]. According to the authors’ feeling even this model needs refinement. Specific effects of the interphase (immobilized layer, transcrystallinity, crystalline polymorph, etc.) which affect the matrix deformation have to be considered. Many model explanations lack to give information why and how cavitation occurs in the nanocomposites with intercalated/exfoliated, finely and coarsely dispersed structures. Note that the toughness in rigid particle filled polymers is linked to cavitation which is followed by stretching of the interparticle matrix ligaments [70]. This effect along with the inhomogeneous distribution of rigid spherical particles was considered in the analytical model of Lauke [71] recently.

Resistance curve approaches of ductile fracture mechanics (J-integral and essential work of fracture (EWF) [72, 73] were mostly used to assess the toughness

of PP nanocomposites. For low aspect ratio nanofillers (i.e. 0D type boehmites) it was found that the critical value (specific EWF) went through a maximum whereas the slope of the resistance curve, i.e. specific plastic work, decrease with increasing nanofiller contents [74, 75]. The scenario is more complex for 1D fillers, such as MWCNT, where a ductile-semiductile transition was observed [76] that basically blurs the EWF application. Karger-Kocsis et al. [77] studying the effect of various nanofillers in PP (boehmite, MWCNT, clay, GR, added in 1 wt% each) concluded that the EWF method can only be adapted for low aspect ratio nanofillers. A further finding was that there is an adverse effect between the energy required to crack initiation and propagation, i.e. both of them can hardly be increased at the same (cf. Fig. 9.3).

Fig. 9.3 Schematic toughness resistance curves for PP nanocomposites



Similar results, tendencies were reported for PP/MMT nanocomposites using the J-integral [65] and EWF [78] approaches. Nevertheless, examples for simultaneous improvements in resistances to crack initiation and propagation can also be found [79]. It is noteworthy that the EWF results on PP nanocomposites are often “scattered” due to the fact that the prerequisites of the EWF applications can only be met with very ductile PP copolymers. Problems linked with unstable necking/tearing can be considered by suitable energy partitioning [73, 80] during EWF which is not always followed.

Finally, toughness decrease in nanocomposites is likely the rule and not the exception. This claim is in concert for example with the ultimate (tensile) properties and pressure-volume-temperature diagram data. Recall that the latter technique evidenced a considerable decay in the free volume upon exfoliation [81] which means restricted molecular motion and thus suggests toughness reduction.

9.2.3.2 Rheological Behavior

It was early recognized that the structure of nanocomposites strongly influences the rheological behavior, especially in the low frequency range (linear viscoelasticity)

[82]. In this range the melt viscosity (studied mostly in shear) increases monotonically with increasing nanoparticles' content irrespective to their shape and incorporation method [82, 83]. Polymer nanocomposites with high aspect ratios (1D and 2D versions) usually exhibit higher viscosities than quasi-spherical types (0D) in the linear viscoelastic range. Surprisingly, boehmite, belonging to the 0D particles, causes a very small increase in the shear viscosity of PP both in the linear and non-linear rheology ranges [75]. As known, PP shows shear thinning behavior (non-linear viscosity range), i.e. the melt viscosity decreases with increasing shear rate. Shear thinning may start at lower shear rates than that of the related matrix polymer with anisometric particles due to their alignment into the flow direction. Note that at very high shear rates, characteristic for injection molding operations, only a small difference in the melt viscosities between the parent PP and its nanocomposite can be found. The latter may be even lower than that of the matrix [84]. The complex viscosity of neat PP as a function of the angular frequency shows Newtonian behavior at low frequencies. The Newtonian range may disappear with increasing nanoparticle content and a transition from liquid-to-solid-like behavior takes place (termed as to rheology percolation), as shown by Prasantha et al. [24] on the example of PP/MWCNT nanocomposites. The related "liquid-solid" change is best visualized through the van Gurp-Palmen plots (phase angle vs. absolute value of complex shear modulus) [24, 85].

The relationship between the shear viscosity and shear rate (in the range of 10^{-3} to 2 s^{-1}) could be well described by the Carreau model [84]. Chafidz et al. [86] reported that the complex shear viscosity as a function of angular frequency (shear rate) can well be described by the Carreau-Yasuda equation. For the shear thinning behavior, determined by rheometer, the Oswald-de Waale (power law) function may also work properly [86]. Information derived from dynamic oscillatory shear, steady shear and elongational flow measurements, eventually combined with "superimposed" techniques like transient/intermittent ones) can deliver a deeper insight in the structure of the nanocomposites and its alteration owing to shear and elongational flows [38, 87, 88]. It was shown for example that the morphological stability of nanocomposites can be successfully studied in rheological measurement [89]. Solomon et al. [90] reported that the course of the storage modulus versus frequency in the viscoelastic range reflects well effects of the intercalation of organoclay (caused by amine surfactants of various chemical build-up).

9.2.3.3 Thermal Behavior

For many applications it is of great importance to know the linear thermal coefficient of expansion (LTCE) of nanoparticle-reinforced composites. It is intuitive that the orientation of 1D and 2D particles makes the LTCE direction dependent. Usually, with increasing nanoparticles' content the LTCE is reduced as shown on example of PP/CNT nanocomposites [91]. Using organoclay at 6 wt % loading the LTCE of PP was decreased by 20% [92]. On the other hand, more moderate results can also be found for PP/clay nanocomposites in the literature.

For the estimation of the LTCE of nanocomposites with various nanoparticles (0D, 1, 2D types) the Chow-model may be successfully adapted as shown by Yoon et al. [93].

Another property of engineering relevance is the HDT. Note that HDT is always enhanced by incorporation of nanoparticles. The related change in PP nanocomposites, yielding at about 40 °C enhancement in HDT at 6 wt% clay content, is originated from a better mechanical stability rather than any increase in the crystallinity and related melting interval. Not surprisingly, the HDT improvement with organoclay is less than with pristine ones [94]. Fornes and Paul [95] proved that the HDT-B (HDT tested by B-method) value of nanocomposites can be calculated by adopting the Halpin-Tsai composite theory for the DMTA properties when coupled with the method of Scobbo. The so-predicted HDT-B values and experimentally measured data exhibited a very good agreement, though for PA/clay nanocomposites.

9.2.3.4 Other Properties

Improvement in the transport properties of 2D nanoparticle-reinforced PPs is the major driving force of commercialization of the related nanocomposites at present. Reduction in the permeability is usually attributed to the fact that the diffusing molecules have to bypass the impermeable platelets (“tortuous path”, labyrinth effect) which are more or less well oriented normal to the diffusion direction. It was found that the Nielsen’s model works well to predict the gas barrier properties in such systems [87]. Recently, more advanced theories were developed addressing changes in the alignment, interphase and bulk properties, as well [96, 97]. Recall that the theoretical models generally consider the silicate layers as perfectly aligned and exfoliated showing a large aspect ratio [87]. However, gas permeability measured is usually markedly below the theoretical predictions [98, 99]. Nevertheless, 2D nanoparticles are far more effective with respect to gas permeation than 0D types [100]. Attention should be called to the fact that permeability is a product of the diffusivity (diffusion coefficient) and equilibrium sorption of the penetrant under given conditions. So, the outcome does not represent a “design parameter”. Nevertheless, studying this behavior useful information can be deduced indirectly, even for the structure of the nanocomposites.

Many reports quoted that the thermal stability (usually studied by TGA) of the polymers increased when containing dispersed nanoparticles. The temperature linked to a given mass loss, and the amount of the char residue increased with increasing clay content. The related increase depended on the clay dispersion, which was controlled by the organophilic surfactant of the clays [101]. It is often claimed that the slowdown in the thermal degradation is due to hampered diffusion of the degradation products from the bulk towards the gas phase. It is worth of noting that all inorganic fillers exhibit some flame retardant effect in their composites. Its manifestation, however, depends on the method selected [102]. Limiting oxygen index (LOI) data showed that there is a large difference between fillers as a

function of their dispersion state (micro- or nanoscale) and aspect ratio [103]. Note that in an LOI test the flame spreads from the top of the specimen downwards. So, in this test the char formation has a great influence. Needless to say that a vertical burn test (e.g. according to UL 94 descriptions) may deliver completely different results. Nowadays, the ultimate method to check the fire retardance is the use of cone calorimetry. In the related tests the heat release rate (HRR) and mass loss rate are registered as a function of time. Numerous works using this method indicated that in presence of different nanoparticles (among which layered silicate were preferentially used) the peak HRR is efficiently reduced, however, with some extension in the overall burning time [103–105]. This was traced to the formation of a carbonaceous/silicate char of thermal insulating properties on the specimen surface [104]. To improve the very poor fire resistance of PP the preferred concept is to make use of intumescent coatings [106]. Intumescent formulations are halogen-free and produce a charred cellular layer upon heating. The related layer is acting as a heat shield by protecting the underlying material from the heat flux of the flame. This concept was adopted for polymer nanocomposites due to two effects: (a) char yielding behavior and (b) reinforcing effect of the clay [107]. Note that the reinforcing effect of the nanoclay is of vital importance as the usual intumescent formulations result in materials of poor mechanical performance. Based on the above behavior layered clay containing PP nanocomposites should have improved resistance to ablation, too.

9.2.4 Processing and Applications

The unique combination of some key properties paved already the way for PP nanocomposites for industrial applications (packaging—due to barrier properties [108], automotive—due to high stiffness, high strength, low density, enhanced HDT, improved mar and scratch resistance [109]). The processing, covering all aspects (welding, joining, etc.) of PP nanocomposites follows the rules established for the neat PPs. Albeit PP nanocomposites are commercialized at present mostly as precompounded grades, in ready to use or in masterbatch (to be “diluted” forms), the in situ “polymerization filling” methods may be the winners in the future.

9.3 Discontinuous Fiber-Reinforced Composites

The history of fiber-reinforced thermoplastic polymers began only some decades ago, when industrial production of the reinforcing fibers (glass in 1935, carbon in 1959, aramid in 1971) and adequate matrix polymers (e.g. PA-6.6 in 1938 and polyethylene terephthalate in 1955) was started. Incorporation of discontinuous fibers into thermoplastics generally yields improvements in mechanical and thermal properties, for instance, stiffness, strength, dimensional stability, service

temperature, resistance to creep and fatigue. These improvements are, however, connected with reduced strain (ductility) characteristics and pronounced anisotropy as a result of the structuring of the reinforcement in the molded parts.

Fiber reinforcement is the best way to transfer commodity or high volume thermoplastics, such as PP into engineering thermoplastics. It is noteworthy that the criteria for engineering thermoplastics—namely, continuous service temperature above 100 °C and tensile strength higher than 40 MPa [110]—can also be met by several plastics without reinforcement.

The relative high annual growth rate of fiber-reinforced composites compared to neat plastics is mostly the result of the substitution of metallic and ceramic items by compression-, injection-, and extrusion-molded composite parts manufactured from discontinuous fiber-reinforced polymers.

9.3.1 *Manufacturing*

The production of discontinuous fiber-reinforced PP composites is usually separated from that of the final shaping that occurs generally by injection molding. Accordingly, PP and the fiber (GF, CF and various NFs) are first processed into a granular, pelletized feedstock. For the incorporation of the fiber extrusion compounding is used. In the eldest version, the PP granules and chopped fibers (<10 mm length) are dry blended before feeding into the hopper of a single- or twin-screw extruder. The extruded composite, in filament (“wire”) form, is cooled and subsequently pelletized (diameter: ~3 mm, length: 3–6 mm). This operation results in severe breakage of the reinforcing fibers: the maximum length generally remains below 0.5 mm in the ready-to-mold granules. In a more advanced version, the fiber (either in chopped or in continuous form) is introduced through a suitable decompression port of the extruder in the already plasticized PP. When rovings, tows are added then the extruder screw also overtake the role of the cutter. In this case the fiber attrition is less severe and thus in the final product the fiber length may surpass 1 mm length. This is the right place to call the attention to the distinction between short and long fiber reinforced PPs: the mean fiber length is below 1 mm for short, while it is above this threshold for long fiber-reinforced grades. In many research works this definition is applied for the initial feedstock, whereas in others for the residual fiber length distribution in the molded parts. Recognizing the beneficial effects of long fibers (enhanced strength and impact resistance) various processes (“wire coating”, cross-head extrusion, different pultrusion methods (using powder coating or melt impregnations) were developed for the production of long fiber-reinforced (mostly long glass fiber, LGF) PP composites after the pioneering activity of ICI Ltd. in 1985 (introduction of Vertron™ types) [111]. In these processes continuous GF or yarns (composed of discontinuous fibers, such as NF variants [112]) are impregnated by the PP melt before cutting to ≤ 10 mm length. In long fiber-reinforced composites the wet-out of the fibers by the matrix is less

perfect compared to traditional compounding, and thus bunched, bundled fibers may be present in the molded items.

The development of discontinuous fiber-reinforced thermoplastics is well reflected by a steady increase in the aspect ratio (length to diameter, l/d) of the fibers both in the parent granules and molded parts. The l/d ratio of short fiber-reinforced grades produced by extrusion melt compounding technique was ≈ 20 earlier, nowadays it lies at ≈ 50 . The next milestone was achieved by pultrusion and powder coating techniques, through which granule size fiber length was set. In the related long fiber-reinforced injection and compression moldable grades the initial aspect ratio of the discontinuous reinforcement (usually GF) is ≈ 1000 and ≈ 2500 , respectively.

A further logical step was to avoid the preparation of the pelletized feedstock. This was solved by merging the preparation of the fiber-reinforced composite with that of its molding in line. Several attempts were made into this direction during modification of the injection molding machines. Although the feasibility of this approach was shown [113, 114] industrial breakthrough occurred when the final part was produced in compression molding [115]. As described in the next paragraph, PP-based GMT were substituted by directly produced long fiber reinforced thermoplastics (D-LFT). In the corresponding D-LFT systems the fiber length range is from 10 to as high as 25–50 mm.

There are some novel processing techniques for discontinuous fiber reinforced PPs, such as fused deposition modelling (FDM). In FDM the composite parts are produced by layer to layer deposition of the molten polymer. The reinforcing fibers in the deposited PP filaments, wires may be GF [116], CF and also NF [117].

The overwhelming majority of discontinuous fiber-reinforced PPs is processed by injection molding. Injection molding comprises the plastification of a given charge of the composite before its injection into a mold with cold walls. After cooling, the solidified parts are ejected and the cycle is repeated. By this way, parts of very complex shapes, with high dimensional accuracy can be produced at extreme high productivity (i.e. very short cycle times). The related machines are sophisticated, highly automatized ones. Injection/compression molding is rarely practiced: here first the melt is injected into the mold before it is subjected to the second compression step yielding the final product [118].

It should be born in mind that the mean fiber length and the fiber length distribution may markedly differ between the feedstock granules and the injection-molded items. Compounding and injection molding are accompanied with severe fiber breakage. This prominently reduces the tensile strength and impact properties. Fiber attrition is influenced by both material- (with increasing fiber content the fiber/fiber interaction is increasing) and processing-related factors (locally acting high stresses due to back pressure or injection speed, convergent and divergent flows at the nozzle, gate design, runner system of the mold etc.—all imposing critical stresses and contributing to fiber/“wall” (surface of the screw, barrel and mold) frictions. Fiber attrition due to various processing parameters was already the topic of works, especially in case of LGF-reinforced PPs [119–121]. Since the processing parameters affect mostly the strength and impact data, these

characteristics were considered when evaluating set changes in the processing [122–124]. Based on the experimental findings, Phelps et al. [125] developed a model to predict the breakage rate assuming that breakage is owing to buckling under hydrodynamic compressive stresses and some off-orientation of the fibers with respect to that of the flow.

All-PP composites can also be prepared by injection molding from chopped consolidated preforms of PP copolymer (matrix) and PP multifilament (reinforcement) [126, 127].

9.3.2 Structure Development and Characterization

Injection molding induces changes in the molecular orientation and crystallization behavior of neat PP [128]. This is also the case for the matrix polymer of short and long fiber reinforced grades. On the other hand, the effects of the skin-core structured matrix are masked by the molding-induced fiber structuring in the reinforced composites. The layering of the fibers and their orientation in each layer in the molded part is due to the melt flow within the mold. For the flow field consisting of shear and elongational flows, processing conditions are not the only important factors; the mold construction (sprue, runner, gate, and cavity geometry inducing converging and diverging flow during processing) is also relevant.

It is widely accepted that fiber orientation in discontinuous fiber-reinforced thermoplastics can adequately be described by the model of Tadmor [129], which involves the fountain or volcano effect discussed by Rose [130]. According to this model, the fiber orientation pattern produced by injection molding can be approximated by a three-layer laminate structure. This is depicted schematically and as it looks in practice in Fig. 9.4. In the surface (S) layers, fibers are oriented parallel to the mold filling direction (MFD). This is caused by the shear flow of the melt along the quickly solidified layer at the mold wall. In the central (C) layer, fibers adopt an orientation perpendicular to the MFD in the plane of the molded item. This kind of alignment is due to the elongational flow at the midplane of the cavity. Factors contributing to the mid-plane elongational flow are diverging flow at the cavity entrance and the fountain effect. The fiber layering can be even more complicated, since particulate fillers tend to migrate toward the mid plane of the molding, where flow speeds are higher [131]. This change, attributed to normal stress effects, again modifies the flow profile and thus the layering and orientation of the discontinuous reinforcement.

Figure 9.4 illustrates the designation of the compact tension (CT) specimens preferentially used. Note that the designation of the CT specimens considers the loading—notching (longitudinal, L or transverse, T) directions in respect to the MFD.

Results of numerous investigations carried out on injection-molded plaques (film-gate, 3–4 mm thick) indicate that ([132], cf. Fig. 9.5):

- Both the fiber layering and alignment increase with fiber volume fraction (V_f).
- The absolute values of the fiber orientation (see later) are closely matched in the S and C layers, and fiber orientation increases with V_f .
- The processing effects (melt, mold temperature, and injection speed) are of secondary importance compared with V_f .

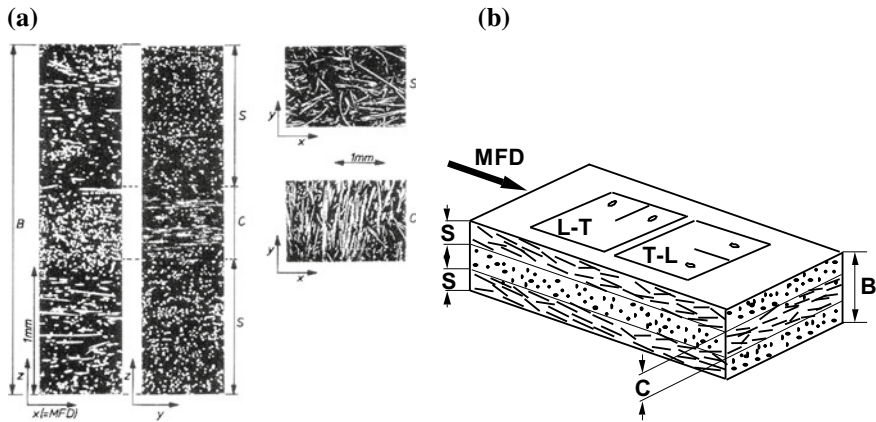


Fig. 9.4 Fiber orientation resulting from injection molding **a** for 40 wt% (=19.4 vol%) long GF reinforced PP; **b** flow induced fiber layering schematically along with specimens (compact tension) preparation. Designations: B—specimen (cavity) thickness, C—central layer thickness, S—surface layer thickness

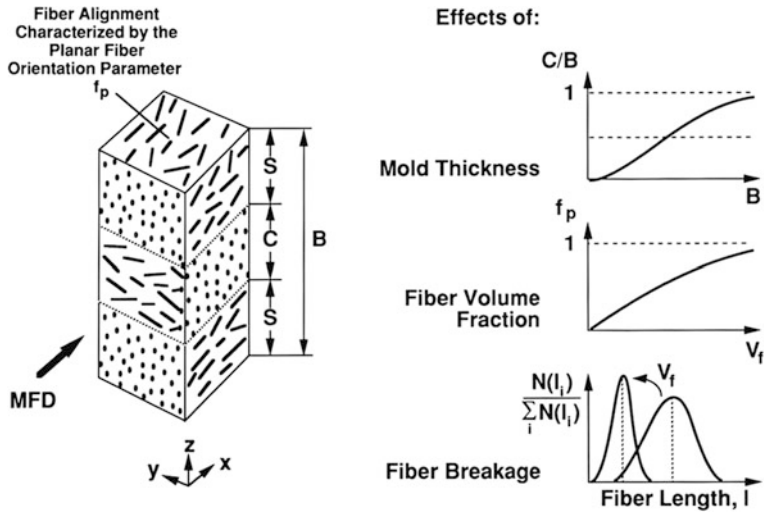


Fig. 9.5 Effects of cavity thickness (B) and V_f on the layering, planar orientation (f_p) and mean fiber length of injection molded discontinuous fiber-reinforced composites

For thinner or thicker items, which in addition involve other gate constructions, these statements are not always valid.

Microstructural investigations carried out on LGF reinforced injection-molded thermoplastics showed significant analogies with short glass fiber (SGF) composites [133–135], namely: (i) the relative thickness of the C layer increases with increasing aspect ratio, and (ii) fiber bending and bunching may occur.

Fiber bunching is connected with the pultrusion pelletizing process used for the production of LGF-reinforced injection moldable composites. Both of the effects of fiber bending and bunching reduce the effective aspect ratio of the reinforcement in the molded part [133, 135].

The aspect ratio of the fibers in the molded item depends on material factors (especially V_f), mold geometry, and processing parameters. Higher fiber loading shifts the aspect ratio distribution curve toward lower values as a result of increased fiber/fiber and fiber/wall interactions causing fiber fracture. This effect is much less pronounced for LGF than for SGF reinforced composites, provided that mold construction for the former system is adequate. It is due to the preliminary orientation of the fibers during manufacturing. The aspect ratio distribution curve of the reinforcement may differ when various layers across the thickness of the molded part are considered [133]. This is mainly due to fiber enrichment in the C layer, differences between bunching and filamentization in the S and C layers, and effects of the flow field on fibers with different aspect ratios.

Distinction between the S and C layers becomes more problematic when in PP composites with compliant NFs or PP fibers, especially at high fiber loading [126, 127].

For the flow features and microstructural development in discontinuous fiber-reinforced thermoplastics, detailed information can be taken from the Ref. [136].

The above treatise makes clear that the microstructural parameters of reinforced injection-molded composites are fiber layering, fiber orientation (they are commonly termed fiber structuring), V_f , effective fiber aspect ratio and its distribution.

For the determination of fiber layering by imaging of polished sections or thin slices via light (reflective or transmission), scanning electron microscopy (SEM), and contact microradiography are preferred. For fiber orientation, microwave, X-ray diffraction, sonic, and thermographic measurements can also be used. A novel powerful technique is the X-ray computed (micro)tomography [137] allowing us to determine both the fiber length and fiber orientation distributions spatially [138–140].

Recall that in Fig. 9.4, a SEM micrographs taken from polished sections along the thickness-MFD ($z-x$) and $y-x$ planes are shown. The evaluation of fiber alignment and mean fiber orientation in a given plane is very time-consuming, as it involves determining the angle distribution under which fibers are aligned. In this respect, image analysis offers the new possibility of getting information about not only in-plane but also spatial orientations [141]. Fiber orientation can be described

either by using mean orientation factors, such as Hermans [142, 143], Krenchel [144], or by vectors [145].

The aspect ratio (since the diameter of the fibers is mainly constant, it can be replaced by fiber length) distribution curves are generally determined from microphotographs of the fibers taken after burning away the matrix. In many cases the matrix polymer can also be removed by solvents.

The above-mentioned microstructural parameters are summarized in a reinforcing effectiveness term (R). This term previously considered the effects of fiber structuring with respect to the loading direction and the fiber loading [146]. This was extended later to include the aspect ratio and aspect ratio distribution [132, 133, 135], and generalized in the form (Eq. 9.1):

$$R = \sum_i T_{rel,i} \cdot f_{p,eff,i} \cdot V_{f,i} \left(\frac{l}{d} \right)_{equ,i} \frac{\left(\frac{l}{d} \right)_{n,i}}{\left(\frac{l}{d} \right)_{m,i}} \quad (9.1)$$

where $T_{rel,i}$ is the relative thickness of the i -th layer normalized to the sample thickness (B), see Figs. 9.4 and 9.5), $f_{p,eff,i}$ is the effective orientation in the i -th layer calculated using the function of planar orientation (f_p) versus $f_{p,eff}$ introduced by Friedrich [146], $V_{f,i}$ is the fiber volume fraction in the i -th layer, $(l/d)_{equ,i}$ is the equivalent aspect ratio in the i -th layer, $(l/d)_{m,i}$ and $(l/d)_{n,i}$ are the mean mass- and number average aspect ratios in the i -th layer, respectively [133].

The reinforcing effectiveness, and the corresponding microstructural efficiency (see later) concepts worked adequately when considering the fracture mechanics-related parameters of discontinuous fiber-reinforced PPs [68, 132, 135]. On the other hand, it can be prophesized that X-ray tomographic inspections along with the related image analysis will give a new impetus to determine or redefine the reinforcing effectiveness parameter.

9.3.3 Properties and Their Prediction

The performance of discontinuous fiber-reinforced composites, including PP-based ones, was already the topic of several books, book chapters and reviews [135, 147–149]. Therefore, next the state of knowledge will be summarized on selected properties thereby considering the molding-induced structuring of the discontinuous reinforcements.

9.3.3.1 Mechanical Response

Tensile tests

The mechanics of discontinuous fiber-reinforced composites is more complex than continuous, aligned fiber containing ones because in the former case the fibers

have different length and spatial orientation. Therefore, the distributions of fiber length and orientation should be considered when modeling the physico-mechanical properties. The “shear lag” theory of Cox [150] assumes that both the fiber and matrix behave as elastic bodies and perfect bonding exist between them along a cylindrical interface. As a consequence, differences in the strain displacements appear in the fiber and matrix along the interface. Though the tensile stress development in the fiber is realistic, the shear strength should fall to zero at the fiber ends instead of showing a maximum according to this model. A further deficiency is that the interface strength is disregarded though it may cause debonding or yielding—associated with subsequent stress redistribution—when the interface or the matrix is weaker. According to the Kelly-Tyson approach [151] the interface strength is balanced by that of the fracture strength of the fiber. The stress builds up from the fiber end toward the middle part is similar to that of the Cox model, but the increase is linear up to a point (stress transfer length) where no strain difference will be between the matrix and fiber. Both models adequately predict the course of the reinforcement efficiency as a function of the fiber aspect ratio. Provided that the fibers are aligned parallel to the applied stress then the E-modulus of the composite (E_c) can be calculated by the modified “rule of mixture” (Eq. 9.2):

$$E_c = \eta_1 E_f V_f + E_m V_m, \quad (9.2)$$

where η_1 is the fiber length efficiency factor representing the average stress in the short divided by the stress in the continuous fiber composite at a similar applied strain [152], E_f, E_m —E-modulus of fibers and matrix respectively; V_f, V_m —volume fraction of fibers and matrix respectively. This equation was refined by Bader and Bowyer [148, 153, 154] who considered that the reinforcing efficiency is a function of the applied strain, as well. Equation (9.2) can be further refined to take the fiber orientation into account:

$$E_c = \eta_0 \eta_1 E_f V_f + E_m V_m \quad (9.3)$$

where η_0 is the mean angle of the fibers to the loading direction. Its value is 1, 0.375 and 0.2 for uniaxial, planar random and spatial random orientations, respectively [148]. Equation (9.3) proved to be useful to estimate the E-modulus of mat-reinforced PP composites [152]. The most popular model to predict the stiffness is credited to Halpin and Tsai (Eqs. 9.4 and 9.5) [155]:

$$E_c = E_m \left(\frac{1 + \xi \eta V_f}{1 - \eta V_f} \right), \quad (9.4)$$

where

$$\eta = \frac{\left(\frac{E_f}{E_m}\right) - 1}{\left(\frac{E_f}{E_m}\right) + \zeta}, \quad (9.5)$$

where η —efficiency factor; ζ —measure of reinforcement geometry which depends on loading conditions.

Its wide use is due to the fact that by suitable choice of the two constants, the Halpin-Tsai equation allows predictions anywhere between the Voigt upper (ζ is infinite) and Reuss lower bound (ζ is zero) rules of mixture equations. Based on the Halpin-Tsai approach Garesci and Fliegner [156] modeled the E -modulus of direct LFT-PP composites whereby considering the V_f , fiber orientation and fiber length distributions. The two latter distributions were assessed in X-ray microtomography and quantified. It is noteworthy that many other equations, already listed for nanocomposites, have been developed and adapted for discontinuous fiber-reinforced PP composites.

The strength prediction is more problematic than that of the stiffness due to the different failure events which may happen even when the fibers are uniaxial aligned (debonding with cavitation, matrix failure, crazing, plastic flow—all at the fiber ends) [148]. This is the possible reason why for optimization of the tensile strength of discontinuous fiber-reinforced composites experimental methods (design of experiments) are used [157]. Though many approaches have been recommended for aligned short fiber composites, one of the most popular ones is based on the Kelly-Tyson equation [152] that considers that the failure is different for fiber below and above the critical fiber length. Since the critical fiber length (aspect ratio) is linked with the interfacial shear strength, this is the right place to comment how it can be tailored. An interfacial shear strength of 4–6 MPa is fairly typical for the adhesion between unmodified PP and GF without specific sizing [152, 158]. Similar values have been reported also for composites with other fibers than GF [159]. These values are, however, far less than shear strength of the PP (when estimated as the half of the yield strength; 15–16 MPa). Values closely matched with the shear strength of PP can be reportedly reached when to the PP matrix a suitable coupling agent (almost exclusively maleic anhydride grafted PP, PP-g-MA) is added and the GF is sized by an appropriate silane [160]. In case of crystalline fibers, such as CF [161], NF [162] and even PP (in case of all-PP composites [163]) a TC layer may form on their surfaces (Fig. 9.6).

The related one-dimensional spherulitic growth is caused by the fiber surface-induced dense heterogeneous nucleation of the crystallizing PP. The TC layer is often quoted for improved stress transfer which is, however, not always experimentally evidenced [46, 164]. It is worth of noting that various surface

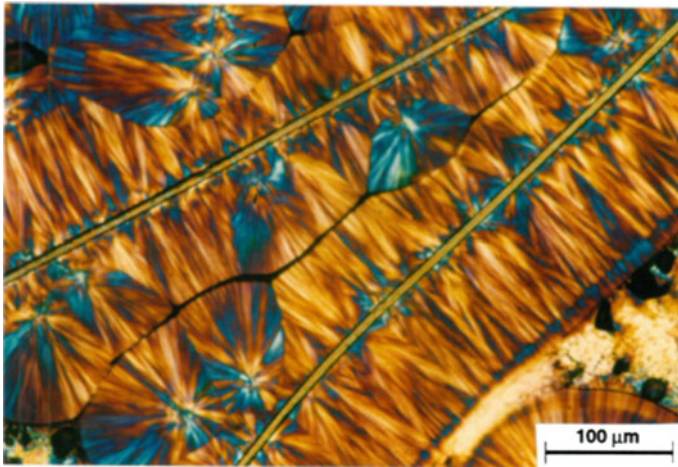


Fig. 9.6 Transcrystalline PP layer formed on the surface of aramide (Kevlar™ 29) fibers. Note: crystallization in quiescent melt at 133 °C

modifications are used for NFs to improve their bonding to PP [165]. Hybridization of fibers is an often practiced tool for property improvements [166]. NFs are hybridized with man-made fibers in order to enhance the strength and reduce its scatter [167]. Nowadays, discontinuous fibers are combined with micron- [168], and especially nanoscale fillers [169, 170] in order to tailor the mechanical and thermal properties of the related composites.

Fracture behavior

Results from standardized toughness testing methods can only be compared when all the specimen- and testing-related conditions are identical. By contrast fracture mechanics may yield toughness which is a material property, i.e. independent of specimen's and testing configurations (but still temperature and frequency dependent). Fundamental aspect of fracture mechanics is that the onset of fracture depends not only on the applied stress but also on intrinsic flaws that act as stress concentrators. Such stress concentration sites are always present in neat and reinforced molded plastics, either as a result of processing or caused by use. The common effects of stress and flaw size are combined in linear elastic fracture mechanics (LEFM) which deals only with bodies that obey the Hookian law, that is, whose deformation is fully elastic. The related terms are the stress intensity factor (K) or fracture toughness and strain energy release rate (G) or fracture energy.

The main criterion of LEFM, namely fully elastic deformation, is very severe for plastics that may undergo pronounced plastic deformation (yielding or tearing) during fracture. In this case, other approaches, are pursued for plastics: J-integral, crack opening displacement, and EWF [171, 172]. These material parameters are included in plastic, elastoplastic, or post-yield fracture mechanics (PYFM). Fracture mechanics methods are aimed at determining that critical parameter at which unstable (LEFM) or stable crack growth (PYFM) takes place.

Fiber reinforcement may affect fracture toughness in different ways. It can be improved, worsened, or held at a constant level by fiber incorporation, depending on the matrix of the composite [132]. The layering and orientation of the fibers in injection-molded items were already shown in connection with Figs. 9.4 and 9.5. On the fracture surface of the specimens, fibers lying parallel or longitudinal to the crack plane (L fibers) can clearly be distinguished from those oriented perpendicularly or transversely to it (T fibers) (Fig. 9.7).

Note that the anisotropic structuring of the fibers yields different fracture mechanical values when specimens with various notch directions (T and L; see Fig. 9.4b) are tested [132, 134, 146]. The load bearing capacity of T fibers aligned in the load direction is considerably higher than that of the L fibers, which have practically no reinforcing effect. Therefore, the fracture mechanical response depends on the relative thickness of the layers containing T and L fibers, respectively.

The degree of fiber orientation in these layers is also important. T fibers completely aligned in the load direction guarantee the best stress transfer and thus the greatest reinforcement. Fiber misalignment along the load direction necessarily reduces the overall reinforcing effect. Friedrich introduced an effective fiber orientation term that takes this fact into account [146].

The influence of fiber aspect ratio on fracture toughness at a given fiber loading depends also on the matrix characteristics. However, with increasing fiber aspect ratio K_c always increases, at least above a given threshold l/d . This is connected with an increase in the performance of the discontinuous-fiber-reinforced composites, since their strength increases with increasing aspect ratio [147].

Recall that all above listed parameters, governing the fracture behavior, were included in the reinforcing effectiveness (R) term. Thus, the fracture mechanics parameters should depend on the R term for discontinuous fiber-reinforced PP composites. This has been proven for both SGF- and LGF-reinforced systems subjected to static [134, 173] and dynamic conditions [174]. Figure 9.8 shows an

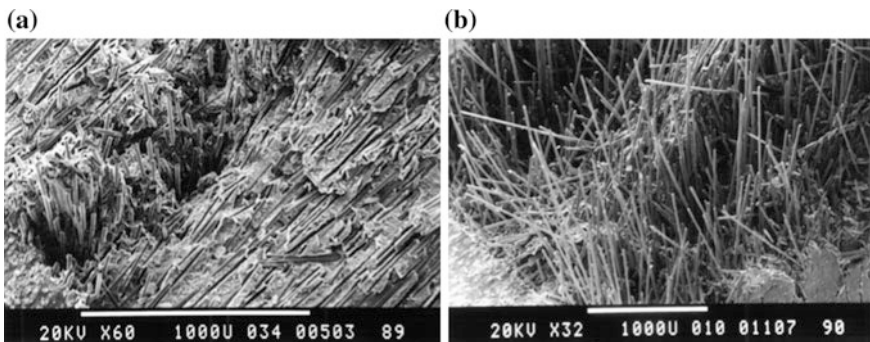
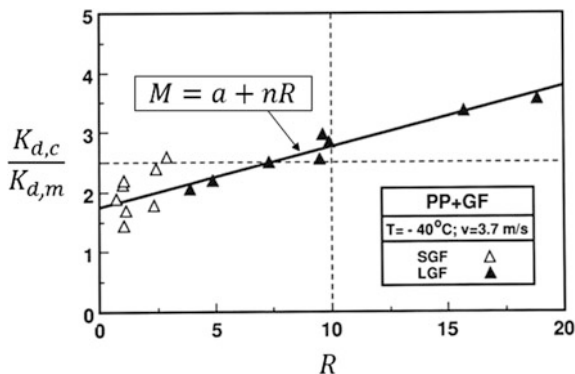


Fig. 9.7 Fracture surface at the razor notch of 40 wt% (=19.4 vol%) SGF (a) and LGF (b) reinforced injection-molded PP. (In this T-L type CT specimen, L fibers can be found on the surface, whereas T fibers in the central layer, as indicated; cf. Fig. 9.4)

Fig. 9.8 Relative dynamic fracture toughness ($\frac{K_{c,d}}{K_{c,m}}$) as a function of the reinforcement efficiency factor R for short and long GF-reinforced PP composites. Notes: V_f content up to 40 wt%; testing conditions: $-40\text{ }^\circ\text{C}$ at 3.7 m/s impact speed (based on [175])



example of high-speed impact tests results that the relative change in the dynamic fracture toughness of the composites compared to the matrix can follows a linear relationship as a function of R (Eq. 9.6):

$$\frac{K_{c,d}}{K_{c,m}} = M = a + nR, \tag{9.6}$$

where M is the microstructural efficiency, a —stress condition factor considering that the matrix fails differently when reinforced than without, n is the energy absorption coefficient, and R is the reinforcement effectiveness.

It is noteworthy that the microstructural efficiency concept worked also properly for the J-integral data of PP composites [173]. It has to be emphasized that dynamic failure mechanisms are the same as those shown and discussed with respect to static loading. Although failure mapping is seldom performed for dynamic measurements, the following effects can be predicted: (i) the frequency embrittlement of the PP matrix promotes brittle matrix cracking, eventually associated with limited craze formation (frequency-dependent T_g), (ii) among the fiber-related failure events, fiber pullout and fracture tend to dominate. Their relative proportions depend not only on the testing conditions but also on the fiber-matrix bonding.

Fatigue

Discontinues fiber-reinforced PP composite parts are widely used in fields in which cyclic subcritical (i.e. fatigue) loading occur. The fatigue performance can be characterized either by the endurance limit (maximum allowed applied stress causing no damage after 10^6 fatigue cycles) or by parameters of the fatigue crack propagation (FCP) curves. The FCP approach is based on the fracture mechanics, i.e. accepting the presence of inherent flaws, inhomogeneity. Such flaws may act as initial cracks and thus the life expectation of the related parts is controlled by the FCP behavior. If the controlling step is, however, the development of crack (or more generally some kind of damage) then the fatigue endurance limit has to be determined via Wöhler curves. To measure the Wöhler curves specimens are subjected to cyclic loading at different maximum stresses at a given loading

configuration. Its modeling is a great challenge because the actual damage mode and sequence should be known and properly parametrized [176].

The fracture mechanics approach can be applied for cycling fatigue of notched specimens. During fatigue slow crack growth occurs under subcritical stress amplitudes; that is, the stress intensity factor amplitude remains below that of the critical value (K_{Ic}). In FCP the crack growth rate per cycle is established as a function of the stress intensity factor amplitude (ΔK). A threshold value ΔK_{th} , which is connected with the onset of fatigue growth, can be read from the FCP curve and may serve for design purpose. After this threshold a stable crack propagation range can be usually found for which the Paris-Erdogan relationship holds (Eq. 9.7):

$$\frac{da}{dN} = A(\Delta K)^m, \tag{9.7}$$

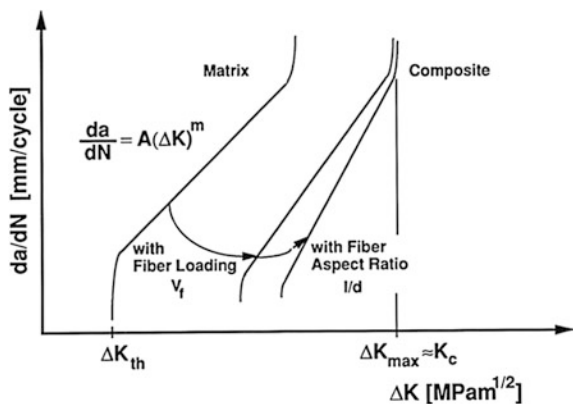
where A is the pre-exponential factor, ΔK is the stress intensity amplitude and m is the exponential term. Note that $\frac{da}{dN}$ can be plotted also as a function of ΔG instead of ΔK [177].

According to the experiments [178–180], the controlling parameters of the FCP behavior are V_f , molding-induced layering (reflected by the notching of the specimens with respect to the MFD) and fiber aspect ratio. Their effects are schematically depicted in Fig. 9.9.

Figure 9.10 makes obvious that LGF extends the damage zone compared to the SGF counterpart thereby improving the resistance to FCP.

Note, however, that all the above parameters are involved in the R -term. Accordingly, there is a good correlation between the crack growth rate and the reinforcing efficiency (R): increasing R results in an improved resistance to FCP. Moreover, it has been shown that $\log(\frac{da}{dN})$ versus $\log M$ data pairs lay on a straight line, also for discontinuous GF-reinforced PP composites [181].

Fig. 9.9 Changes in the stable FCP behavior due to microstructural parameters, schematically. *Note:* Scheme in double logarithmic scaling [181]



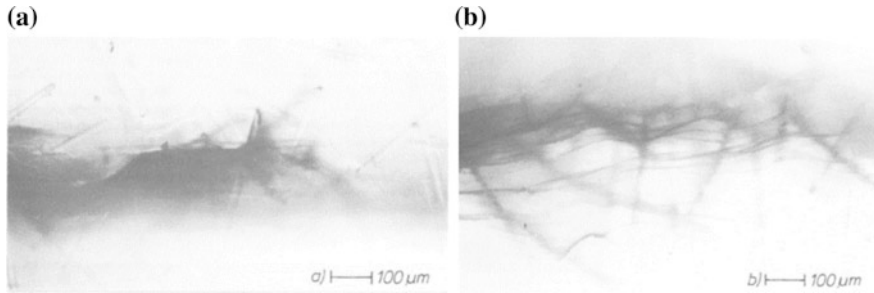


Fig. 9.10 Transmitted light pictures on the crack tip damage zone showing the matrix- (craze bands) and fiber-related (stress concentration at fiber end, debonding, pull-out) failure events in 10 wt% SGF (a) and LGF-reinforced PP (b), respectively [178]

Creep

The long-term creep behavior is of paramount importance since many composite parts have to withstand to a constant load during their lifespan. Different models have been proposed and adapted for thermoplastics like PP [182, 183] and their discontinuous fiber-reinforced composites [184, 185] to describe their creep behavior. Exploiting the viscoelastic feature of polymeric materials, the preferred way is to increase the temperature to accelerate the time dependence of the creep and create master curves based on the time-temperature superposition principle (TTSP). Accordingly, short-term creep experiments, performed at various temperatures, are used to create a master curve, which describes the long-term deformation at a reference temperature. Usually, the Williams-Landel-Ferry [186] or the Arrhenius equation, or a combination of them, are applied to determine the shift factor that is needed for the construction of the long-term master curve (supposing load and time independent shift factor parameters). Based on short term measurements such as tensile ($\epsilon_2(t_2)$) and creep ($\epsilon_1(t_1, t_0)$) tests of $t_M = 10$ h performed on PP/GF samples at different load levels ($\sigma(t_0) \rightarrow \epsilon_0$) Vas and Bakonyi [182, 185] developed a novel statistical phenomenological method for modeling the creep process (ϵ_1) and assessing the statistical properties of the creep strain (ϵ_{1B}) and lifetime (t_{1B}) to failure. A kind of load-time superposition principle realized by nonlinear symmetry (R) and variable transformations (S_1, S_2) was used to approximate the mean creep-strength curve ($\epsilon_{1B}-t_0$ or $\epsilon_{1B}-t_{1B}$) and the whole mean creep process as a master curve ($\epsilon_{1B}(t_0): t_0 \leq t_1 \leq t_{1B}$) at arbitrary creep load levels ($0 \leq t_0 \leq t_{2B}$) also outside the measuring range (Fig. 9.11). Weibull based probabilistic approach enabled to estimate the confidence intervals of the curves and the creep failure data. The method can be applied to modeling the stress relaxation process as well.

Fracture mechanics approaches can also be used to study the time dependent crack growth at constant load, termed as to static fatigue (Eq. 9.8):

Computer aided design (CAD) is a technique that has been successfully applied to optimization of mold construction for molded parts. In CAD design of an injection-molded part, the first step is to visualize the weak sites, that is, the weld lines. The next step is to change the position and/or type of runner and gate so that weld lines do not evolve or, if this is impossible, are positioned where low stresses in the part during service can be predicted. The next phase is modelling the flow in the mold, subdivided into FEs, and characterizing the melt flow patterns in these mold segments. For the calculation of the flow patterns, rheological parameters, determined experimentally or estimated by the software, are used. The flow modelling is repeated in several steps until optimized mold filling occurs. The aim is to get the same material flow in all segments of the mold resulting in smooth surfaced, warpage-free products with controlled shrinkage [192].

9.3.3.3 Thermal Properties

As mentioned before, crystalline reinforcing fibers usually work as heterogeneous nucleants and even may promote TC growth. Due to this nucleation, the undercooling (supercooling), meaning the temperature interval between the melting and crystallization of PP, is reduced. As a consequence, injection molded parts may be earlier ejected thereby increasing the productivity. Similar to nanocomposites, incorporation of discontinuous fibers markedly enhances the HDT. Parallel to that also the thermal expansion coefficient is reduced. On the other hand, the thermal expansion coefficient may show a strong direction dependence owing to the fiber local orientation.

To enhance the thermal conductivity, hybridization of GF and NF with CFs and with suitable micro- (such as boron nitride) and nanofillers (CNT, GR, inorganic “fullerenes” [193]) are the preferred strategies. Based on results achieved by PP/CF composites it was reported that the polymer coupling agent (PP-g-MA) does not affect the thermal conductivity [194]. Modeling of the thermal conductivity followed the theories developed for the mechanical behavior of short fiber composites [188, 195, 196]. The byside effect of the fiber/nanofiller hybridization is often an enhanced resistance to thermal degradation. Like to nanocomposites [197], this improvement is traced to the formation of a protective char layer on the burning surface and/or to an enlarged diffusion path of the burnable volatile degradation products from the bulk toward the surface.

PP is an easy burning material due to its high carbon and hydrogen contents. Therefore, flame retardants are incorporated when the specification in the related application field requires a flame retarded PP grade. Though different classifications exist [198], the flame retardants work either in the gaseous or in the condensed phase via various chemical and physical mechanisms interfering with that of the combustion. The flame retarding effect of $\text{Al}(\text{OH})_3$ and $\text{Mg}(\text{OH})_2$ is due to their endothermic degradation whereby water is released which “cools” the flame and dilutes the composition of the burning pyrolysis gas. Unfortunately, their required amount may be as high as 65 wt% in order to meet the V-0 rating of the UL94

classification [199]. This high loading is undesirable having a negative impact on the processability and mechanical properties of the related composite. The nowadays preferred phosphorous containing flame retardants act in the gas, and eventually, also in the condensed phase (char formation). Its amount may be below 5 wt% P-content in a fire-proof PP. Intumescent coatings form a carbonaceous foamed mass when exposed to heat, and work as a heat shield and barrier layer against the diffusion of the evolved degradation products [106]. It is noteworthy that NFs, being combustible themselves, may cause a “candlewick” effect that should be depressed by suitable surface treatments [200]. Vadas et al. [201] investigated the effect of ammonium polyphosphate in an injection-moldable all-PP composites. The LOI was enhanced from 18 to 29.5% and the UL-94 classification changed from HB to V-2 when the composite contained 15 wt% ammonium polyphosphate flame retardant.

9.3.3.4 Other Properties

Some application fields, such as bipolar plate in fuel cells [202], housing of electronic devices (electromagnetic interference (EMI) shielding [203], require electric conductive PP composites. For this purpose, generally PP/SCF (short carbon fiber) composites have been prepared. For high conductivity the requirement is to reach the percolation threshold. The percolation threshold is assigned to a long-range connection of randomly distributed particles. PP/SCF conductive composites showed a conductivity of 10^{-6} S/m when containing more than 3 wt% of CF, and an optimal EMI shielding efficiency of 25 dB when containing 20 wt% of CF [204]. The percolation threshold loading can be reduced when conductive fillers (any kind) with different aspect ratios are simultaneously present. This hybridization strategy is now exhaustively followed. The related development is fueled also by the need of electric conductive filaments for FDM. Krause and Pötschke found for example that electric (and thermal conductive) PP composites can be produced at low SCF/carbonaceous nanofiller (MWCNT or GR) loading (7.5 vol%) [205].

9.3.4 Processing and Applications

Among the guidelines for processing of short and long fiber reinforced thermoplastic, priority is given to processing parameters and mold constructions that contribute to preserving the initial aspect ratio, that is, the fiber length of the reinforcement. Avoiding fiber breakage requires molding at minimal frictional heating. On a given reciprocating injection molding machine this can be achieved by slow screw rotation, low injection speed, low back pressure, and high barrel temperature. Processing of LGF reinforced thermoplastics is very similar to that of SGF composites. It is recommended, however, to choose a 10–20 °C higher barrel temperature and a special “low work” screw. This screw is characterized by a long

feed section with constant root and wide, deep flights. This section is followed by a low gradual compression zone without kneading or mixing elements; the screw ends in a constant-root metering section with flat flights. In addition, certain aspects of mold construction have to be considered (short runners, large film or fan gates).

Service conditions for short fiber reinforced thermoplastic composite parts often require a given well-defined fiber structuring. For injection-molded items, a new technique called multiple live-feed injection molding was developed. In this method, a packing head is inserted between the mold and the head of the injection-molding machine. The melt flow, and thus fiber orientation in the packing stage, can be modified accordingly by a programmable movement of the pistons of the packing head that pressurizes the solidifying melt directly [206]. A similar approach, called dynamic packing injection molding, has been developed recently [207]. In this method oscillatory shear is imposed on the gradually cooled melt during the packing, solidification stage. Albeit this yields some reduction in the mean fiber length, the improved orientation of the fibers and that of the matrix compensate this effect and results in strongly enhanced tensile strength compared to conventional injection molding for both SGF- and LGF-PPs. In injection molded parts the development of weld lines (“cold” and “hot” ones whether the melt streams are opposed or merging side by side) can hardly be avoided. In order to diminish the parallel layering of the fibers in the weld line several processing options, such as “push-pull” injection molding, sequential filling [208] are possible.

The application of short and long fiber-reinforced PP composites is very broad covering practically all sectors. Long fiber-reinforced versions are preferred composites for automotive applications. Nowadays, substantial efforts are made to reinforce PP with recycled discontinuous CF and use them in the automotive sector [209, 210].

9.4 Mat-Reinforced Composites

Mat-reinforced thermoplastics (MRT), belonging to the family of “organosheets”, are usually defined as semi-finished blanks consisting either of continuous or discontinuous (chopped) long fiber mat impregnated with a thermoplastic polymer. Final shaping of these blanks, cut to size, occurs mostly in hot flow (compression) molding for which the blanks are preheated.

MRT sheets were first presented in the 1967 by PPG Industries and Union Carbide under the trademark Azdel[®] as an alternative material to stamped metal for economical production of large parts [211, 212]. Short cycle time (20–60 s), as well as superior mechanical properties together with low weight, allowed MRT to occupy a niche of semi-structural elements in the automotive industry.

Physical and mechanical properties of composites are strongly affected by numerous factors: nature of the reinforcement and matrix, content and architecture

of the reinforcement, adhesion between reinforcement and matrix, etc. Reinforcement in the form of mat delivers MRT mechanical performance that place it between short fiber injection molded and advanced long fiber reinforced composites [213]. Although MRTs are available with various polymeric matrices: poly (butylene terephthalate), poly(ether imide), polycarbonate, PA-6, etc.—the most popular, due to a low price and widespread availability, is PP. Fibers of different nature could be used for MRT—GF, CF, NF, etc.

Traditional and still most popular reinforcement type for MRT is GF mat. The corresponding organosheets are called as GMT. GFs ensure MRTs with a tensile strength in the range of 68–108 MPa, and modulus in the range of 3.9–6.2 GPa. Such level of mechanical performance stipulates typical application of GMT in automotive for semi-structural parts, e.g. undercover, seat back frame, load floor, etc. Mat architectures determine mechanical performance of GMT. For instance, short chopped fibers provide better surface finish as well as filling of deep complex mold cavity, while continuous randomly oriented fiber mat gives high stiffness and impact strength [214]. First serial produced GMT part—front-end for Chevrolet Monza—dated back to 1975 [215]. Since that time GMT has been successfully implemented for decades, and today is commercially produced by a number of companies. The best known tradenames are: Azdel[®], Symalite[®], Isosport[®], Elastopreg[®] and others.

Recently, the focus of research has been shifted toward NFs as prospective reinforcements for ecologically friendly composites. Respective MRTs are named as natural mat thermoplastics (NMTs). Despite of certain advantages of NFs covering wide availability, low cost and density as well as ecofriendly image, the mechanical properties of NFs are generally lower than those with man-made reinforcements. Thus, NMT with hemp, jute or flax fibers exhibits almost half of the tensile strength of GMT. At the same time, the tensile modulus of hemp or flax fiber reinforced NMTs is comparable with that of GMT. Moreover, NFs have more than twice lower density than GF, therefore demonstrating better specific (relative to density) properties. The last fact enables application of NMTs in cars, but restrains it for non-structural parts enduring minimal loads. Possible applications of NMTs could be door panels, sun visors, spare-tire covers, seat foundations, instrumental panels, etc.) [216]. Commercially available NMT sheets are either melt impregnated or semi-finished needle punched mats.

Lack of the examples of carbon mat thermoplastics (CMT) could be explained by the infeasibility to fully implement the superior structural properties of CF in the form of mat. Nonetheless, CMT could be a prospective solution for the application of recycled CFs.

All-PP or “self-reinforced” PP (SR-PP) composites containing mat reinforcements have also been produced [217]. In these cases, the processing window was ensured by using random PP copolymers [218] or beta PP homopolymer matrices [217].

9.4.1 Manufacturing

Manufacturing of MRT sheets originally occurred earlier in two distinct phases: mat production and its impregnation to produce semi-finished blank. However, recently integral solutions combining these two processes have appeared. They are named as ‘direct’ processes which were already introduced in the previous section.

Sheets production techniques could be specified according to the mat placement’s approach—dry-laid or wet-laid (melt impregnation and slurry deposition method respectively) [219]. The *dry-laid* technique implies one step impregnation and lamination of the reinforcement mat in a double-belt press (DBP). The consolidated sheet has a thickness of 2–4 mm. They can be divided into two grades—*stampable* and *hot flowing* (Fig. 9.12). *Stampable* versions contain chemically bonded swirl mat composed of endless fiber rovings. Such mat structure restricts the deformability of the material during stamping. As a consequence, the molded part

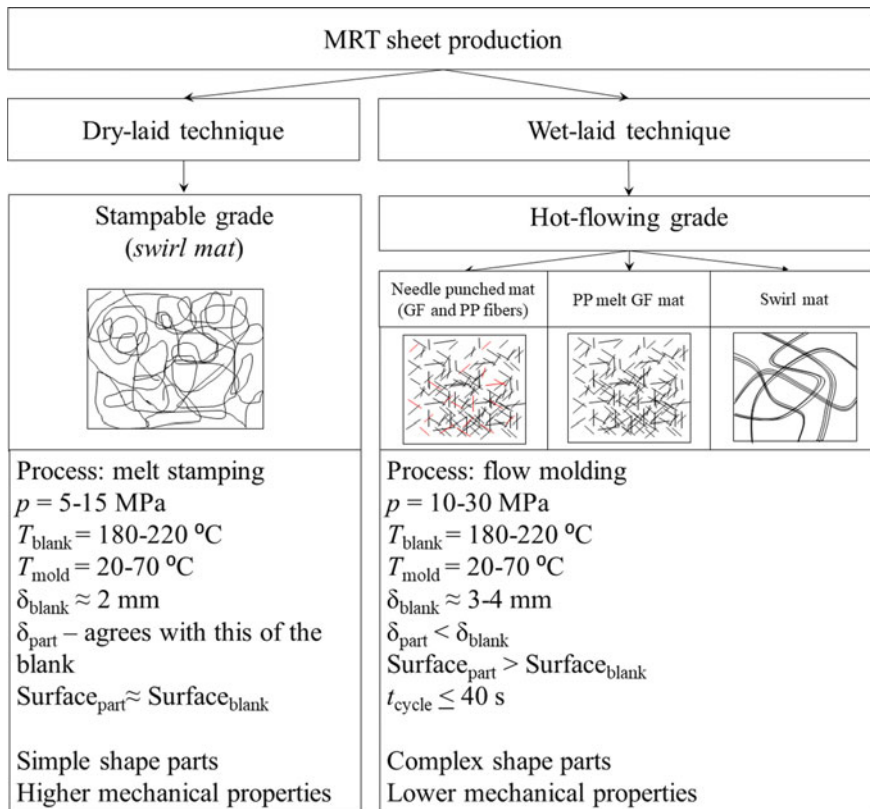


Fig. 9.12 Methods of the production of MRT sheets and its manufacturing technologies: p —pressure; T_{blank} , T_{mold} —temperature of the preheated blanks and the mold, respectively; δ_{blank} , δ_{part} —thickness of the blank and part; t_{cycle} —cycle time

surface area as well as thickness does not strongly differ from those of the blank. In other words, the complexity of the part's shape is limited. *Hot flowing* grade MRTs are formed by needling of discontinuous or continuous fibers. They exhibit good deformability when manufactured to the final parts. Eventually, complex parts containing ribs, thickness alteration and inserts could be molded. Although hot flowing grade MRTs provide lower mechanical performance than stampable ones, they dominate the market. This is due to the offered design freedom and high productivity (very short cycle times).

Wet-laid methods originated from papermaking industry. Among them the *slurry* and *foam deposition* techniques should be noted. Both techniques imply mixing of the PP powder or fiber with chopped reinforcing fibers, water and binder, depositing the corresponding blend on a moving conveyer belt and draining. These steps are followed by drying, heating, cooling, compacting and consolidation of the organosheets. In *slurry deposition* method the raw materials are dispersed in a very large quantity of water. In the resulting MRTs the reinforcing fibers are “fully” impregnated. By contrast, *foam deposition* method involves dispersing of aqueous foam, thus enabling to produce *partially consolidated* MRT. The term ‘*partially consolidated*’ means, essentially, that fibers are impregnated by the polymer only locally. So the resin acts as a binder, bundling the fibers together and forming 3D skeleton structure, that exhibits higher (comparatively to monolithic) specific flexural properties [220]. Partially consolidated GMTs are developed by Hanwha Azdel (SuperLite[®]), Quadrant (SymaLite[®]—product, consisting of GF and thermoplastic fibers) and Owens Corning.

9.4.2 Structure Development and Characterization

Conventional MRT part forming

The manufacturing process of MRT parts comprises blank cutting, its preheating to the melting temperature and compression molding. Preheating of the sheet could be implemented by IR radiation, hot air convection or contact thermal conductivity. Selection of the preheating depends mostly on the type of the reinforcement and mat production's method. For example, GMT as well as melt-impregnated NMT could generally be heated either by IR radiation or by air convection. However, the story is different for needle punched NMT, that needs longer heating time, and, as a consequence, should be heated by conduction [216].

Typical *hot stamping* process parameters, required to form a part with swirl mat MRT, are the following: pressure—5 to 15 MPa, blank temperature—180 to 220 °C, mold temperature—20 to 70 °C. The thickness and surface area of the resulting composite parts conforms those of the blanks [219]. In contrast, *hot-flowing grade* mat require higher pressure, usually 10–30 MPa. The final composite part has lower thickness comparatively to the blank, and higher surface area. The cycle time does not exceed 60 s.

MRT production line comprises the following units: tray for organosheets, preheating oven, feeding unit, press with the mold, removal robot and, optionally, postprocessing unit. Transfer between different line components can be implemented manually, but in most cases is carried out automatically by robots and conveyers.

Partially consolidated MRT

In conventional MRT sheets the reinforcement is well impregnated (though void content may reach several %), while partially consolidated MRT exhibit 3D framework structure. Partially consolidated MRTs are also referred as lightweight reinforced thermoplastics (LWRT) and produced with the areal density as low as 1200 g/m². In contrast, the areal density of traditional MRTs ranges between 2000 and 2500 g/m².

Due to springback effect stipulated by the fiber relaxation during the preheating of LWRT, the thickness of the composite part could be up to six times higher than that of the original organosheet. This issue provides three positive effects:

- Relative to the mechanical performance, higher thickness accompanied with lower density delivers the composite higher specific bending stiffness. This could be easily illustrated by the following expression (Eq. 9.9):

$$\bar{S} = \frac{S}{\rho} = \frac{E}{\rho} \cdot I = \frac{E}{\rho} \cdot \frac{bh^3}{12}, \quad (9.9)$$

where \bar{S} – specific bending stiffness, S – bending stiffness, ρ – density, E – flexural modulus, I – axial moment of inertia, b – part cross section width, h – part cross section height. Note, that expression is written for the rectangular cross section.

- With respect to the manufacturing process a lower pressure (less than 0.5 MPa) than for traditional MRT is required. The related technology is therefore essentially thermoforming, that—besides evident process simplification—permits integration of functional and decoration surfaces in one shot.
- The third benefit belongs to the acoustic performance of the resulting composite. As the increased “voided” thickness represents a greater pass along with multiple reflection and absorption possibilities for the sound, the partially consolidated MRTs exhibit excellent noise reduction. Thus, headliner manufactured from partially consolidated GMT demonstrates doubled sound absorption coefficient at frequencies higher than 2000 Hz than those from polyester or polyurethane reinforced with GF [221].

The mentioned issues make LWRT very attractive materials for automotive interior components, such as door trims, sunshades, headliners, trunk trims, parcel shelves, etc.

Direct Long Fiber Thermoplastics

As mentioned above, originally the manufacturing of the semi-finished thermoplastic sheets and the production of the final parts occurred separately. However, the breakthrough idea to combine these processes has appeared in 1990s, and

become a well-established integrated production technology soon. This technique traced back to GMT and is called as *direct long fiber thermoplastic*. The specific feature of D-LFT is incorporation and impregnation of the reinforcement fibers with the PP matrix directly during the compounding and plastification of the composites. For the first step—compound production—extrusion technology is used.

For the second step two variants are available: compression or injection molding. Accordingly, two types of D-LFT are distinguished: open machine process (compression molding cf. Fig. 9.13) and close machine process (injection molding). Each method has certain pros and cons. Thus, compression molding enables shorter cycle time, higher fiber length and consequently better mechanical properties, but at the same time formed parts have flashes and require post-processing. Whereas injection molding provides parts with an accurate contour and excellent surface quality, allows to integrate various inserts, but require longer cycle time and yields more sever fiber length degradation.

Despite definite increase of the capital costs, D-LFT provides certain benefits to the production, as well as to the structural performance of the composite parts. First of all, the discarded step of additional heating and plastification of the blanks, allows to diminish residual stresses in the composite part. Second, the manufacturer has more freedom in materials' formulation and adoption of the process to demands of the actual part. Third, long GFs (12–50 mm) provide outstanding mechanical properties to the composite. However, a drawback of D-LFT is the alignment of the fibers and resulting anisotropy generated by the flow processing [219].

The initial step of the D-LFT process includes melting and degassing of PP as well as its blending with cut fibers, introduced in form of rovings, by virtue of the extrusion process. Accordingly, the extruder acts as fiber cutter, at the same time cf. Fig. 9.13. It is imperative to maintain the length of the reinforcing fibers, as high as possible, in the molded part. Therefore, fiber-protection screw geometries, non-return valves, shut-off nozzles and runner systems as well as large screw

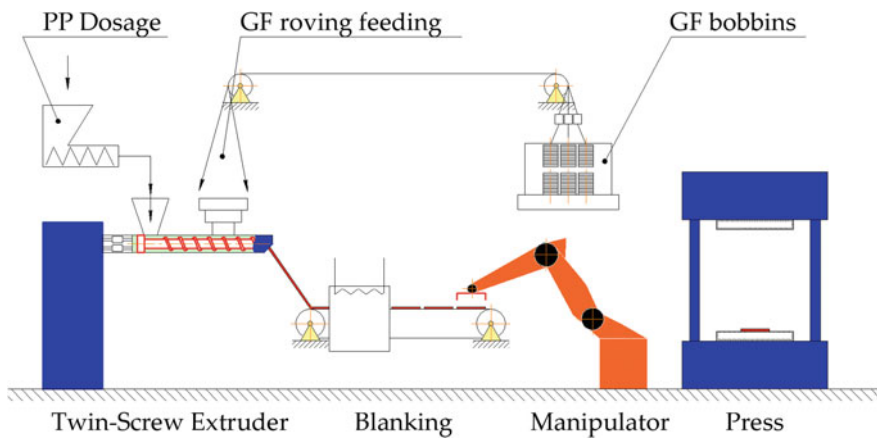


Fig. 9.13 LFT production method schematically

diameters are recommended [222]. Further, the extruded mixture goes through the slit die and applied to the conveyer belt. Next step is either pressing or injection molding.

Composite parts molded from long fiber (12–50 mm) D-LFT compounds show tensile strength and modulus values in the range of 100–125 MPa and 8.2–9.2 GPa, respectively. Their flexural strength, modulus and notched Charpy impact energy are lay in the ranges: 180–200 MPa, 8.2–9.0 GPa and 26–30 kJ/m², respectively. Such mechanical performance predestinates LFT compounds to apply them for semi-structural and structural automobile parts. Typical applications are body panels, seat pans, sound shields, front-end assemblies, structural body parts, truck panels and housings, doors, tailgates and fender sections. The commercially produces LFT PP compounds are Celstran[®] and Stamax[®].

D-LFT foam

Further development step in injection molded D-LFTs has been done in the direction of foaming. Adding of a blowing agent into the LFT compound during the plastification phase allows obtaining LFT foam with compact surface layers and porous structure in the core. D-LFT foam technology approach was introduced by Roch et al. [222, 223] from Fraunhofer ICT as an alternative to MuCell[®] process. The relative D-LFT foam technique utilized nitrogen as a blowing agent at a concentration of 3 wt%. Nitrogen was pre-compressed up to 350 bar and introduced as a supercritical fluid into the melt compound in twin-screw extruder via a gas injector. A ‘breathing mold’ technique was used to obtain integral foam sheets. GF-reinforced PP composites with and without foaming, yielding different thicknesses, were produced and their properties compared. Thus, 5.8 mm samples demonstrated 300% gain in flexural rigidity compared to the unfoamed reference with 3.6 mm thickness. The accompanied weight saving is amounted 35%. Another advantage, provided by foaming, was a diminishing in fiber alignment and in the related mechanical anisotropy. Further benefit of the incorporation of long GFs incorporation into foamed PP was some toughness improvement.

9.4.3 Properties and Their Prediction

9.4.3.1 Mechanical Response

As it was mentioned earlier the mechanical response of MRT are determined by the mat architecture and nature of the fibers. The static mechanical properties of MRT reinforced with NF, GF, and CF are presented in Table 9.1.

Mechanical properties of continuous fiber or swirl mat GMT (GMT-C) outperforms those of the discontinuous fiber GMT (GMT-D). As for tensile and flexural properties, the difference is less distinct, but for the fracture toughness (K_Q) it is essential [228]. The reason of it is explained by the internal structure provided by mat. Thus, swirl mat brings GMT-C mesh-like internal structure (Fig. 9.14a). Deformation and breakage of such structure occur locally, so that stress could be effectively redistributed and transferred on the other fibers in the network before

Table 9.1 Mechanical properties of PP based MRTs. Designations: SMC—Sheet Molding Compound

Reinforcement	Fiber mass fraction (wt%)	Density (kg/m ³)	Tensile		Flexural		Ref.
			σ (MPa)	E (GPa)	σ (MPa)	E (GPa)	
Neat PP	0	900	0.7–1.7	1.9–3.5	–	–	[213]
SR-PP	50	800-900	31–99	2.4–2.7	–	–	[217]
NMT							
Flax	40	1190	57	8.8	81	4.2	[213, 224]
Hemp	40	1190	52	6.9	–	–	[213]
Jute	40	1190	27	3.7	–	–	[213]
Bamboo		1010	30	3.6	–	–	[213]
GMT							
GMT20	20	1070	68.6	3.9	93	3.4	[225, 226]
GMT30	30	1110	78.4	4.4	98	3.9	
GMT40	40	1180	90–108	5.6–6.2	138–160	4.9–6.1	
UD45	45	1270	254	11.8	215	9.8	
CMT	25	1140	~ 175	~ 20	~ 240	~ 16	[227]
SMC	30–40	1700–2300	60–160	10–15	120–250	8–14	[225]
Steel	–	7800	450–650	190–210	–	200	–

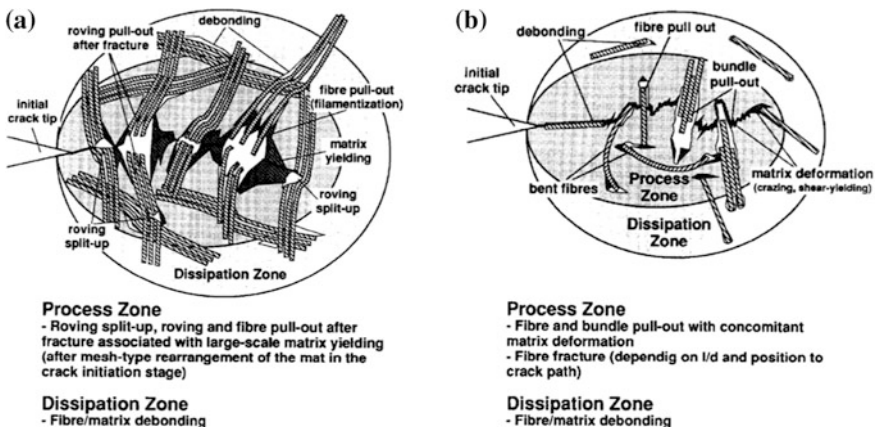


Fig. 9.14 Schematic representation of failure mode in **a** GMT-C and **b** GMT-D [228] ([211] reproduced with the permission of Springer Nature)

failure. This possibility is completely missing for GMT-D structure (Fig. 9.14b), where the failure is immediately stipulated either by ‘fiber-matrix’ debonding, fiber pull-out and fracture, or matrix deformation. As a result, GMT-C demonstrates larger than GMT-D damage zone, that in case of GMT-C, could reach up to 30 mm in diameter [228–231].

The recycling prospective of MRT depends on the fiber type. Thus, Bourmaud et al. [232] studied the degradation of flax-PP and glass-PP nonwoven composites. They found out, that after three compression moulding recycling cycles, the decrease in modulus is about 40% for flax reinforced PP, and only 4% for glass reinforced PP. At the same time both flax- and glass-PP demonstrated significant strength reduction (70 and 75%, respectively).

9.4.3.2 Rheological Behavior

Modern approaches to the process engineering involve wide use of simulation, that provides significant cost and time savings. Consequently, detailed knowledge of the rheological behavior of the material under molding conditions are essential for process modelling. A number of studies are dedicated to experimental investigations and mathematical modelling of GMT stamping rheology [233–238]. The squeeze flow technique is often chosen for rheological testing of GMT, due to its experimental simplicity, suitability for continuous fiber materials and its broad similarity to the pressing process [235].

Two flow models could be used to describe possible flow behavior in a biaxial flow geometry. The first one is ‘shear flow’ model that assumes zero velocity of the fluid at the plate surface. The second one is ‘biaxial extension’ model, where complete slip occurs at the plate surfaces. Both models are described by power-law constitutive equations, that take into account anisotropy and non-Newtonian flow effects (Eqs. 9.10 and 9.11) [239]:

$$\tau = A_s \dot{\gamma}^m, \quad (9.10)$$

$$\sigma = A_e \dot{\varepsilon}^m, \quad (9.11)$$

where τ and σ are shear and strain stresses respectively; A_s and A_e —shear and extensional power law constants; γ and ε —shear and strain rates respectively.

The shear and extensional viscosities (η_s and η_e) at particular strain rate could be given by Eqs. 9.12 and 9.13:

$$\eta_s = A_s \dot{\gamma}^{m-1}, \quad (9.12)$$

$$\eta_e = A_e \dot{\varepsilon}^{m-1}. \quad (9.13)$$

Kotsikov et al. [235] concluded, that squeezing flows of GMT cannot be modelled as pure shear flow without introducing large errors in the prediction of squeezing forces. In contrary, biaxial extension model provides good agreement with the experimental results.

Dweib and Brádaigh [237, 238] considered the constitutive equation for a transversally isotropic power-law fluid (Eq. 9.14):

$$\begin{bmatrix} \sigma_{xx} \\ \sigma_{yy} \\ \sigma_{zz} \end{bmatrix} = \begin{bmatrix} \eta_1 & 0 & 0 \\ 0 & \eta_2 & 0 \\ 0 & 0 & \eta_1 \end{bmatrix} \cdot \begin{bmatrix} \dot{\epsilon}_{xx} \\ \dot{\epsilon}_{yy} \\ \dot{\epsilon}_{zz} \end{bmatrix} - \begin{bmatrix} P \\ P \\ P \end{bmatrix}, \quad (9.14)$$

where σ_{xx} , σ_{yy} , σ_{zz} —normal components of the stress tensor in x , y and z directions; η_1 , η_2 —fluid viscosities; $\dot{\epsilon}_{xx}$, $\dot{\epsilon}_{yy}$, $\dot{\epsilon}_{zz}$ —strain rates in x ; y and z ; P —hydrostatic pressure.

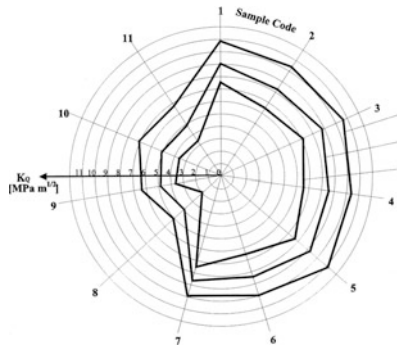
They modelled squeezing flow as a pure extensional flow and also as a combination of shearing and extensional flows. They determined, that the extensional viscosity at 180 °C and constant closing speed of 0.5 mm/s, in x and z directions lied in the range of 0.79–0.85 MPa·s, and in y direction it was slightly higher (0.9–1.2 MPa·s) [238].

9.4.3.3 Thermal Behavior

During the service life semi-structural automotive parts are generally subjected to fairly high mechanical and thermal loads. For instance, in hot climate the temperature of some components can rise up to 80 °C or beyond. So, it is very important to possess information about the behavior of MRT under a combination of thermal and mechanical loads. One of the main parameters that characterize the thermal behavior of composites under the mechanical load is HDT. For GMT the HDT ranges from 145 to 158 °C, while for NMT reinforced with flax—from 140 to 145 °C [219]. However, HDT data only hint for thermal operation limits because the real structures are subjected to loadings highly different from a clear flexure used in HDT determination.

The effect of temperature on the creep behavior of continuous fiber GMT was investigated by Dassapa et al. [240]. Short-term creep tests consisting of 30 min creep followed by 1 h recovery were conducted at five stress levels at the range of 20–60 MPa, and at 14 temperatures at the range of 25–90 °C. The researchers concluded that continuous fiber GMT should not be used at stresses over 60 MPa, particularly when the temperature exceeded 50 °C, due to significant increase of the creep rate.

Czigány et al. [241] studies temperature influence on the fracture behavior of GMT. Diagram in Fig. 9.15 demonstrates the fracture toughness of GMT-C (Index 1–7) and GMT-D (Index 8–11) at various temperatures: –40 °C, room temperature (RT), and +90 °C [241]. The values of fracture toughness of GMT-C was almost twice higher than those of GMT-D at all temperatures. Temperature rise influenced negatively the fracture toughness. The highest value of K_Q is observed at –40 °C, i.e. the temperature below T_g . At RT impact strength of both, GMT-C and GMT-D reduced by almost 20%, at +90 °C by 30–40% (Fig. 9.15).



Sample no.	Fracture toughness (K_{Ic}) (MPa $m^{1/2}$)		
	$T = -40^{\circ}C$	$T = RT$	$T = +90^{\circ}C$
1	10.78±0.32	8.99±0.89	7.46±0.54
2	10.41±0.17	8.20±0.33	6.43±0.11
3	10.69±0.71	8.82±0.51	7.13±0.47
4	10.45±0.28	8.60±0.08	6.56±0.05
5	11.02±0.19	9.28±0.39	7.81±0.28
6	10.01±0.71	8.47±0.32	6.56±0.50
7	10.10±0.13	8.71±0.47	7.65±0.42
8	5.07±0.36	3.99±0.21	2.04±0.16
9	6.34±0.20	4.83±0.19	3.53±0.25
10	7.05±0.27	5.06±0.28	3.61±0.42
11	6.72±0.43	4.94±0.17	3.42±0.14

Fig. 9.15 Fracture toughness of swirl mat (Index 1-7) and long fiber (Index 8-11) GMT at different temperatures ([241] reproduced with the permission of Elsevier)

9.4.3.4 Other Properties

As it was mentioned above, the fatigue behavior differs for GMT-C and GMT-D. Thus, the fatigue endurance limit of GMT-C after 10^6 fatigue cycles can be given by 25–30% of the static tensile strength [229]. This issue limits swirl mat thermoplastics application mostly for impact resistant parts, while GMT-Ds are more suitable for long-term loading conditions.

9.4.4 Applications

Some examples of GMT parts application are presented in Table 9.2.

Table 9.2 Examples of MRT composites application

Year	Part	Ref.
1975	Front-end/retainer for Chevrolet Monza	[215]
1977	Front support frame for Pontiac Firebird, Chevrolet Camaro	
1978	Seat pan for Chevrolet Corvette	
1992	Technical front-end VW Golf III	
1993	Battery tray for Suzuki Wagon R	[242]
1997	Hatchback door DC W 168	[215]
1997	Fuel tank cover for Toyota Harrier Hybrid	[242]
2002	Front seat structure for Bentley Continental	
2003	Hatchback door Nissan Murano	[215]
2004	Lightweight underbody systems of the BMW series: E 60/61, E 63/64, E 8x and E 9x	
2009	Battery tray for Mitsubishi i-MiEV	[242]
2014	Front-end for Mercedes S-Class Coupé	

9.5 Fabric-Reinforced Composites

Reinforcement in the form of fabric provides composite with higher strength and stiffness compared to short and long fiber reinforced versions. This is mostly due to different mechanisms of carrying load in the corresponding composite structures. The main structural element in fabric is yarn, that particularly overtakes the mechanical load applied to the structure. Distribution of the load in a textile is carried out by friction forces between fibers, that results in higher critical length of the fibers, and consequently—higher strength of the material. The other aspect is that the fiber content in fabric-reinforced composites is in the range of 45–55 vol%, which is higher than those in discontinuous fiber-reinforced grades (20–35 vol%). This is associated with better mechanical performance *per se*. Another distinct feature of fabric reinforced composites is a certain anisotropy of their properties. This fact allows to create customized structures with tailored properties in the required directions.

Better mechanical properties and possibility of creation structures with tailored properties, provided by the fabric, together with good formability through the thermoplastic matrix, enable the applications of fabric reinforced polypropylene (FR-PP) in structural automotive parts. Fabrics with various weaving styles are currently available. The most popular fabrics are schematically presented at Fig. 9.16.

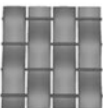
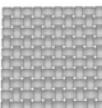
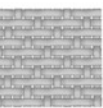
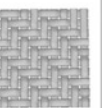
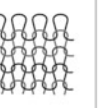
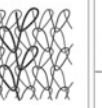
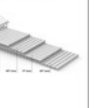
Fabrics						
1D	2D					3D
Unidirectional  Low drapeability/ no crimp • Predominant stress and stiffness in one direction • Good handling characteristics	Plain weave  Low drapeability/ high crimp	Satin weave  Good drapeability/ low crimp	Twill weave  Average drapeability/ average crimp	Wet-knitted  Excellent drapeability/ moderate crimp	Warp-knitted  Excellent drapeability/ moderate crimp	Multiaxial  Average drapeability/ no crimp • Strength and stiffness in three directions • Time saving, cost-effective technology
		• Strength and stiffness in two directions • Very good handling characteristics • Possibility to 'hybridize' fabric, by mixing fibers of various nature				

Fig. 9.16 Typical fabrics used as reinforcements in composites

However, despite of certain advantages of FR-PP, their production is associated with definite challenges. The FR-PP manufacturing could be basically divided into two stages: impregnation and consolidation. Consolidation does not expose serious problems, but impregnation of the fabric with the molten PP is not an easy task due to a high viscosity of the PP melt (200–2000 Pas [243]). Traditionally,

the impregnation and consolidation processes are separated. The impregnated product is semi-finished sheet or prepreg (also called as “organosheet”), while the result of the consolidation stage is the composite part. “Direct” processing routes, implying in line fabrication of both semi-finished material and composite parts have appeared two decades ago, and now they represent established manufacturing techniques (Fig. 9.17) [244]. The processing techniques of semi-finished FR-PP sheets production, and composite parts’ forming will be discussed in Sect. 9.6.1.

By compression molding of PP fabrics themselves—called hot compaction method—all-PP composites having identical polymer components can be produced. Hot compaction means that a thin skin of high tenacity polymer fibers or tapes melts and upon cooling this melted material recrystallizes to form the matrix of a self-reinforced composite [245–247]. This composites is commercialized under the name of CURV[®].

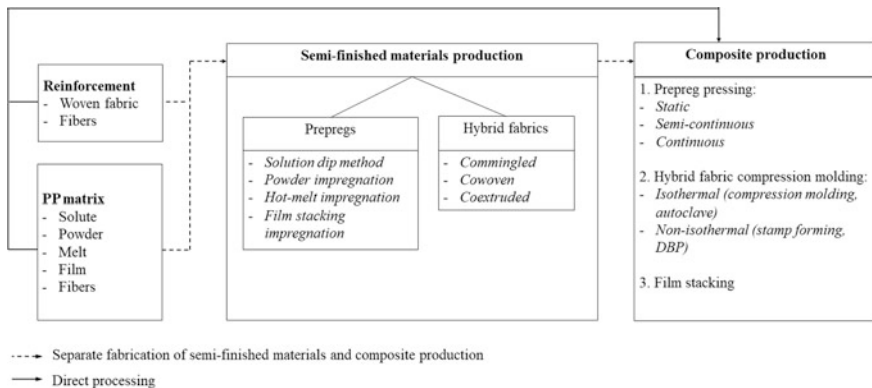


Fig. 9.17 Principal scheme of the production of FR-PP in sequential and direct ways, respectively

9.5.1 Manufacturing

The manufacturing techniques of semi-finished materials could be classified based on the matrix state during combining the fabric with the matrix (Fig. 9.17). Thus, impregnation with the solute PP matches to solution dip method [248, 249], powder—to powder impregnation [250, 251], film—to film stacking [252], melt—to hot-melt impregnation [253, 254]. Combining the reinforcement with PP in the form of fibers termed to as hybrid fabric (commingled and co-woven) technology. Each of these compounding techniques are reviewed below.

Solution dipping

Solution dip impregnation method is probably the earliest thermoplastic prepreg fabrication technique [248, 249]. Its another name is “solvent impregnation”, that illustrates the necessity to use a solvent in order to reduce the viscosity of PP, and therefore facilitate the impregnation. The solution dip method generally assumes two manufacturing steps. The first one is conveyance of the reinforcement textile through the bath with the solute PP. Then, the impregnated fabric goes through a heating chamber, where the solvent is completely evaporated to prevent void formation (Fig. 9.18). The solvent removal is usually the most problematic issue of this technique, because the amount of the diluent required to decrease the high-molecular weight polymer viscosity to an acceptable threshold could reach 85 vol% and more. Beyond that, the semi-crystalline PP can only be dissolved at rather high temperature (>180 °C) due to its excellent resistance to common solvents. Hence, these issues limit the application of solvent impregnation prominently.

Powder impregnation

The aim of the processing by the powder impregnation technique is to bring matrix and fibers to the intimate contact in order to minimize the flowing distance during consolidation [255]. The matrix material should be ground so, that the particles diameter is comparable with that of the fiber diameter. The powder is scattered over the textile, and stick to the fibers via electrostatic attraction. The powder-coated material is then consolidated in a DBP (Fig. 9.18) or interval press to semi-finished products.

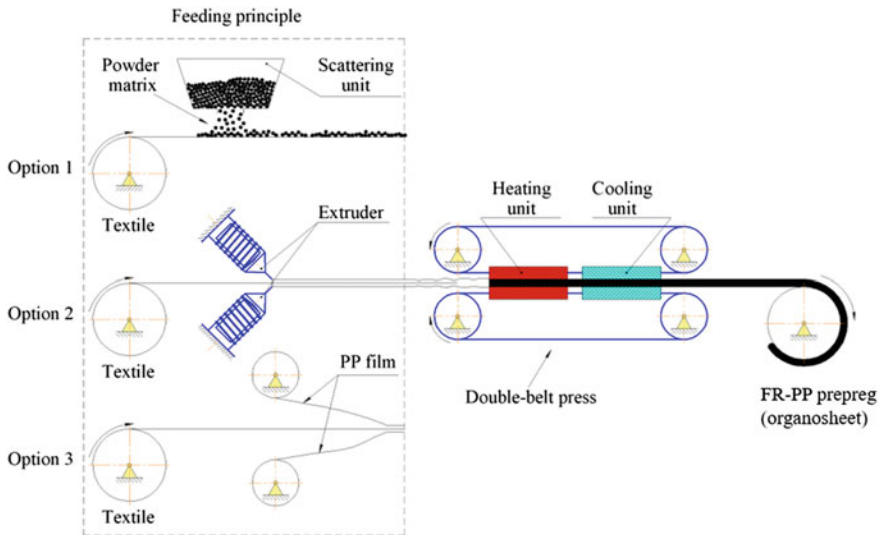


Fig. 9.18 Schematic representations of the continuous powder, hot melt and film stacking impregnation processes using a DBP

The consolidation behavior of FR-PP during powder impregnation process was described by Connor et al. [255]. The proposed model assumes that melt particles form drops, and each drop generates a “bridge” between the adjacent fibers. During the impregnation process every single resin ‘bridge’ spreads along the fibers due to the applied pressure and capillary forces. The bridges distribution pushes out the air from the composite and reduce the inter-fiber spacing.

Powder impregnation technique was first implemented by Price [250, 256] in 1970s for glass roving. However, fabric impregnation is also possible with this process [244], but not really feasible due to economic reasons (substantial loss of powder during handling).

Hot melt and film stacking impregnation

Hot melt impregnation [253] and film stacking are very similar processes which imply either direct extrusion of the matrix material in the molten state onto the textile material or feeding of the matrix in film form on both surfaces of the fabric (cf. Fig. 9.18). Both methods require DBP, that apply constant pressure and heat simultaneously. In case of film-stacking method DBP provides heat and pressure necessary for impregnation, while in case of hot melt process it additionally supports the distribute of the PP melt through/in the fabric [257].

Hot melt impregnation could be considered as a liquid flow through porous media and this process could be mathematically described by Darcy law (Eq. 9.15):

$$\vec{V} = -\frac{\vec{K}}{\mu} \nabla p, \quad (9.15)$$

where \vec{V} —velocity vector; \vec{K} —preform permeability vector; μ —dynamic viscosity of the resin; ∇p —pressure gradient.

The pressure gradient consists of two contributions: (i) mechanical pressure applied to the fluid, and (ii) capillary forces acting between the molten matrix and the reinforcing fibers. The permeability is clearly a key parameter in impregnation modelling and it strongly depends on the fibers architecture. This parameter could be defined either analytically or experimentally [258]. Although experimental techniques are well established, they normally require a large set of carefully controlled tests that are usually rather time-consuming. Analytical approaches are also widely used, but as all predictive techniques, they involve definite assumptions which generally impair the accuracy of the methods. A popular model to predict the permeability is the Kozeny-Carman equation (Eq. 9.16) [259]:

$$K = \frac{r^2}{4k} \cdot \frac{\epsilon^3}{(1 - \epsilon)^2}, \quad (9.16)$$

where r —is the radius of the particles; ϵ —is the porosity; k —is the Kozeny constant.

The Kozeny-Carman equation is based on a capillary model and thus it is inherently a one-dimensional model that works well only for isotropic medium. Gutowsky et al. [260] expanded the application of the Kozeny-Carman equation to describe the permeability of anisotropic preforms. However, Kozeny-Carman and Gutowsky approaches are restricted to a simplified geometry and applicable only for UD fiber architecture (i.e. not working for woven and stitched preforms). Computer modelling approaches help us, however, to investigate complex preform geometries, define pressure and velocity fields, and to calculate the permeability vectors accordingly [258].

Hybrid yarns, fabrics

Hybrid fabrics containing both the matrix and reinforcement fibers, can be principally divided into two groups: commingled and co-woven fabrics. Commingled fabric consists of hybrid yarns in which the matrix and reinforcement are “blended” intimately at the level of the filaments (Fig. 9.19a). Co-woven fabric includes separate PP and reinforcing yarns (GF, CF, NF, etc.) (Fig. 9.19b). The positive effect of such hybridization lies in diminishing of the distance that resin must flow to achieve impregnation [255].

Hybrid yarns can be manufactured by means of various techniques: commingling in an air jet [262], on-line commingling, that utilizes air texturing instead of air jet texturing [263, 264], co-wrapping, core-spinning [262] and stretch-breaking [262]. The last option—stretch-broken commingled fibers—is a prospective opportunity for recycled CF [265]. Hybrid yarns could be later processed to the fabrics using standard weaving techniques.

Both, commingled and co-woven hybrid fabrics are used as drapable preforms and transformed into the shaped final composite parts through the consolidation process applying heat and pressure [266]. A mathematical model of the commingled fabric consolidation was developed by van West et al. [267]. This model utilizes the Darcy’s law to describe the radial flow of the resin across the fiber bundle by considering that the permeability changes with the V_f during the consolidation process.

‘Hybrid’ yarn can also be prepared by coextrusion when PP homopolymer is coated with PP copolymer having lower melting temperature followed by intensive stretching. The woven fabric from the coextruded yarn is the preform of the all-PP composites [268, 269]. This composites is commercialized under the name of PURE[®].

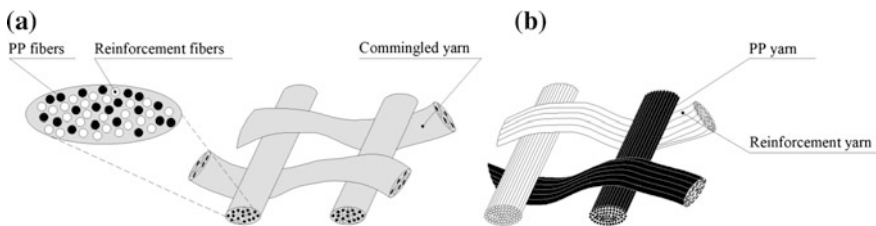


Fig. 9.19 Commingled (a) and co-woven (b) hybrid textile structures [261]

9.5.2 Structure Development and Characterization

Manufacturing techniques for composite parts production from FR-PP could be divided into three groups, namely *prepreg pressing*, *hybrid fabric pressing* and *film stacking*. As mentioned previously, for mass production ‘direct’ processing routes, i.e. in-line production of both the semi-finished impregnated material and composite part, are also feasible.

Prepreg pressing

Pressing of the FR-PP organosheets does not principally differ from that of stampable grade MRT described in Sect. 9.4. The process includes the same manufacturing steps: prepreg preheating, transferring to the mold, pressing and demolding of the part. The distinct feature of FR-PP prepregs is their zero flowability. Therefore, the shaping is restricted by the fabric structure. The usual processing temperature for FR-PP lays in the range of 160–220 °C, pressure—in the range of 5–10 MPa, and processing time—less than 5 min. FR-PP organosheets are produced under the tradenames: Tepex[®], GMTex[®] and others.

Sandwich panels consisting of FR-PP skins and either foam or honeycomb PP core can be also produced by hot pressing. A comprehensive overview in this field is given in Ref. [270]. Sandwich panels with GF FR-PP and PP honeycomb are commercially produced under the tradename MonoPan[®].

Hybrid fabric pressing

As mentioned previously, the main target of the hybridization of the reinforcement fabric with PP is to diminish the matrix flow distance. This distance in a typical commingled material amounts to 20–40 μm [262]. Another advantage of hybrid fabrics over impregnated prepreg sheets resides in better drapability that allows the preform to conform easily to a complex mold surface [266].

To form a composite part from hybrid fabrics it is necessary to melt the matrix fibers, impregnate the reinforcement and consolidate the material. The distinct feature of the described process is that impregnation and consolidation occur in one-shot. Forming techniques for hybrid fabrics could be principally divided into two groups: isothermal and non-isothermal [271]. During the isothermal process the mold and material are thermo-cycled together above the melting temperature of PP [272–274]. Consequently, manufacturing techniques associated with the isothermal consolidation process are compression molding and autoclave forming. These techniques provide perfect consolidation state and excellent performance, but strongly limit the production rate. In contrast, non-isothermal consolidation occurs when the fabric is preheated above the PP melting temperature in an external heating unit and then transferred into the mold maintained at a temperature below the “solidification” of PP [261, 271, 275]. Preheating could be implemented by hot air, IR or contact heating. Nevertheless, non-isothermal technique requires very fast transfer of the preform to the mold in order to avoid significant heat loss. For example, the temperature of four-layer stack of woven GF/PP preform drops from 220 °C to T_m (160–170 °C) within only 20 s [262]. Manufacturing technique utilizing non-isothermal processes for commingled and co-woven fabrics is stamp

forming. A typical stamp forming processing cycle consists of material heating above the melting temperature of PP, applying pressure, and further cooling below the solidification (between the crystallization and glass transition temperature) while maintaining pressure [267]. The pressure necessary to consolidate hybrid fabric is generally lower than that of GMT, as there is no need for fabric structure to move with the flowing matrix in order to fill the mold.

Properties of a composite part produced of commingled or co-woven fabric strongly depend on the processing parameters, such as melting temperature, mold temperature, pressure and holding time. Additionally, impregnation and consolidation time of the hybrid fabrics are dependent on the fabric structure, yarn dimensions and shape, number of fibers per yarn, fiber diameter, and quality of commingling. A number of works were dedicated to the determination of the optimal (from mechanical performance point of view) parameters for both, isothermal and non-isothermal forming. Some results of the research activity in this field are presented in Table 9.3.

Average process parameters for isothermal process are the following: mold temperature—190 to 205 °C, average holding time—5 to 8 min, pressure—0.4 to 4.5 MPa. By contrast, non-isothermal consolidation process exhibit lower holding time (less than 60 s) and lower mold temperature 60–100 °C, while the pressure level is nearly the same (2.3–4.0 MPa).

Commingled fabrics are produced under the tradename Twintex[®], ThermoPly[®], and others.

Film stacking technique

Film stacking manufacturing process is suitable for the laboratory scale production [252, 279]. This technique utilizes a hot press and allows to produce either organosheets or laminates with the sizes limited by the sizes of the mold.

Various processing parameters for film stacking technique are mentioned in the literature. Thus, Kim and Lee [252, 279] produced PP prepregs reinforced with the woven CF fabric and defined the following processing parameters: mold temperature—230 °C, slowly increased pressure—up to 28 MPa, time to pressure rise—10 min. Russo et al. [280] produced laminates from 8 layers of plain weave type glass fabric (204 g/m²) and 2 types PP films (35–40 μm), produced of PPs with difference flow grades—70 g/10 min and 12 g/10 min. For the first one the following processing parameters were used: temperature—190 °C, pressure—2.5 MPa, holding time—45 min. The second one required slightly higher values of temperature and pressure (210 °C and 4 MPa respectively) and same processing time—45 min. Scarponi et al. [281] manufactured hemp FR-PP laminates with the following parameters: temperature—200 °C, pressure—5 MPa, holding time—10 min. Okumura et al. [282] produces CF FR-PP laminate with the following processing parameters: temperature—180 °C, pressure—14.6 MPa, holding time—20 min.

Film-stacking method is widely used for production of self-reinforced PP composites [283, 284]. In this case the matrix (viscosity, type) and the reinforcement (fabric type, content) can be combined in a wide range in order to ensure the necessary processing window and to tailor the properties of the resulting composites.

Table 9.3 Optimal processing parameters for composite manufacturing from commingled fabrics

Process	Fabric parameters	Laminate parameters	Optimal processing parameters				Ref.
			T_0 (°C)	T_{mold} (°C)	t (min)	p (MPa)	
Isothermal	GF/PP warp-knitted fabric 450 g/m ² $v_{GF} = 60$ wt%	12 layers Flat laminate	–	205	8	4.5	[273]
	GF/PP twill $v_{GF} = 60$ wt%	Flat laminate	–	200	5	0.7	[274]
	GF/PP Tubular weft-knits	10 layers	–	200	5	4.0	[276]
	GF/PP twill 745 g/m ² $v_{GF} = 60$ wt%	4 layers	–	200	4	0.4	[277]
	Flax/PP UD fabric (flax—warp, PP—weft)	–	–	190	20	0.5	[278]
Non-isothermal	GF/PP twill 650 g/m ² $v_{GF} = 60$ wt%	8 layers [8 (0/90)] _T Flat laminate	220	60	0.75	2.3	[261]
	GF/PP twill 1485 g/m ² 743 g/m ² $v_{GF} = 60$ wt%	3 layers of 1485 g/m ² and 6 layers of 743 g/m ² Flat laminate	190	100	1	4.0	[275]

9.5.3 Properties and Their Prediction

9.5.3.1 Mechanical Response

FR-PP exhibits higher level of static and dynamic mechanical properties than MRT. Thus, the tensile strength, tensile modulus, flexural strength and flexural modulus of Twintex[®] with 60 wt% of GF are in the range of 300–400 MPa (ISO 527), 14–20 GPa (ISO 527), 280–380 MPa (ISO 14125) and 13–18 GPa (ISO 14125), respectively [285]. The impact strength of Twintex[®] amounts 160–200 kJ/m² (ISO 180). FR-PPs exhibit significant strain rate dependent deformation behavior [286, 287]. Thus, tensile and compression modulus and strength increases with the increasing strain rate, while shear modulus and strength tends to decrease [286]. Compared to GF/PP, woven fabric reinforced all-PP composites demonstrates

lower tensile properties (strength in the range of 55–85 MPa, and Young's modulus in the range 1.7–2.3 GPa [284]) but significantly higher impact strength—250 to 550 kJ/m² [283].

The interfacial strength plays a significant role in the mechanical behavior of FR-PP, as it is responsible for the efficient load transfer. The specific feature of the PP matrix, which influences the adhesion, is its non-polar nature. Due to this reason PP does not adhere well to most of the fibers. In order to improve the interfacial adhesion between PP matrix and reinforcement two basic strategies have been developed. The first one implies fiber surface modifications with coupling agents, plasma treatment, wet oxidation, whiskerization, etc. The purpose of the surface treatment is to increase the surface energy, induce chemically active functional groups or increase the surface roughness of the fiber to enhance the physical bonding with the matrix. The most commonly used and industrially adopted method for GF modification is treatment with the silanes bearing alkoxy silane groups. After hydrolysis, the silanol groups formed react with the hydroxyl groups on the GF surface [288]. Silanes are not effective for untreated CFs as they do not contain –OH group. Nevertheless, hydroxyl groups can be generated on the CF surface by plasma, wet chemical or electrochemical oxidation treatments. As for the NFs, they are also incompatible with PP matrix due to a polar nature of cellulose. One possible treatment for NFs are silanization [289]. The interested reader could find more information on NF modification in Ref. [165].

The second strategy introduces polar functional groups into the PP. The polar groups in PP chains are generated by reactions with species that contain specific functional groups in their structures, such as ester, carboxylic acid or anhydride groups [290]. The most popular interfacial compatibilizers are: PP-g-MA, PP grafted with maleic acid (PP-g-MAA), and styrene butadiene styrene block copolymer grafted with maleic anhydride, etc. However, combination of both strategies is also commonly used to improve the adhesion between fibers and PP matrix.

Some fiber treatments reduce the strength of the individual fibers, but the increased 'fiber-matrix' adhesion leads to a higher interfacial strength and higher mechanical response of the whole composite. Thus, Han et al. [288] investigated the influence of plasma treatment followed by silane application on CFs. They demonstrated, that albeit 1 min plasma treatment together with the silane treatment decreased the filament strength from 3.68 to 3.23 GPa, the interlaminar shear strength (ILSS) showed 48.7% growth.

Okumura et al. [282] investigated the effects of removal of sizing and PP-g-MAA content on the mechanical properties of carbon FR-PP. They reported, that the flexural strength of the samples, containing 1 wt% of PP-g-MAA, reached the value of 453 MPa at about 50 vol% of CF content, that is more than twice higher than for the untreated sample. Removal of the sizing agent increased the flexural strength even more.

Russo et al. [291] studied the effect of the PP-g-MA compatibilizer on the mechanical behavior of plain weave glass FR-PP. Thus, PP-g-MA increased the flexural strength of the composite from 97.9 to 183.0 MPa, and the flexural

modulus from 15.3 up to 17.1 GPa. However, improved adhesion deteriorated the falling weight impact resistance.

Alcock et al. prepared woven fabric reinforced all-PP composites from coextruded tapes (reinforcement content ca. 90%). They concluded that the developed composite's tensile properties outperformed the GMT-PP and remain slightly below the woven glass fiber reinforced PPs [268]. All-PP composites possess excellent falling weight resistance [292], which can be tailored by the consolidation quality of the composite (depends mainly on consolidation temperature and pressure) [284].

9.5.3.2 Rheological Behavior

The rheological behavior of FR-PP is defined by its both constituents—thermoplastic matrix and textile. The predominant flow mechanisms in FR-PP governed by the matrix are resin percolation and transverse squeeze flow (Fig. 9.20). On the other hand, the formability, shaping of FR-PP is controlled by the fabric. The main deformation modes determined by the textile are bending, fiber straightening, yarn buckling, as well as intra- and inter-ply shear (in-plane and out-of-plane shear correspondingly) [293, 294]. Bending mode is characterized by relatively small deformations, and consequently is associated with single curved shapes. At the same time in-plane shear enables higher deformations and is representative to double curved shapes. In fact, in-plane shear behavior is a key deformation mode of textile reinforced composites utilizing GFs and CFs fibers [295]. At the same time, for all-PP composites deformation modes connecting with the fibers plays much more important role [296].

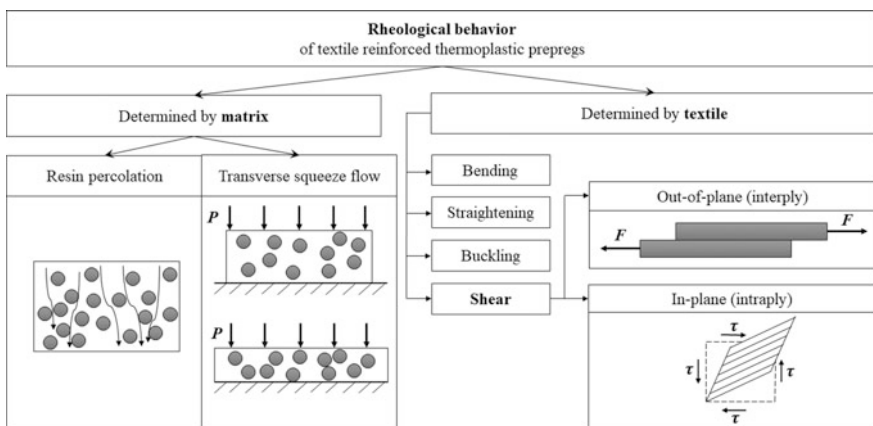


Fig. 9.20 Forming mechanisms of thermoplastic textile reinforced prepregs determined by their constituents (based on Ref. [300])

The rheology of textile composites could be characterized experimentally, by using picture frame and bias extension tests [297–299]. On the other hand, prospective prediction methods have been developed, as well [300].

Numerous works were dedicated to the prediction of the forming behavior of a textile. Four prediction methods are mentioned in literature, namely: kinematic, continuous, semi-discrete and mesoscopic. All the described approaches are based on the different assumptions and have their certain pros and cons [293]. Thus, kinematic approach (also called as fishnet or geometrical mapping algorithm [301]), assumes that yarns are inextensible, warp and weft yarns can freely rotate at the intersections points while slide is prohibited. Modell, based on kinematic approach, is also called as a ‘trellis model’, and consists of a mapping of the fabric geometry from an initial to a final surface with an in-plane shearing as the only deformation mechanism [302]. Major benefit of the fishnet algorithms is that they deliver results very fast, but disregarding mesh deformation possibilities except of shearing. As a consequence, kinematic approach is primary used at the initial design stage. *Continuous* method treats the textile as a continuous medium during forming, moreover the inherent anisotropy can be taken into account. Standard FEs (shell, membrane, 3D) could be used to simulate textile forming with the continuous approach [293, 303]. However, this method does not fully characterize the mechanical behavior of the textile. Semi-discrete approach assumes the textile as a set of woven cells, where one-unit cell is submitted to the loads of its neighboring yarn. Mesoscopic or meso-scale approach is the most accurate one, as it considers the textile as a set of yarns connecting to each other, where each fiber bundle is modelled. The principal difference of the mesoscopic method from the listed above approaches are accounting of the contact of the yarns with friction and possible slipping between them.

Nevertheless, none of the described above predictive methods includes the influence of the viscous matrix, and consequently cannot take into account the influence of processing conditions (i.e. temperature, rate of loading, contact forces, interplay friction, etc.), that appear during thermoforming (Fig. 9.21). Below, we will describe modelling approaches that take into consideration both, matrix and fabric behavior.

Rheological models for the forming behavior of composite materials with one or two families of reinforcing fibers were first presented by Rogers [305]. Rogers’ models are based on the set of material models known as ideal fiber reinforced materials [306, 307]. The specific feature of these models is a kinematic constraint of fibers inextensibility accompanied with the assumption of the material incompressibility and a suitable anisotropic constitutive relationship. Fibers are considered as linear elastic, whereas the matrix—linear viscoelastic material. The relevant constitutive equation for viscoelastic matrix was a simple generalization of the elastic equation, in which algebraic designation of moduli and strains were replaced by relaxation moduli and strain rates.

Johnson [302] extended Rogers’ work and proposed a rheological model for textile reinforced thermoplastic prepregs, which takes into account fabric

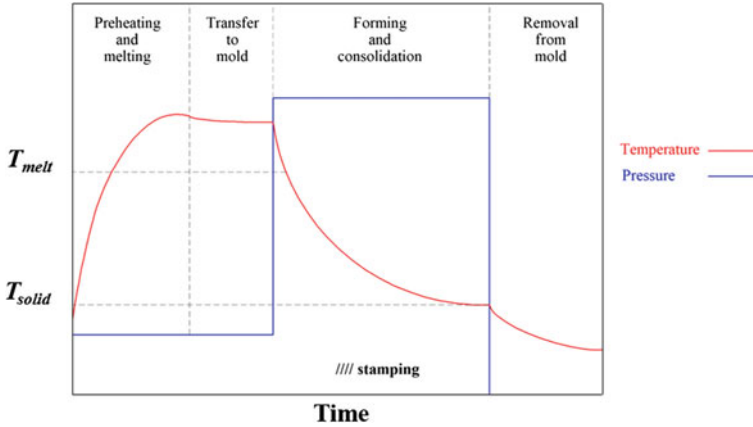


Fig. 9.21 Principle stages of pressure and temperature in the processing of thermoplastic prepregs (based on Ref. [304])

deformation together with the resin viscosity (so called “biphase model”). Johnson’s model assumes textile reinforced thermoplastic sheet to be a continuum with continuously distributed fibers. Each ply comprises an incompressible anisotropic Newtonian viscous fluid and two families of high stiffness inextensible fibers (Eq. 9.17) [300]:

$$\begin{pmatrix} \sigma_{11} \\ \sigma_{22} \\ \sigma_{12} \end{pmatrix} = \underbrace{\begin{pmatrix} 4\eta_1 & 2\eta_1 & 0 \\ 2\eta_1 & 4\eta_1 & 0 \\ 0 & 0 & 2\eta_1 \end{pmatrix} \begin{pmatrix} d_{11} \\ d_{22} \\ d_{12} \end{pmatrix}}_{\text{Viscous part}} + \underbrace{E_1 \begin{pmatrix} \varepsilon_{11} \\ 0 \\ 0 \end{pmatrix} + E_2 \begin{pmatrix} c^4 & c^2s^2 & c^3s \\ c^2s^2 & s & cs^3 \\ c^3s & cs^3 & c^2s^2 \end{pmatrix} \begin{pmatrix} \varepsilon_{11} \\ \varepsilon_{22} \\ \varepsilon_{12} \end{pmatrix}}_{\text{Elastic part}}, \tag{9.17}$$

where σ_{ij} —element stress components, η_1 —viscosity, d_{ij} —the velocity gradient, E_1, E_2 —elasticity modulus, $c = \cos \phi, s = \sin \phi, \varepsilon_{ij}$ —strain components.

The basic assumptions and appropriate equations of the Johnson’s model are listed below:

- (a) *Incompressibility condition* express mathematically, that fluid volumes are preserved (Eq. 9.18):

$$\text{tr}(\mathbf{d}) = 0, \tag{9.18}$$

where tr—trace of a tensor, \mathbf{d} —Eulerian rate of strain tensor.

- (b) *Inextensibility condition* expresses that the strain rate components in the fiber direction are equal to zero (Eqs. 9.19 and 9.20):

$$\text{tr}(\mathbf{A}\mathbf{d}) = \text{tr}(\mathbf{B}\mathbf{d}) = 0, \quad (9.19)$$

$$\mathbf{A} = \mathbf{a} \cdot \mathbf{a}; \mathbf{B} = \mathbf{b} \cdot \mathbf{b}, \quad (9.20)$$

where \mathbf{a} , \mathbf{b} —unit vectors, that denote fiber orientation.

- (c) *Fibers rotation with the fluid* elements during deformation, which leads to Eqs. 9.21 and 9.22 for the orientation vectors:

$$\frac{D\mathbf{a}}{Dt} = \mathbf{a} \cdot \nabla \mathbf{v}, \quad (9.21)$$

$$\frac{D\mathbf{b}}{Dt} = \mathbf{b} \cdot \nabla \mathbf{v}, \quad (9.22)$$

where $\frac{D}{Dt}$ is time derivative defined as (Eq. 9.23):

$$\frac{Dg}{Dt} = \frac{\partial g}{\partial t} + \mathbf{v} \cdot \nabla g, \quad (9.23)$$

where \mathbf{v} —velocity vector.

- (d) *Constitutive equation* for a Newtonian viscous fluid with two families of inextensible fibers (Eqs. 9.24 and 9.25):

$$\boldsymbol{\sigma} = -p\mathbf{I} + S_a\mathbf{A} + S_b\mathbf{B} + 2\eta_1\mathbf{d} + 2\eta_2(\mathbf{A}\mathbf{d} + \mathbf{d}\mathbf{A} + \mathbf{B}\mathbf{d} + \mathbf{d}\mathbf{B}) + 2\eta_3(\mathbf{C}\mathbf{d} + \mathbf{d}\mathbf{C}), \quad (9.24)$$

$$\mathbf{C} = \frac{1}{2}(\mathbf{a}\mathbf{b} + \mathbf{b}\mathbf{a})(\mathbf{a} \cdot \mathbf{b}), \quad (9.25)$$

where $-p\mathbf{I}$ —arbitrary hydrostatic pressure term [305], S_a, S_b —fiber tension stresses, which are the reaction to the inextensibility constraints in the fiber directions, η_1, η_2 —in-plane viscosities related to shear along and transverse to the fibers, η_3 —viscosity, that is related to trellis deformation in the fiber plane where the fabric angle changes.

- (e) *Equilibrium equation* (9.26):

$$\frac{\partial \sigma_{ij}}{\partial x_j} = 0, \quad (9.26)$$

where $\boldsymbol{\sigma}$ —stress.

However, the model proposed by Johnson is idealized as it neither considers fabric weave nor includes any interaction effects between the warp and weft fibers. Interaction between fibers is included through their influence on the viscosity parameters and on the fabric locking angle. The author noted that viscoelastic and thermal effects could be included to the presented model by allowing the viscosity

to be rate and temperature dependent. In his further work Johnson [300] extended the proposed rheological model for temperature-dependent viscoelastic material and implemented it in the explicit FE code PAN-STAMP (originally intended to the metal stamping) to characterize the in-plane behavior of each ply in the laminate media.

Luca et al. [308] simulated textile thermoplastic forming by utilizing ‘biphase model’ in which matrix has a thermo-viscous behavior, while woven fibers are treated as elastic. The out-of-plane shearing between the adjacent layers was handled using viscous-friction and contact constraints. The heat transfer assumed to be predominantly one-dimensional (through-the-thickness), and tool-to-ply and ply-to-ply heat transfer was simulated via the mechanical contact. However, limited in-plane heat transfer was also considered and modelled using conventional anisotropic heat conduction. The proposed simulation technique was verified with the experiment and demonstrated consistent agreement in predicting of ply wrinkling and fiber reorientation.

Nishi et al. [309] simulated the forming behavior of the woven thermoplastic prepreg during the non-isothermal thermoforming process. The modelling process was performed as a complex thermal-mechanical analysis, that took into account the mechanical response of the anisotropic nonlinear textile and temperature dependence of isotropic elasto-plastic matrix. The thermoplastic textile prepreg was simulated as a macroscale model consisting of a layer of fabric and placed around two layers of matrix. The authors proposed the combined shell and membrane model, where the textile was simulated with membrane elements, while matrix—with shell elements. They adapted the micromechanical model proposed by Ivanov et al. [310] to the membrane element in order to describe the in-plane behavior of the prepreg, while shell elements were responsible for the bending stiffness. The authors also considered the heat transfer on the contact surface between prepreg and tool during the non-isothermal forming process. The resulting FE model accurately predicted in-plane shear response and demonstrated a good agreement with the bias-extension experimental measurements. A similar approach was utilized by Gong et al. [311].

Harrison et al. [312] created an analytical constituent-based multi-scale energy model for the prediction of complex rheological behavior of viscous FR-PP prepreg. The developed model took into account the fabric weave architecture, the V_f as well as the PP rheology. The prepreg was modelled as two-phase structure composed of stacked textile and matrix layers. The developed model was not fully predictive, as it did not take into account the meso-scale kinematics. However, the proposed model gave accurate and quick prediction of FR-PP forming behavior at different shear rates and temperatures without recourse to either textile composite characterization experiments or sophisticated FE simulations. In his further work Harrison incorporated the constituent-based multi-scale energy model into the non-orthogonal one [313]. Next, he combined multi-scale energy model with macro-scale and successfully implemented it in FE codes Abaqus Standard and Abaqus Explicit [314]. In a later study [315] he demonstrated the possibility of

modelling of a press forming of 0/90 cross-ply GF-PP using the double-dome geometry by comparison of the obtained numerical results with the experimental.

9.5.3.3 Thermal Behavior

The real life operation conditions of composite structures predominantly involve combined thermo-mechanical loading. For automotive application a typical temperature range is from $-40\text{ }^{\circ}\text{C}$ up to $80\text{ }^{\circ}\text{C}$, thus it is essential to understand the mechanical behavior of FR-PP in this temperature window. With increasing temperature, the stiffness and strength of thermoplastics normally decreases, whereas the failure strain increases. These effects become dramatic when exceeding the polymer's T_g . This is the reason why matrix-dominated properties (shear, transverse stiffness and strength, compression strength) are reduced with the temperature rise. By contrast, the mechanical properties of man-made reinforcement are not essentially influenced by the temperature in a wide temperature range. As a consequence the effect of elevated temperature on the fiber-dominated properties (tensile, bending strength, etc.) is much less significant [316, 317].

Although the recommended operation temperature of semi-crystalline PP is far below its melting temperature, the glass transition region should be taken into account. Thus, if the temperature rises above T_g , the macromolecules motion in the amorphous regions increases, in such a manner enhancing ductile character of PP. The glass transition region of PP matrix ranges from $-10\text{ }^{\circ}\text{C}$ up to $+20\text{ }^{\circ}\text{C}$ [317].

Hufenbach et al. [318] investigated the thermal-mechanical behavior of glass FR-PP produced of a commingled fabric (twill weave Twintex[®]) under static load. The tested samples had a [(0/90)]₄ lay-up and contained 51 vol% of the reinforcement. The authors defined Young's modulus and tensile strength at 23 and $80\text{ }^{\circ}\text{C}$ in 0° , 45° and 90° directions (Table 9.4).

Obviously, the off-axis mechanical properties of woven GF-PP composites are more influenced by the temperature than those in warp- and weft-directions [319], see also Table 9.4.

The compression strength of FR-PP in fiber direction is strongly influenced by the matrix stiffness, as it prevents fibers from kinking. Therefore, glass FR-PP demonstrates almost 70% drop of compression strength between -40 and $80\text{ }^{\circ}\text{C}$

Table 9.4 Mechanical properties of woven GF-PP at 23 and $80\text{ }^{\circ}\text{C}$ [318]

Direction	$T\text{ (}^{\circ}\text{C)}$	$E\text{ (GPa)}$	$\sigma^+\text{ (MPa)}$	Damping values $\tan \delta\text{ (-)}$
0°	23	14.2	299	0.02861
	80	13.8	268	0.04863
45°	23	5.5	115	0.03267
	80	2.9	58	0.05862
90°	23	14.7	280	0.03008
	80	13.3	257	0.04901

(from 256 to 79 MPa) [317]. At T_m the compression strength falls to zero [319]. The in-plane Poisson's ratio is considered to be constant at the mentioned temperature range [317].

However, static properties are not enough for reliable structural design of automotive components. It is necessary to understand cyclic (fatigue) and dynamic (crash and impact) properties under combined thermo-mechanical loading conditions. Bureau and Denault [320] tested woven GF reinforced PP composites under cyclic sinusoidal load at -40 , 23 and 50 °C and compared the obtained results with polyester based composite. The flexural fatigue modulus was reported in terms of 'normalized modulus' (modulus at a given cycle divided by the initial one). The maximum flexural fatigue stresses obtained were 300 MPa at -40 °C, 186 MPa at 23 °C, and 175 MPa at 50 °C that corresponded accordingly to 88, 75 and 121% of the yield stress of FR-PP. However, none of the examined PP based samples failed after 2×10^6 cycles. At 50 °C FR-PP demonstrated slightly higher fatigue resistance than at -40 °C and even significantly better performance has been found at 23 °C, which is very close to T_g of the PP matrix.

Anyway, despite the fact that woven GF PP composites lose their static mechanical properties with the temperature rise, their fatigue performance remains quite high: $2 \dots 3 \times 10^6$ cycles when tested at fatigue levels equivalent to the yield stress, and about 4×10^6 cycles when tested at 84% of its yield stress [320].

Bocz et al. pointed out that for woven fabric reinforced self-reinforced PP composites has been much lower amount of intumescent flame retardant (IFR) can be efficient in PP than for traditional PP and PP composites. V-0 classification in UL-94 test can be achieved with only 9 wt% of IFR additive. It was proved that the significant shrinkage, exhibited by the highly-stretched PP tapes when exposed to heat, is the key factor behind the self-extinguishing behavior of flame retarded SRCs with rather low additive content (only 9 wt% IFR) [321, 322].

9.5.3.4 Other Properties

Due to its relatively low glass transition temperature, PP matrix demonstrates ductility properties even at RT, thus providing its composites considerably improved fatigue performance in comparison with a conventional thermoset composite [272]. Fatigue performance of FR-PP depends on both fiber orientation and load mode. Thus, Ferreira et al. [323] examined the fatigue behavior of glass FR-PP with three different layups: 0 ; $+30/-30/0^\circ$; and $+45/0/-45^\circ$. The authors demonstrated that 0° laminate shows 1.5–1.8 higher fatigue strength than those with the other lay-ups tested (Fig. 9.22).

Three typical stages of stiffness loss could be distinguished during the fatigue damage accumulation. The first one is rather short (do not exceed 5% of loading time) and it demonstrates a progressive stiffness reduction. The second stage corresponds to a gradual stiffness degradation and lasts the majority of all fatigue life (75–85%). The third stage is associated with the stiffness catastrophic drop until failure and lasts 10–20% of the fatigue life [272, 324].

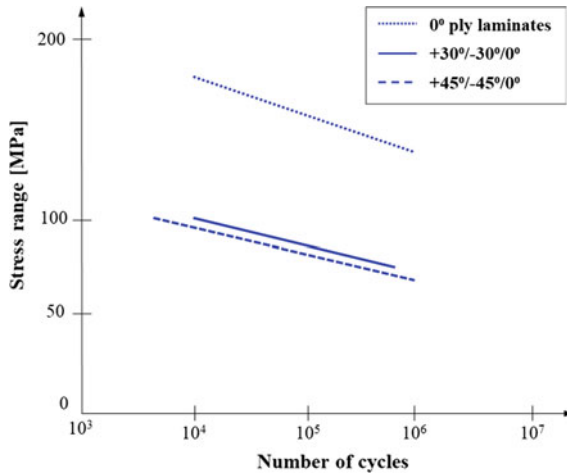


Fig. 9.22 Summary of Wöhler fatigue behavior of woven GF-PP ($V_f = 0.338$) at different layups (based on Ref. [323])

Besides service temperatures the processing conditions could influence significantly the fatigue performance of FR-PP [272]. Thus, low cooling rates, low molding temperatures, low pressures, or short heating cycles obviously leads to poor microstructural characteristics, which consequently negatively affect the fatigue performance (Fig. 9.23). Bureau and Denault [272] examined the fatigue response of the woven GF reinforced PP under various molding conditions: SCC—slow cooling conditions, ETC—extreme temperature conditions, LPSC—low pressure stamping conditions, HPSC—high pressure stiffness conditions and RC—reference forming conditions (Table 9.5).

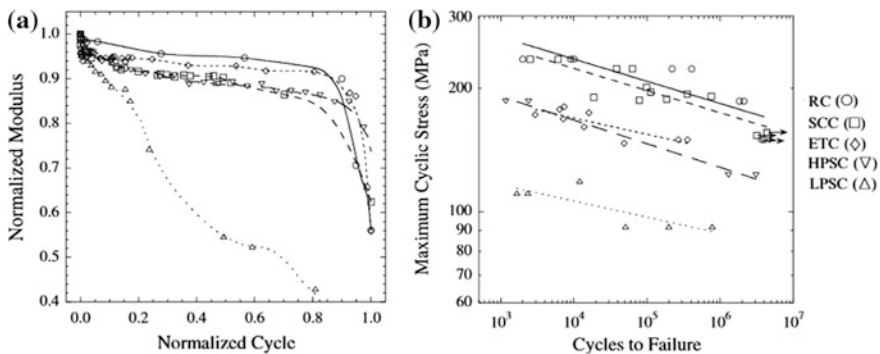


Fig. 9.23 Fatigue performance of woven GF reinforced PP: **a** normalized flexural modulus as a function of number of cycles at a maximum stress level of 75% of the flexural strength for RC, SCC, ETC and LPSC, and 62% for HPSC; **b** maximum cycle stress for various ([272] reproduced with the permission of Elsevier)

Table 9.5 Processing conditions used for the molding of woven GF reinforced PP [272]

Conditions	Temperature (°C)	Holding time (min)	Cooling rate (°C/min)	Pressure (MPa)
RC	200	5	10	0.70
SCC	200	5	1	0.35 ^a
ETC	315	20 ^b	10	0.35 ^a
PSC	160	10	10	0.70
LPSC	200 ^c	— ^d	10	0.11
HPSC	200 ^c	— ^d	10	0.10

^aA lower pressure was used to prevent matrix flow due to the long duration of molten stage

^bA longer time was used to maximize matrix degradation

^cPSC plate is preheated to temperature in an infrared oven and then placed upon a mold prior to stamping

^dUndetermined: stamping was done at constant closing speed until desired pressure was reached

The best fatigue performance from the flexural stiffness point of view was demonstrated by the composites formed under RC and ETC process conditions (Fig. 9.23a). However, composites formed under RC and SCC conditions exhibited “indefinite” fatigue life ($>3-4 \times 10^6$ cycles) at the cyclic stress of 150 MPa (Fig. 9.23b).

Mathieu et al. [325] studied the durability characteristics of glass FR-PP under the influence of the environmental conditions typical for civil engineering constructions. They defined the long-term properties of FR-PP under the influence of tap and 3% salt water at 13, 50 and 70 °C as well as freeze/thaw cycles. The loss of elastic modulus after 168 days in salt solution amounted to 9, 20 and 23% at 23, 50 and 70 °C respectively, while in tap water the loss of modulus was 12, 19 and 20%. The degradation of flexural strength under the same testing conditions amounted to 19, 30 and 44% for immersion in salt solution, and 11, 20 and 24%—for immersion in tap water. Freeze/thaw cycling (800 cycles) resulted in 8 and 32% loss of flexural strength and 0 and 22% loss of elastic modulus for unsaturated and saturated in water samples.

9.5.4 Processing and Applications

Excellent energy absorption capacity and advanced fatigue performance together with high lightweight potential, and high production capacity qualifies FR-PP for crash resistant as well as semi-structural and structural components in automotive application. The typical examples of using FR-PP in automobiles could be: seat pan [326], floor panels [327], A-, B- and C-pillars [92], different protection shields [328] and so on.

9.6 Laminate Composites

Laminated composites consist of several monolayers (plies) containing endless fibers with various orientation angles (Fig. 9.24). Each monolayer comprises the reinforcement in the form of UD fibers (or tapes) embedded in the matrix. Next we refer to such monolayers as UD-PP.

Conceptually, the production of laminated composites from UD-PP does not differ from that of FR-PP, and consists of two basic stages, namely impregnation and consolidation. These steps can be either separated or combined in one production line. For detailed description of these production concepts interested reader is addressed to Sects. 9.4 and 9.5. Although the manufacturing methods of the semi-finished UD-PP does not principally differ from those of FR-PP, the production routes of composite parts involve also techniques typical for UD composites, i.e. pultrusion, filament winding (FW), etc. (Fig. 9.25).

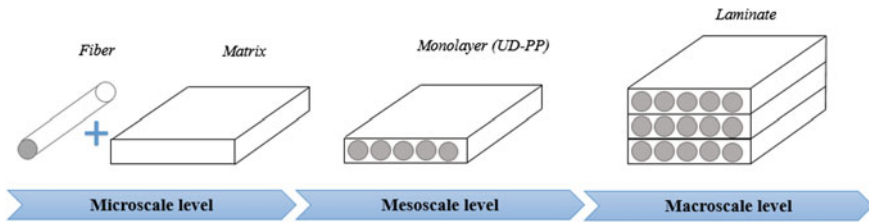


Fig. 9.24 Different structural levels of laminated composites

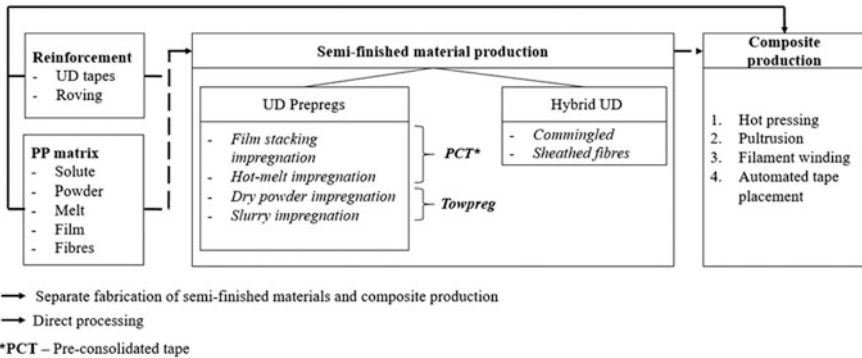


Fig. 9.25 Principal scheme of the UD-PP sequential production

9.6.1 Manufacturing

As it was mentioned before, the manufacturing techniques of UD-PP preregs are very similar to those of FR-PP and already introduced in Sect. 9.5. However, some of the techniques have certain distinguishing features which will be highlighted below.

UD thermoplastic preregs are differently classified. Thus semi-finished materials impregnated with solute, melt or film polymer are called as ‘pre-consolidated tapes’ (PCT), while preregs impregnated with powder are called as ‘towpregs’ (Fig. 9.26). UD-PP towpregs are produced under the tradenames FibrFlex[®], TenCate Cetex[®], PolyStrand[®], and others.

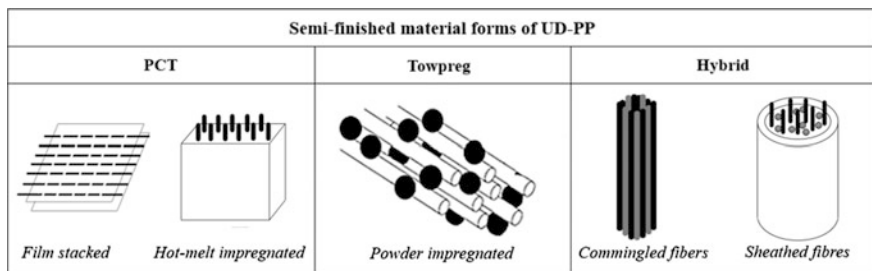


Fig. 9.26 Semi-finished material forms of UD-PP

Hybrid UD reinforcements could be in the form of commingled or sheathed fibers. In the latter case the roving or fibers are mingled with very fine matrix powder and jacketed by a thin polymer sheath [329, 330].

Film stacking is the most widely used method to produce small quantity of the UD-PP, while for the mass production hot melt, *dry powder* or *slurry* methods are far more suitable. A distinct feature of all the mass production techniques of UD-PP is the utilization of ‘pultrusion-like’ equipment. This involves the pulling of a continuous fiber tow through an “impregnation medium”, which is either the polymer melt or dry polymer powder, or a fluid dispersion of polymer powder. This is followed in-line with suitable post-treatments.

Hot melt pultrusion

Basically, hot melt pultrusion lines for UD-PP prepreg production consists of the following units: creel; fibers guidance, spreading, preheating and drying; polymer feeder; impregnation and consolidation cell; cooling chamber, pulling and cutting units (Fig. 9.27).

However, feeding unit could be implemented by different ways. Thus, it could be either an injection [331] or an extrusion equipment [332, 333]. Both variants are currently used. For example, Nunes et al. [332, 334] produced PP-based PCTs with GF and CF reinforcements via a pultrusion line utilizing an extrusion feeder

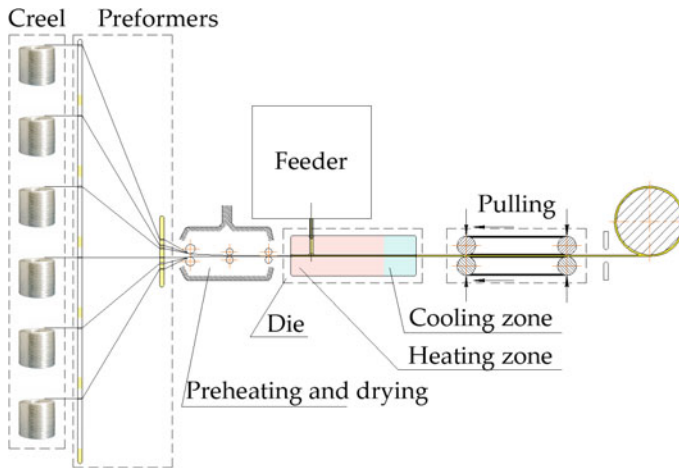


Fig. 9.27 Hot melt thermoplastic pultrusion production line

(cross-head extrusion die). The width of the resulting tape was 25 mm and the fiber content was 45 and 60 wt% for CF and GF, respectively. The same principle is utilized by CompTape B.V. (Delft, Netherlands) [333], that commercially produce PCTs with PP matrix. Poon et al. [335] also adapted an extruder feeding systems for UD-PP prepreg production.

By contrast Thermoplastic Pultrusion Technologies (Yorktown, Virginia, USA) used injection polymer feeder [331]. The major difference between injection and extrusion feeding units is in the polymer supply (intermittent vs. continuous, respectively). Note that an injection feeder requires higher pressures, as well as, stricter process control compared to the extrusion one.

Nunes et al. [336, 337] demonstrated that the impregnation quality of pultruded PCT is better than that of powder impregnated towpreps. However, hot melt pultrusion technique is not free from shortcomings. The main drawbacks of this technology are: (i) impregnation is affected by the matrix viscosity, and (ii) the polymer melt should have high enough thermooxidative stability.

Dry powder processing

Dry powder prepegging method was developed by Price in 1973 [338]. In this technique finely ground PP particles, suspended in dry air, are deposited onto the fiber tow exploiting of aerodynamic, gravitation, van der Waals and electrostatic forces. A typical powder-coating line comprises wind-off block, fibers' spreader, fiber pre-heating and coating sections, consolidation oven and wind-up unit (Fig. 9.28) [339–342]. The coating section could either include a simple powder feeder and a vibrating bath, or a more complicated powder feed hopper creating fluidized bed. There are several methods to create fluidized powder beds which have been surveyed by Padaki and Drzal [343].

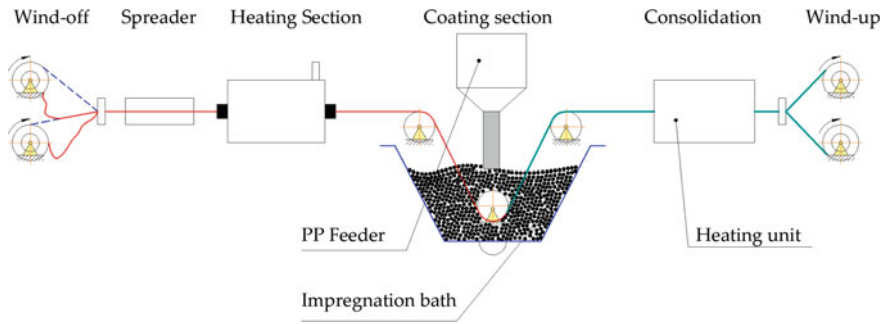


Fig. 9.28 Schematic diagram of the powder-coating line set-up (based on Ref. [340])

A research group in Polytechnic Institute of Leiria (Portugal) [340, 344, 345] conducted a comprehensive research study on the dry powder impregnated towpreg manufacturing. It was reported that particles size is one of the most important processing parameters. Thus, the optimum PP particles size from the point of view of production capacity should be 400 μm , while to guarantee adequate mechanical properties the particle size should not exceed 320 μm [344]. The optimized processing conditions were: linear fiber pulling speed in the range of 1.1–1.2 m/min, coating chamber and consolidation oven temperature at 55 and 280 $^{\circ}\text{C}$, respectively, and relative humidity in the coating chamber at 80%.

Despite of the great advantage of dry powder prepregging, namely independence of the matrix viscosity, it has definite drawbacks. One of them is the high friction between dry fibers and guide rollers that causes fibers damage. Electrostatic forces that stipulate particles deposition on the tows do not guarantee good process control due to the high loss of polymer powder. As a result, it is quite difficult to achieve consistent V_f in towpregs. Moreover, it is practically impossible to attain a uniform powder distribution in the towpreg. The last fact causes the appearance of pores and microvoids in the final product.

Slurry processing (wet impregnation)

Slurry processing implies drawing of the reinforcing fibers through a medium consisting of a liquid carrier with suspended polymer particles [343, 345, 346]. The presence of a liquid phase reduces the friction force between the tow fibers and guide pins, thus minimizing fibers damage. Moreover, capillary forces help the penetration of particles into the tow yielding some interlocking effect [347]. However, wet powder impregnation process requires the removal of the liquid carrier prior to consolidation that decreases the cost efficiency and production capacity [348].

9.6.2 Structure Development and Characterization

Production technologies for laminated composite manufacturing could be roughly divided into two groups—‘continuous’ and ‘discrete’ methods. ‘Continuous’ techniques include pultrusion and filament winding (FW), while ‘discrete’ ones the hot pressing and automated tape placement (ATP).

Pultrusion of UD-PP composites

The very first attempts to produce laminated thermoplastic composite by means of pultrusion process were taken in 1980th [349]. Since that time a great number of investigations were dedicated to the different aspects of the thermoplastic pultrusion technology. Today pultrusion is a well-established manufacturing technique of thermoplastic profiles. A typical thermoplastic pultrusion line includes block of creels with the bobbins of fibers, guiding device, fibers’ preheater, set of two dies, pulling and cutting mechanism (Fig. 9.29).

The main difference of a thermoplastic pultrusion line from thermoset one resides in a presence of two dies working for heating and cooling, respectively. The matrix flow occurs in a heating die that, due to higher viscosity of thermoplastic matrix, is much shorter in length than the thermoset analogue. Moreover, the cavity of the heating die section of thermoplastic pultrusion is tapered over a larger length than the thermoset one. This cavity profile is aimed at generating back flow of the matrix melt in order to achieve the desired impregnation and compaction of the profile [350]. A cooling die is intended for the consolidation of the profile.

Nunes and co-workers [334] defined the optimal processing parameters for production of laminated GF-PP composite profiles using a laboratory scale pultrusion line. This pultrusion processing window was given by the following parameters: pre-heating chamber—170 to 180 °C, consolidation die temperature—280 °C, cooling die temperature—25 °C, and linear pultrusion speed—0.2 to 0.3 m/min. Similar results were obtained for GF-PP by Poon et al. [335], and for

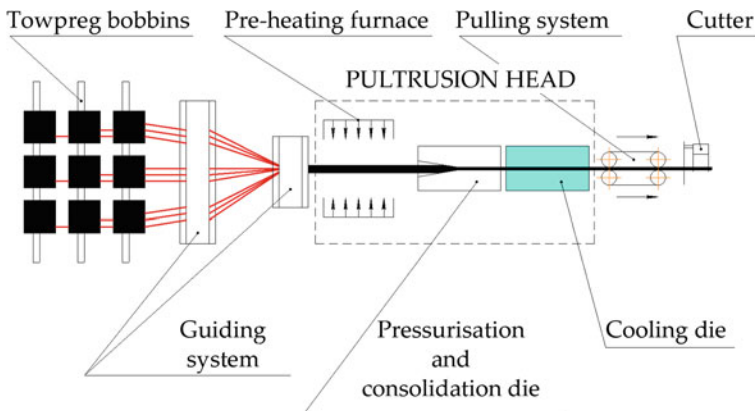


Fig. 9.29 Schematic diagram of thermoplastic pultrusion production line

flax fibers reinforced PP by Angelov et al. [351]. However, a line speed up to 2 m/min was achievable, depending on the section thickness of the profile [352]. Despite of maturity of the thermoplastic pultrusion process, its main drawback is that the angle of the reinforcement with respect of the production is limited. Thus, only UD laminates can be produced by means of pultrusion.

Filament winding

Filament winding (FW) is an automated manufacturing technique that enables to produce axially symmetric shell bodies with continuous fiber reinforcement placed at different angles. However, the reinforcement angles, feasible by FW, are limited for geodesic ones.

By contrast to thermoset the thermoplastic FW offers in situ (on-line) consolidation of composite product, thus enabling to eliminate post-consolidation procedure and, consequently, to attain better economic efficiency and higher production rates. The thermoplastic FW process consist of two steps: (i) heating of the prepreg up to the polymer melting temperature and (ii) applying compaction pressure and consolidation of the prepreg with the substrate laminate at the contact region (Fig. 9.30). A FW production line typically consists of a winding machine, creel, pre-heating and heating units, consolidation roller and mandrel.

The key issue in the successful implementation of thermoplastic FW is the heating that can be achieved by a variety of methods, i.e. direct flame, hot gas, IR radiation, ultrasonic [355] and laser energy. Funk and Neitzel [356, 357] estimated the feasibility of each heating method from the technical and economical positions. They determined, that laser heating enables the highest winding speed (up to 140 m/min) but at the same time is accompanied by high investment and processing costs. IR heating method exhibited lower (compared to laser) expenditures together with lower winding speed (not more than 27 m/min). Direct flame and hot gas

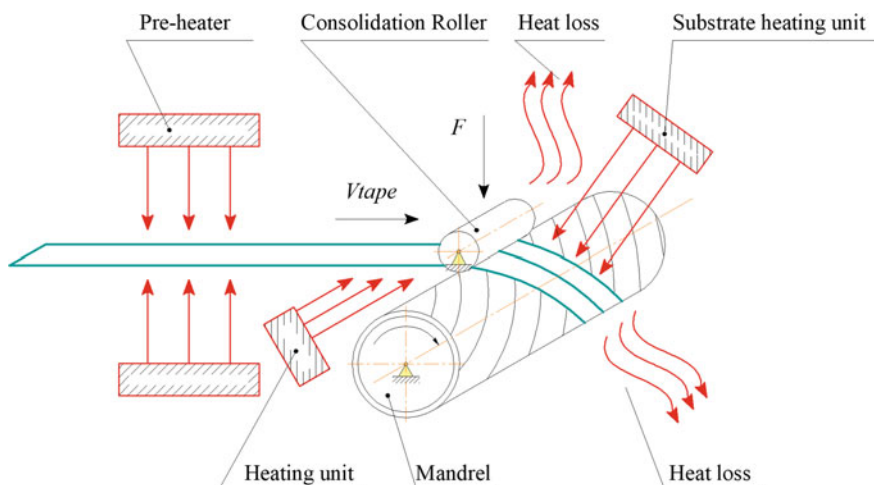


Fig. 9.30 Schematic diagram of thermoplastic FW process (based on Ref. [353, 354])

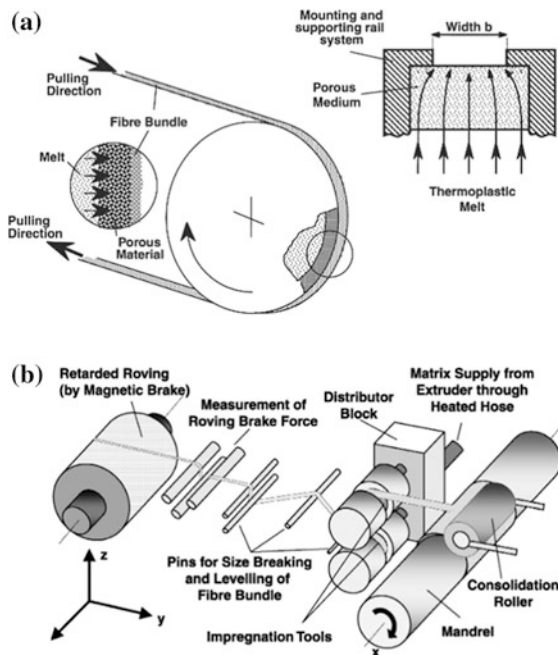
techniques are low-cost options allowing an average winding speed in the range of 18–60 m/min.

Dai and Ye [353] defined the processing window for GF-PP rings produced with a FW technique utilizing hot gas heating and constant compaction line pressure. Optimal processing parameters for composite tubes produced from commingles GF roving were obtained by Dobrzanski et al. [358] by means of Taguchi method.

The feasibility of a direct processing route for FW (D-FW) that involved the fibers' impregnation, winding and consolidation in line, was first demonstrated by Astrom and Pipes in 1990th [359]. For the fiber impregnation the authors have chosen a combination of powder impregnation in an agitated powder bed. The powder-impregnated fibers entered in a small pultrusion die before depositing them onto the mandrel. Besides a very low processing speed (0.7 m/min), for this D-FW other technological restrictions, such as high void content and weak consolidation, had to be taken into account.

Henninger and Friedrich [360, 361] informed about an on-line melt impregnation technique using an 'impregnation wheel'. The working principle of this technique involves an impregnation of a reinforcement tow with the molten polymer squeezed by a pressure through a porous ring (Fig. 9.31a). The supply of polymer melt is provided by a normal single screw extruder and a flexible heated hose. The schematic diagram of D-FW line utilizing 'impregnation wheel' technology is presented in Fig. 9.31b. The maximum achievable winding speed causing no degradation in the mechanical properties was 15 m/min, and the maximum processing temperature was given by 230 °C [361].

Fig. 9.31 D-FW production line: **a** working principle of an 'impregnation wheel' technology; **b** schematic diagram of the D-FW production line ([360, 361] reproduced with the permission of Elsevier)



As it was mentioned before the possible fiber architecture with FW process is limited by geodesic angle. The next discussed technology is free of this restriction.

Automated Tape Placement

Automated tape placement (ATP) is a manufacturing technique, that allows to create large scale flat, single- and even double-curved laminate composite products without any limitation on the reinforcing angle. ATP is a logical extension of a thermoplastic tape placement technology, that becomes possible with the advances in automation/robotics [362]. The ATP process is similar to FW and involves the prepreg's melting (at least locally) and bounding it to the laminate substrate by application of a compaction force exerted by a consolidation roller (Fig. 9.32). During the consolidation procedure the prepreg tapes are cooled to the tool temperature. Possible heating methods for ATP are the same as for FW. However, due to a high production capacity demands, the most effective heat source for ATP is laser [363–366].

The laser-assisted ATP rates could reach 160 m/min [364], thus allowing cost-effective production of fully consolidated load-optimized 3D structural components for automotive, aerospace, sport and other industries. An extensive research in this field was conducted by Fraunhofer Institute for Production Technology (Fraunhofer IPT) [364, 365, 367, 368]. This research group developed a production system for ATP [364] and a multi-material-head for ATP which is able to process thermoplastic and thermoset tapes, as well as dry fiber roving covered with adhesive [367]. Moreover, they demonstrated the feasibility of combining of ATP produced shell parts with 3D-printed thermoplastic structures [369].

Hot pressing manufacturing technique for UD-PP composites does not principally differ from that for FR-PP which is described in details in Sect. 9.5.

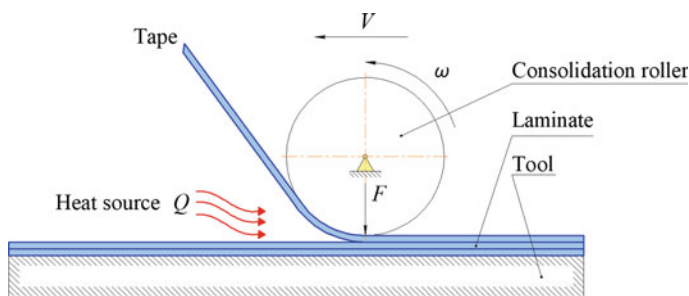


Fig. 9.32 Schematic diagram of ATP technology

9.6.3 Properties and Their Prediction

9.6.3.1 Mechanical Response

Due to their reinforcement architecture UD-PP composites demonstrate the highest level of mechanical response in longitudinal direction when compared with FR-PP, GMT, LFT and other PP based composites (Fig. 9.2).

The static mechanical properties of UD-PP can be defined either experimentally and also well-predicted by theories. Mechanical testing methods for UD composites are well established laboratory techniques that are ruled by a number of standards. Thus, ISO 527-5 is a relevant international standard for tensile testing of UD composites, ASTM D 695, ASTM D 3410, DIN 65 380 and others—for compression testing, ASTM D 790—for flexural testing. However, there are further relevant testing standards summarized in Ref. [172]. Some mechanical testing results of UD-PP are presented in Table 9.6. More information about the properties of UD-PP reinforced with NFs a concerned reader could find in an overview paper of Malkapuram et al. [289].

Table 9.6 Mechanical properties of UD-PP

Reinforcement type (prepreg type)	Production technique	V_f (%)	ρ (kg/m ³)	Tensile		Flexural		Ref.
				σ (MPa)	E (GPa)	σ (MPa)	E (GPa)	
Flax (commingled)	Pultrusion	38	800	145	15.1	101	14.3	[376]
Flax	Hot pressing	17.4–31.8	1000–1070	–	–	89.9–212.4	11–22	[377]
Kenaf (film stacking)	Vacuum bag	≈44	–	120	~ 14	–	–	[378]
Kenaf (film stacking)	Hot pressing	–	–	~ 83–93	~ 5	–	–	[379]
GF (towpreg)	Pultrusion	56.2	–	305	29.9	>117	22.5	[344]
		52.1	1322–1767	>336	33.9	158–241	28.6	[332]
	FW	59	–	431	31	–	–	[344]
GF (commingled)	Pultrusion	37.1	1519	545.9	24.9	595	26.2	[332]
		50	1480	515	33.4	335	28.8	[376]
GF (PCT)	pultrusion	30	–	355	71.3	329	16.8	[332]
GF (PCT) Plytron [®]	–	35	1480	680	22.5	570	22	[380]
CF	–	40	–	1421	–	750	90	[381]

The mechanical properties of UD-PP can be improved by interphase engineering. The related methods do not differ from those for FR-PP described in Sect. 9.5 [370–374].

The theoretical prediction of the mechanical properties of UD in longitudinal direction is based on the rule of mixture [375]. However, this prediction is rather rough and can be used only for engineering evaluations.

The effective properties of the laminated composites consisting of several UD monolayers are defined by the orientation, thickness, and stacking sequence of the individual layers. The theory that describe the linear elastic behavior of laminated composites subjected to in-plane loads and bending moments is referred as Classical Laminate Theory (CLT) [382, 383]. CLT is a well-known analytical predictive technique widely used by engineers and researchers to determine linear elastic properties of composites. To evaluate the failure response of the laminated composites different failure criteria are considered. In general, fiber reinforced composites exhibit various types of internal failure, namely: fiber breakage, matrix deformation and cracking, fiber debonding, fiber pull-out and delamination. The development of fiber reinforced composites failure criteria has been conducted for more than 30 years by the researchers all over the world. The progress in failure prediction approaches was summarized in a comprehensive review conducted by Orifici et al. [384].

9.6.3.2 Rheological Behavior

The rheological behavior of UD-PP is governed by the same laws as FR-PP and is well described in Sect. 9.5.3.2.

9.6.3.3 Thermal Behavior

Thermal properties of composites are the main parameters that define thermal response, performance and reliability of the related structures. Generally thermal properties of laminated composites depend on a number of variables, i.e. reinforcement type, its content and laying angle, void content, temperature, etc. Consequently, it is highly desirable to control and tailor the composite thermal properties. Apart from traditional experimental methods, a number of predictive methods for thermal conductivity, diffusivity and specific heat determination exist [385, 386]. One of the most widely used methods to predict the thermal conductivity of UD composites is thermal-electrical analogy method. This is based on the similarity of the partial differential equation governing the thermal potential and electric potential distribution. According to this analogue the effective thermal conductivity of a composite could be determined as the equivalent electrical resistance by the Ohm's law [387].

9.6.3.4 Other Properties

Fatigue

The UD-PP composites are mainly developed for long term load-bearing applications, and therefore fatigue response of such composites is of great importance. The UD composite behavior under cyclic load is governed by diffuse damage accumulation. A general concept of UD composites tension-tension fatigue behavior was proposed by Talreja [388]. This concept implies that at low cycle fatigue catastrophic fiber damage is dominant, at intermediate cycle—progressive fiber-bridged matrix cracking and/or interfacial shear failure is prevalent, while for high cycle—failure initiated in the matrix and arrested by the fibers can be considered as typical.

Van den Oever and Peijs [389] examined the fatigue performance of UD-GF-PP with both unmodified and MAH-modified matrices under longitudinal tensile (Fig. 9.33a), transverse and shear (Fig. 9.33b) loads. The authors found only a slight improvement in fatigue performance for the UD-PP with maleic anhydride modified matrix.

The influence of interfacial strength of the UD-PP on the fatigue performance was also studied by Gamstedt et al. [390]. Enhancement of the interfacial strength between fibers and matrix with MAH led to better fatigue resistance and prolonged fatigue life.

Zushi et al. [381] defined the fatigue endurance limit (that can be used for design) for UD-PP reinforced with CFs as 500 MPa, that is one third of the static tensile strength.

Electric conductivity

Damage sensing/location and self-healing are the present hot topics in the field of advanced laminate composites, including PP-matrix based ones, as well. Joo et al. [391] demonstrated that addressable conducting network (ACN) technique is

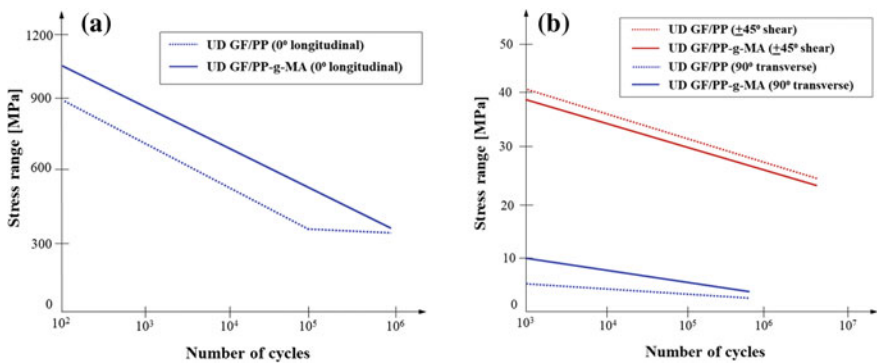


Fig. 9.33 Fatigue performance of UD-PP composites: **a** Longitudinal fatigue data for 0° laminate; **b** transverse and shear fatigue data for 90° off-axis laminates and ±45° angle-ply laminates correspondingly (based of Ref. [389])

promising method for damage sensing of composites. This technique utilizes the electrically conductive network of composite itself as sensor. Structural delamination or matrix cracking can be evaluated through resistance change by interruption of the through-thickness electric current flow. Metallic line electrodes on the top and bottom of the composite laminate, arranged in a grid pattern, serve to detect the change in the resistivity. To set the required through-thickness electric conductivity CNT and the like may be incorporated into the PP matrix or between the UD-CF laminae. It is noteworthy that composites containing both traditional fibrous and nanoscale reinforcements are referred to as hierarchical, multiscale or fuzzy composites. The beauty of this ACN approach is that it may work also for self-healing of the related composites when triggering resistive heating. The cited work showed that damage sensing was possible with high accuracy and the self-healing efficiency, measured in flexural tests, was as high as 96%.

9.6.4 Processing and Applications

UD-PP tapes and towpregs may be the feedstock for a vast variety of laminated composite products. Pultrusion is the preferred technique to produce profiles with various cross sections. FW allows the production of rotary bodies, i.e. pressure vessels, tanks, pipes, etc. ATP enables to create large-scale structures with single and double curvatures for aerospace, automotive and sport industries. However, technological versatility together with the ability to vary the laminate layup provides engineers a certain freedom, when creating laminated PP composite structures.

9.7 Conclusion and Outlook

The good mechanical and thermal properties of PP can be markedly enhanced by incorporation of reinforcements the range of which cover nanoparticles through textile architecture to UD aligned endless fibers. Beside of structural properties, the composites can be ensured with functional ones, such as thermal and electrical conductivities when for example carbonaceous nanofillers are introduced additionally. The latter nanofillers may play a key role in the preparation of smart composites having for example self-sensing and self-healing possibilities.

A general trend in the manufacturing of PP composites is the combination of several steps in-line. In the corresponding direct processes, the preparation and storage of semi-finished parts are avoided. Among the novel in situ preparation methods a bright future can be predicted the additive manufacturing methods, such as fused deposition of PP filaments with endless fiber reinforcement.

In the field of PP nanocomposites the R&D works will focus on using carbonaceous nanofillers to achieve functional properties. Considerable efforts will be

dedicated to model the structure-property relationships in nanocomposites whereby considering the actual dispersion state (agglomeration phenomena) of the nanoadditives.

Hybridization of the reinforcing fibers may drive the development of discontinuous fiber-reinforced injection-moldable composites. Use of recycled CFs in PP matrix may be a viable contribution to circular economy targeting the reuse of discarded composites. Tomographic inspections may result in new definition of the microstructure and its efficiency (i.e. fiber orientation distribution, fiber length alignment, fiber layering) in molded parts. The related works may contribute to more reliable flow modeling, as well. Textile engineering using commingled fibers will likely be the driver for the development of textile-reinforced PP composites. This note holds also for the related all-PP composites. The traditional processing techniques using UD fiber-reinforced PP preforms, such as filament winding, tape laying, may face to sever competition with additive manufacturing versions.

As far as the testing of PP composites concerns the general trend is to assess and describe their long-term performance including creep and fatigue.

References

1. Karger-Kocsis J, Kmetty Á, Lendvai L et al (2015) Water-assisted production of thermoplastic nanocomposites: a review. *Materials* 8(1):72–95. <https://doi.org/10.3390/ma8010072>
2. Zapata P, Quijada R (2012) Polypropylene nanocomposites obtained by in situ polymerization using metallocene catalyst: influence of the nanoparticles on the final polymer morphology. *J Nanomater* 2012:6. <https://doi.org/10.1155/2012/194543>
3. Azinfar B, Ahmad Ramazani SA, Jafariesfad N (2014) In situ preparation and property investigation of polypropylene/fumed silica nanocomposites. *Polym Compos* 35(1):37–44. <https://doi.org/10.1002/pc.22631>
4. Ahmad Ramazani SA, Tavakolzadeh F, Baniasadi H (2010) Synthesis of polypropylene/clay nanocomposites using bisupported Ziegler-Natta catalyst. *J Appl Polym Sci* 115(1):308–314. <https://doi.org/10.1002/app.31102>
5. Cardoso RDS, Oliveira JDS, Ramis LB et al (2018) Ziegler-Natta catalyst based on MgCl₂/clay/ID/TiCl₄ for the synthesis of spherical particles of polypropylene nanocomposites. *J Nanosci Nanotechnol* 18(7):5124–5132. <https://doi.org/10.1166/jnn.2018.15308>
6. Milani MA, González D, Quijada R et al (2013) Polypropylene/graphene nanosheet nanocomposites by in situ polymerization: synthesis, characterization and fundamental properties. *Compos Sci Technol* 84:1–7. <https://doi.org/10.1016/j.compscitech.2013.05.001>
7. Funck A, Kaminsky W (2007) Polypropylene carbon nanotube composites by in situ polymerization. *Compos Sci Technol* 67(5):906–915. <https://doi.org/10.1016/j.compscitech.2006.01.034>
8. Huang Y, Qin Y, Zhou Y et al (2010) Polypropylene/graphene oxide nanocomposites prepared by in situ Ziegler – Natta polymerization. *Chem Mater* 22(13):4096–4102. <https://doi.org/10.1021/cm100998e>
9. Kaminsky W (ed) (2013) Polyolefins: 50 years after Ziegler and Natta II. Polyolefins by metallocenes and other single-site catalyst. *Advances in polymer science*, vol 258. Springer, Heidelberg. <https://doi.org/10.1007/978-3-642-40805-2>

10. Kalaitzidou K, Fukushima H, Drzal LT (2007) A new compounding method for exfoliated graphite–polypropylene nanocomposites with enhanced flexural properties and lower percolation threshold. *Compos Sci Technol* 67(10):2045–2051. <https://doi.org/10.1016/j.compscitech.2006.11.014>
11. Chiu F-C, Chu P-H (2006) Characterization of solution-mixed polypropylene/clay nanocomposites without compatibilizers. *J Polym Res* 13(1):73–78. <https://doi.org/10.1007/s10965-005-9009-7>
12. Ljungberg N, Bonini C, Bortolussi F et al (2005) New nanocomposite materials reinforced with cellulose whiskers in atactic polypropylene: effect of surface and dispersion characteristics. *Biomacromol* 6(5):2732–2739. <https://doi.org/10.1021/bm050222v>
13. Karger-Kocsis J, Lendvai L (2018) Polymer/boehmite nanocomposites: a review. *J Appl Polym Sci* 135(24):45573. <https://doi.org/10.1002/app.45573>
14. Kato M, Matsushita M, Fukumori K (2004) Development of a new production method for a polypropylene-clay nanocomposite. *Polym Eng Sci* 44(7):1205. <https://doi.org/10.1002/pen.20115>
15. Karger-Kocsis J (2000) Reinforced polymer blends. In: Paul DR, Bucknall CB (eds) *Polymer blends*, vol 2. Wiley, New York, pp 395–428
16. Song P, Cao Z, Cai Y et al (2011) Fabrication of exfoliated graphene-based polypropylene nanocomposites with enhanced mechanical and thermal properties. *Polymer* 52(18):4001–4010. <https://doi.org/10.1016/j.polymer.2011.06.045>
17. Bouaziz A, Jaziri M, Dalmas F et al (2014) Nanocomposites of silica reinforced polypropylene: correlation between morphology and properties. *Polym Eng Sci* 54(9):2187–2196. <https://doi.org/10.1002/pen.23768>
18. Dabrowska I, Fambri L, Pegoretti A et al (2015) Spinning, drawing and physical properties of polypropylene nanocomposite fibers with fumed nanosilica. *Express Polym Lett* 9:277–290. <https://doi.org/10.3144/expresspolymlett.2015.25>
19. Zohrevand A, Aji A, Mighri F (2014) Morphology and properties of highly filled iPP/TiO₂ nanocomposites. *Polym Eng Sci* 54(4):874–886. <https://doi.org/10.1002/pen.23625>
20. Lin Y, Chen H, Chan C-M et al (2008) High impact toughness polypropylene/CaCO₃ nanocomposites and the toughening mechanism. *Macromolecules* 41(23):9204–9213. <https://doi.org/10.1021/ma801095d>
21. Zhao H, Li RKY (2005) Crystallization, mechanical, and fracture behaviors of spherical alumina-filled polypropylene nanocomposites. *J Polym Sci, Part B: Polym Phys* 43(24):3652–3664. <https://doi.org/10.1002/polb.20654>
22. Pracella M, Chionna D, Fina A et al (2006) Polypropylene-POSS nanocomposites: morphology and crystallization behaviour. *Macromol Symp* 234(1):59–67. <https://doi.org/10.1002/masy.200650209>
23. Prashantha K, Lacrampe MF, Krawczak P (2011) Processing and characterization of halloysite nanotubes filled polypropylene nanocomposites based on a masterbatch route: effect of halloysites treatment on structural and mechanical properties. *Express Polym Lett* 5(4):295–307. <https://doi.org/10.3144/expresspolymlett.2011.30>
24. Prashantha K, Soulestin J, Lacrampe MF et al (2009) Masterbatch-based multi-walled carbon nanotube filled polypropylene nanocomposites: assessment of rheological and mechanical properties. *Compos Sci Technol* 69(11):1756–1763. <https://doi.org/10.1016/j.compscitech.2008.10.005>
25. Szentes A, Varga C, Horváth G et al (2012) Electrical resistivity and thermal properties of compatibilized multi-walled carbon nanotube/polypropylene composites. *Express Polym Lett* 6(6):494–502. <https://doi.org/10.3144/expresspolymlett.2012.52>
26. Prashantha K, Soulestin J, Lacrampe MF et al (2009) Taguchi analysis of shrinkage and warpage of injection-moulded polypropylene/multiwall carbon nanotubes nanocomposites. *Express Polym Lett* 3(10):630–638. <https://doi.org/10.3144/expresspolymlett.2009.79>
27. Hassan ML, Mathew AP, Hassan EA et al (2014) Improving cellulose/polypropylene nanocomposites properties with chemical modified bagasse nanofibers and maleated polypropylene. *J Reinf Plast Compos* 33(1):26–36. <https://doi.org/10.1177/0731684413509292>

28. Hubbe MA, Rojas OJ, Lucia LA et al (2008) Cellulosic nanocomposites: a review. *BioResources* 3(3):929–980
29. Utracki LA, Sepéhr M, Boccaleri E (2007) Synthetic, layered nanoparticles for polymeric nanocomposites (PNCs). *Polym Adv Technol* 18(1):1–37. <https://doi.org/10.1002/pat.852>
30. Utracki LA, Kamal MR (2002) Clay-containing polymeric nanocomposites. *Arab J Sci Eng* 27(1):43–67
31. Gao Y, Zhang Y, Williams GR et al (2016) Layered double hydroxide-oxidized carbon nanotube hybrids as highly efficient flame retardant nanofillers for polypropylene. *Sci Rep* 6:35502. <https://doi.org/10.1038/srep35502>
32. Nagendra B, Rosely CVS, Leuteritz A et al (2017) Polypropylene/layered double hydroxide nanocomposites: influence of LDH intralayer metal constituents on the properties of polypropylene. *ACS Omega* 2(1):20–31. <https://doi.org/10.1021/acsomega.6b00485>
33. Tripathi SN, Srinivasa Rao GS, Mathur AB et al (2017) Polyolefin/graphene nanocomposites: a review. *RSC Adv* 7(38):23615–23632. <https://doi.org/10.1039/C6RA28392F>
34. Hári J, Horváth F, Móczó J et al (2017) Competitive interactions, structure and properties in polymer/layered silicate nanocomposites. *Express Polym Lett* 11(6):479–492. <https://doi.org/10.3144/expresspolymlett.2017.45>
35. Hári J, Dominkovics Z, Fekete E et al (2009) Kinetics of structure formation in PP/layered silicate nanocomposite. *Express Polym Lett* 3(11):692–702. <https://doi.org/10.3144/expresspolymlett.2009.87>
36. Lee SH, Youn JR (2008) Experimental and theoretical study on shear flow behavior of polypropylene/layered silicate nanocomposites. *Adv Compos Mater* 17(3):191–214. <https://doi.org/10.1163/156855108X345225>
37. He S, Zhang J, Xiao X et al (2017) Study on the morphology development and dispersion mechanism of polypropylene/graphene nanoplatelets composites for different shear field. *Compos Sci Technol* 153:209–221. <https://doi.org/10.1016/j.compscitech.2017.10.024>
38. Battisti M, Perko L, Arunachalam S et al (2018) Influence of elongational flow generating nozzles on material properties of polypropylene nanocomposites. *Polym Eng Sci* 58(1):3–12. <https://doi.org/10.1002/pen.24361>
39. Huang Z-X, Meng C, Zhang G et al (2017) Manufacturing polymer/clay nanocomposites through elongational flow technique. *Mater Manuf Process* 32(12):1409–1415. <https://doi.org/10.1080/10426914.2017.1339316>
40. Reichert P, Nitz H, Klinke S et al (2000) Poly(propylene)/organoclay nanocomposite formation: influence of compatibilizer functionality and organoclay modification. *Macromol Mater Eng* 275(1):8–17. [https://doi.org/10.1002/\(SICI\)1439-2054\(20000201\)275:1%3c8:AID-MAME8%3e3.0.CO;2-6](https://doi.org/10.1002/(SICI)1439-2054(20000201)275:1%3c8:AID-MAME8%3e3.0.CO;2-6)
41. Garcia-López D, Picazo O, Merino JC et al (2003) Polypropylene–clay nanocomposites: effect of compatibilizing agents on clay dispersion. *Eur Polym J* 39(5):945–950. [https://doi.org/10.1016/S0014-3057\(02\)00333-6](https://doi.org/10.1016/S0014-3057(02)00333-6)
42. Koo CM, Kim MJ, Choi MH et al (2003) Mechanical and rheological properties of the maleated polypropylene–layered silicate nanocomposites with different morphology. *J Appl Polym Sci* 88(6):1526–1535. <https://doi.org/10.1002/app.11782>
43. Li W, Karger-Kocsis J, Thomann R (2009) Compatibilization effect of TiO₂ nanoparticles on the phase structure of PET/PP/TiO₂ nanocomposites. *J Polym Sci, Part B: Polym Phys* 47:1616–1624. <https://doi.org/10.1002/polb.21752>
44. Ray SS (2010) A new possibility for microstructural investigation of clay-based polymer nanocomposite by focused ion beam tomography. *Polymer* 51(17):3966–3970. <https://doi.org/10.1016/j.polymer.2010.06.025>
45. Schneider S, Eppler F, Weber M et al (2016) Multiscale dispersion-state characterization of nanocomposites using optical coherence tomography. *Sci Rep* 6:31733. <https://doi.org/10.1038/srep31733>

46. Karger-Kocsis J, Varga J (1999) Interfacial morphology and its effects in polypropylene composites. In: Karger-Kocsis J (ed) *Polypropylene: an A-Z reference*, vol 2. Polymer Science and Technology Series. Springer Netherlands, Dordrecht, Netherlands, pp 348–356. https://doi.org/10.1007/978-94-011-4421-6_50
47. Zhang S, Minus ML, Zhu L et al (2008) Polymer transcrystallinity induced by carbon nanotubes. *Polymer* 49(5):1356–1364. <https://doi.org/10.1016/j.polymer.2008.01.018>
48. Abdou JP, Braggin GA, Luo Y et al (2015) Graphene-induced oriented interfacial microstructures in single fiber polymer composites. *ACS Appl Mater Interfaces* 7(24):13620–13626. <https://doi.org/10.1021/acsami.5b03269>
49. Nakajima H, Yamada K, Iseki Y et al (2003) Preparation and characterization of polypropylene/mesoporous silica nanocomposites with confined polypropylene. *J Polym Sci, Part B: Polym Phys* 41(24):3324–3332. <https://doi.org/10.1002/polb.10700>
50. Zhang MQ, Rong MZ, Friedrich K (2003) Processing and properties of nonlayered nanoparticle reinforced thermoplastic composites. In: Nalwa HS (ed) *Handbook of organic-inorganic hybrid materials and nanocomposites*, vol 2. Nanocomposites. American Scientific Publishers, Los Angeles, pp 113–150
51. Karamipour S, Ebadi-Dehaghani H, Ashouri D et al (2011) Effect of nano-CaCO₃ on rheological and dynamic mechanical properties of polypropylene: experiments and models. *Polym Test* 30(1):110–117. <https://doi.org/10.1016/j.polymertesting.2010.10.009>
52. Hu H, Onyebueke L, Abatan A (2010) Characterizing and modeling mechanical properties of nanocomposites-review and evaluation. *J Miner Mater Charact Eng* 9(4):275–319. <https://doi.org/10.4236/jmmce.2010.94022>
53. Kalaitzidou K, Fukushima H, Miyagawa H et al (2007) Flexural and tensile moduli of polypropylene nanocomposites and comparison of experimental data to Halpin-Tsai and Tandon-Weng models. *Polym Eng Sci* 47(11):1796–1803. <https://doi.org/10.1002/pen.20879>
54. Rouhi S, Alizadeh Y, Ansari R (2016) Molecular dynamics simulations of the interfacial characteristics of polypropylene/single-walled carbon nanotubes. *Proc Inst Mech Eng Part L: J Mater: Des Appl* 230(1):190–205. <https://doi.org/10.1177/1464420714557167>
55. Rezaiean N, Ebadi-Dehaghani H, Khonakdar HA et al (2016) Microstructure and properties of polypropylene/clay nanocomposites. *J Macromol Sci Part B* 55(10):1022–1038. <https://doi.org/10.1080/00222348.2016.1230462>
56. Spencer PE, Sweeney J (2009) Modeling of polymer clay nanocomposites for a multiscale approach. In: Karger-Kocsis J, Fakirov S (eds) *Nano- and micromechanics of polymer blends and composites*. Carl Hanser Verlag GmbH & Co. KG, Munich, pp 545–578
57. Mallick PK, Zhou Y (2003) Yield and fatigue behavior of polypropylene and polyamide-6 nanocomposites. *J Mater Sci* 38(15):3183–3190. <https://doi.org/10.1023/A:1025161215708>
58. Lv Y, Huang Y, Kong M et al (2014) Creep lifetime prediction of polypropylene/clay nanocomposites based on a critical failure strain criterion. *Compos Sci Technol* 96:71–79. <https://doi.org/10.1016/j.compscitech.2014.03.011>
59. Pedrazzoli D, Pegoretti A (2014) Long-term creep behavior of polypropylene/fumed silica nanocomposites estimated by time–temperature and time–strain superposition approaches. *Polym Bull* 71(9):2247–2268. <https://doi.org/10.1007/s00289-014-1185-3>
60. Drozdov AD, Høg Lejre AL, Christiansen Jd (2009) Viscoelasticity, viscoplasticity, and creep failure of polypropylene/clay nanocomposites. *Compos Sci Technol* 69(15):2596–2603. <https://doi.org/10.1016/j.compscitech.2009.07.018>
61. Ramsaroop A, Kanny K, Mohan T (2010) Fracture toughness studies of polypropylene- clay nanocomposites and glass fibre reinforced polypropylene composites. *Mater Sci Appl* 1(5):301–309. <https://doi.org/10.4236/msa.2010.15044>
62. Karger-Kocsis J (1989) Fracture of short-fibre reinforced thermoplastics. In: Friedrich K (ed) *Application of fracture mechanics to composite materials*, vol 6. Composite Materials Series. Elsevier Applied Science, Amsterdam, pp 189–247

63. Pegoretti A (2009) Creep and fatigue behavior of polymer nanocomposites. In: Karger-Kocsis J, Fakirov S (eds) Nano- and micromechanics of polymer blends and composites. Hanser, Munich, pp 301–339. <https://doi.org/10.3139/9783446430129.009>
64. Karger-Kocsis J (2009) On the toughness of “nanomodified” polymers and their traditional polymer composites. In: Karger-Kocsis J, Fakirov S (eds) Nano- and micromechanics of polymer blends and composites. Hanser, Munich, pp 425–470. <https://doi.org/10.3139/9783446430129.012>
65. Chen L, Wong SC, Pisharath S (2003) Fracture properties of nanoclay-filled polypropylene. *J Appl Polym Sci* 88(14):3298–3305. <https://doi.org/10.1002/app.12153>
66. Bureau MN, Perrin-Sarazin F, Ton-That MT (2004) Polyolefin nanocomposites: essential work of fracture analysis. *Polym Eng Sci* 44(6):1142–1151. <https://doi.org/10.1002/pen.20107>
67. Chan C-M, Wu J, Li J-X et al (2002) Polypropylene/calcium carbonate nanocomposites. *Polymer* 43(10):2981–2992. [https://doi.org/10.1016/S0032-3861\(02\)00120-9](https://doi.org/10.1016/S0032-3861(02)00120-9)
68. Karger-Kocsis J (1999) Dependence of the fracture and fatigue performance of polyolefins and related blends and composites on microstructural and molecular characteristics. *Macromol Symp* 143(1):185–205. <https://doi.org/10.1002/masy.19991430115>
69. Ou Y, Yang F, Yu ZZ (1998) A new conception on the toughness of nylon 6/silica nanocomposite prepared via in situ polymerization. *J Polym Sci, Part B: Polym Phys* 36(5):789–795. [https://doi.org/10.1002/\(SICI\)1099-0488\(19980415\)36:5%3c789:AID-POLB6%3e3.0.CO;2-G](https://doi.org/10.1002/(SICI)1099-0488(19980415)36:5%3c789:AID-POLB6%3e3.0.CO;2-G)
70. Argon AS, Cohen RE (2003) Toughenability of polymers. *Polymer* 44(19):6013–6032. [https://doi.org/10.1016/S0032-3861\(03\)00546-9](https://doi.org/10.1016/S0032-3861(03)00546-9)
71. Lauke B (2017) Fracture toughness modelling of polymers filled with inhomogeneously distributed rigid spherical particles. *Express Polym Lett* 11(7):545–554. <https://doi.org/10.3144/expresspolymlett.2017.52>
72. Arencón D, Velasco JI (2009) Fracture toughness of polypropylene-based particulate composites. *Materials* 2(4):2046. <https://doi.org/10.3390/ma2042046>
73. Bárány T, Czigány T, Karger-Kocsis J (2010) Application of the essential work of fracture (EWF) concept for polymers, related blends and composites: a review. *Prog Polym Sci* 35(10):1257–1287. <https://doi.org/10.1016/j.progpolymsci.2010.07.001>
74. Turcsán T, Mészáros L, Khumalo VM et al (2014) Fracture behavior of boehmite-filled polypropylene block copolymer nanocomposites as assessed by the essential work of fracture concept. *J Appl Polym Sci* 131(13). <https://doi.org/10.1002/app.40447>
75. Pedrazzoli D, Tuba F, Khumalo V et al (2014) Mechanical and rheological response of polypropylene/boehmite nanocomposites. *J Reinf Plast Compos* 33(3):252–265. <https://doi.org/10.1177/0731684413505787>
76. Satapathy BK, Ganß M, Weidisch R et al (2007) Ductile-to-semiductile transition in PP-MWNT nanocomposites. *Macromol Rapid Commun* 28(7):834–841. <https://doi.org/10.1002/marc.200600892>
77. Karger-Kocsis J, Khumalo VM, Bárány T et al (2013) On the toughness of thermoplastic polymer nanocomposites as assessed by the essential work of fracture (EWF) approach. *Compos Interfaces* 20(6):395–404. <https://doi.org/10.1080/15685543.2013.807145>
78. Bureau MN, Ton-That M-T, Perrin-Sarazin F (2006) Essential work of fracture and failure mechanisms of polypropylene–clay nanocomposites. *Eng Fract Mech* 73(16):2360–2374. <https://doi.org/10.1016/j.engfracmech.2006.04.012>
79. Saminathan K, Selvakumar P, Bhatnagar N (2008) Fracture studies of polypropylene/nanoclay composite. Part I: effect of loading rates on essential work of fracture. *Polym Test* 27(3):296–307. <https://doi.org/10.1016/j.polymertesting.2007.11.008>
80. Karger-Kocsis J (1996) For what kind of polymer is the toughness assessment by the essential work concept straightforward? *Polym Bull* 37(1):119–126. <https://doi.org/10.1007/bf00313827>

81. Utracki LA, Simha R, Garcia-Rejon A (2003) Pressure – volume – temperature dependence of poly- ϵ -caprolactam/clay nanocomposites. *Macromolecules* 36(6):2114–2121. <https://doi.org/10.1021/ma0215464>
82. Giannelis EP, Krishnamoorti R, Manias E (1999) Polymer-silicate nanocomposites: model systems for confined polymers and polymer brushes. In: Granick S (ed) *Polymers in confined environments*. *Advances in Polymer Science*, vol 138. Springer, Berlin, pp 107–147. https://doi.org/10.1007/3-540-69711-x_3
83. Privalko VP, Shumsky VF, Privalko EG et al (2002) Viscoelasticity and flow behavior of irradiation grafted nano-inorganic particle filled polypropylene composites in the melt state. *Sci Technol Adv Mater* 3(2):111. [https://doi.org/10.1016/S1468-6996\(00\)00011-6](https://doi.org/10.1016/S1468-6996(00)00011-6)
84. Gu SY, Ren J, Wang QF (2004) Rheology of poly(propylene)/clay nanocomposites. *J Appl Polym Sci* 91(4):2427–2434. <https://doi.org/10.1002/app.13403>
85. Trinkle S, Friedrich C (2001) Van Gorp-Palmen-plot: a way to characterize polydispersity of linear polymers. *Rheol Acta* 40(4):322–328. <https://doi.org/10.1007/s003970000137>
86. Chafidz A, Kaaressina M, Al-Zahrani S et al (2014) Multiwall carbon nanotubes filled polypropylene nanocomposites: rheological and electrical properties. *Polym Eng Sci* 54(5):1134–1143. <https://doi.org/10.1002/pen.23647>
87. Sinha Ray S, Okamoto M (2003) Polymer/layered silicate nanocomposites: a review from preparation to processing. *Prog Polym Sci* 28(11):1539–1641. <https://doi.org/10.1016/j.progpolymsci.2003.08.002>
88. Okamoto M, Nam PH, Maiti P et al (2001) A house of cards structure in polypropylene/clay nanocomposites under elongational flow. *Nano Lett* 1(6):295–298. <https://doi.org/10.1021/nl0100163>
89. Reichert P, Hoffmann B, Bock T et al (2001) Morphological stability of poly(propylene) nanocomposites. *Macromol Rapid Commun* 22(7):519–523. [https://doi.org/10.1002/1521-3927\(20010401\)22:7%3c519:AID-MARC519%3e3.0.CO;2-W](https://doi.org/10.1002/1521-3927(20010401)22:7%3c519:AID-MARC519%3e3.0.CO;2-W)
90. Solomon MJ, Almusallam AS, Seefeldt KF et al (2001) Rheology of polypropylene/clay hybrid materials. *Macromolecules* 34(6):1864–1872. <https://doi.org/10.1021/ma001122e>
91. Bikiaris D (2010) Microstructure and properties of polypropylene/carbon nanotube nanocomposites. *Materials* 3(4):2884–2946. <https://doi.org/10.3390/ma3042884>
92. Karian H (ed) (2003) *Handbook of polypropylene and polypropylene composites*. CRC Press, Boca Raton (Revised and Expanded. *Plastics Engineering*)
93. Yoon PJ, Fornes TD, Paul DR (2002) Thermal expansion behavior of nylon 6 nanocomposites. *Polymer* 43(25):6727–6741. [https://doi.org/10.1016/S0032-3861\(02\)00638-9](https://doi.org/10.1016/S0032-3861(02)00638-9)
94. Manias E, Touny A, Wu L et al (2001) Polypropylene/montmorillonite nanocomposites. Review of the synthetic routes and materials properties. *Chem Mater* 13(10):3516–3523. <https://doi.org/10.1021/cm0110627>
95. Fornes TD, Paul DR (2003) Modeling properties of nylon 6/clay nanocomposites using composite theories. *Polymer* 44(17):4993–5013. [https://doi.org/10.1016/S0032-3861\(03\)00471-3](https://doi.org/10.1016/S0032-3861(03)00471-3)
96. Bharadwaj RK (2001) Modeling the barrier properties of polymer-layered silicate nanocomposites. *Macromolecules* 34(26):9189–9192. <https://doi.org/10.1021/ma010780b>
97. Martínez-Hermosilla GA, Mesic B, Bronlund JE (2015) A review of thermoplastic composites vapour permeability models: applicability for barrier dispersion coatings. *Packag Technol Sci* 28(7):565–578. <https://doi.org/10.1002/pts.2125>
98. Ellis TS, D'Angelo JS (2003) Thermal and mechanical properties of a polypropylene nanocomposite. *J Appl Polym Sci* 90(6):1639–1647. <https://doi.org/10.1002/app.12830>
99. Gorrasí G, Tortora M, Vittoria V et al (2003) Transport properties of organic vapors in nanocomposites of organophilic layered silicate and syndiotactic polypropylene. *Polymer* 44(13):3679–3685. [https://doi.org/10.1016/S0032-3861\(03\)00284-2](https://doi.org/10.1016/S0032-3861(03)00284-2)
100. Gómez M, Bracho D, Palza H et al (2015) Effect of morphology on the permeability, mechanical and thermal properties of polypropylene/SiO₂ nanocomposites. *Polym Int* 64(9):1245–1251. <https://doi.org/10.1002/pi.4909>

101. Tang Y, Hu Y, Song L et al (2003) Preparation and thermal stability of polypropylene/montmorillonite nanocomposites. *Polym Degrad Stab* 82(1):127–131. [https://doi.org/10.1016/S0141-3910\(03\)00173-3](https://doi.org/10.1016/S0141-3910(03)00173-3)
102. Wang L, He X, Wilkie CA (2010) The utility of nanocomposites in fire retardancy. *Materials* 3(9):4580–4606. <https://doi.org/10.3390/ma3094580>
103. Wagenknecht U, Kretzschmar B, Reinhardt G (2003) Investigations of fire retardant properties of polypropylene-clay-nanocomposites. *Macromol Symp* 194(1):207–212. <https://doi.org/10.1002/masy.200390084>
104. Gilman JW, Jackson CL, Morgan AB et al (2000) Flammability properties of polymer – layered-silicate nanocomposites. Polypropylene polystyrene nanocomposites. *Chem Mater* 12(7):1866–1873. <https://doi.org/10.1021/cm0001760>
105. Arao Y (2015) Flame retardancy of polymer nanocomposite. In: Visakh PM, Arao Y (eds) *Flame retardants: polymer blends, composites and nanocomposites*. Engineering Materials. Springer International Publishing, Cham, pp 15–44. https://doi.org/10.1007/978-3-319-03467-6_2
106. Le Bras M, Bourbigot S (1999) Intumescent fire retardant polypropylene formulations. In: Karger-Kocsis J (ed) *Polypropylene: an A-Z reference*. Polymer Science and Technology Series, vol 2. Springer Netherlands, Dordrecht, pp 357–365. https://doi.org/10.1007/978-94-011-4421-6_51
107. Tang Y, Hu Y, Wang S et al (2003) Intumescent flame retardant–montmorillonite synergism in polypropylene-layered silicate nanocomposites. *Polym Int* 52(8):1396–1400. <https://doi.org/10.1002/pi.1270>
108. Manikantan MR, Varadharaju N (2011) Preparation and properties of polypropylene-based nanocomposite films for food packaging. *Packag Technol Sci* 24(4):191–209. <https://doi.org/10.1002/pts.925>
109. Garcés JM, Moll DJ, Bicerano J et al (2000) Polymeric nanocomposites for automotive applications. *Adv Mater* 12(23):1835–1839. [https://doi.org/10.1002/1521-4095\(200012\)12:23%3c1835:AID-ADMA1835%3e3.0.CO;2-T](https://doi.org/10.1002/1521-4095(200012)12:23%3c1835:AID-ADMA1835%3e3.0.CO;2-T)
110. Utracki LA (1987) Present and future trends in polymer blends technology. *Int Polym Process* 2(1):3–12. <https://doi.org/10.3139/217.870003>
111. Lutz A, Harmia T (1999) Impregnation techniques for fiber bundles or tows. In: Karger-Kocsis J (ed) *Polypropylene: an A-Z reference*, vol 2. Springer Netherlands, Dordrecht, pp 301–306. https://doi.org/10.1007/978-94-011-4421-6_43
112. Uawongsuwan P, Yang Y, Hamada H (2015) Long jute fiber-reinforced polypropylene composite: effects of jute fiber bundle and glass fiber hybridization. *J Appl Polym Sci* 132(15). <https://doi.org/10.1002/app.41819>
113. Hawley RC, Jones RF (2005) In-line compounding of long-fiber thermoplastics for injection molding. *J Thermoplast Compos Mater* 18(5):459–464. <https://doi.org/10.1177/0892705705054413>
114. Yan X, Shen H, Yu L et al (2017) Polypropylene–glass fiber/basalt fiber hybrid composites fabricated by direct fiber feeding injection molding process. *J Appl Polym Sci* 134(44):45472. <https://doi.org/10.1002/app.45472>
115. Bourban P-E, Manson J-A (1999) Integrated manufacturing. In: Karger-Kocsis J (ed) *Polypropylene: an A-Z reference*, vol 2. Springer Netherlands, Dordrecht, pp 341–347. https://doi.org/10.1007/978-94-011-4421-6_49
116. Carneiro OS, Silva AF, Gomes R (2015) Fused deposition modeling with polypropylene. *Mater Des* 83:768–776. <https://doi.org/10.1016/j.matdes.2015.06.053>
117. Milosevic M, Stoof D, Pickering K (2017) Characterizing the mechanical properties of fused deposition modelling natural fiber recycled polypropylene composites. *J Compos Sci* 1(1):7. <https://doi.org/10.3390/jcs1010007>
118. Yang C, Huang H-X, Li K (2010) Investigation of fiber orientation states in injection-compression molded short-fiber-reinforced thermoplastics. *Polym Compos* 31(11):1899–1908. <https://doi.org/10.1002/pc.20986>

119. Giusti R, Zanini F, Lucchetta G (2018) Automatic glass fiber length measurement for discontinuous fiber-reinforced composites. *Compos Part A: Appl Sci Manuf* 112:263–270. <https://doi.org/10.1016/j.compositesa.2018.06.016>
120. Inoue A, Morita K, Tanaka T et al (2015) Effect of screw design on fiber breakage and dispersion in injection-molded long glass-fiber-reinforced polypropylene. *J Compos Mater* 49(1):75–84. <https://doi.org/10.1177/0021998313514872>
121. Vaxman A, Narkis M, Siegmann A et al (2012) Short-fiber thermoplastics composites: fiber fracture during melt processing. In: Nicolais L (ed) *Wiley encyclopedia of composites*. Wiley, New York. <https://doi.org/10.1002/9781118097298.weoc225>
122. Barbosa SE, Kenny JM (1999) Processing of short fiber reinforced polypropylene. II: statistical study of the effects of processing conditions on the impact strength. *Polym Eng Sci* 39(10):1880–1890. <https://doi.org/10.1002/pen.11581>
123. Puch F, Hopmann C (2015) Experimental investigation of the influence of the compounding process and the composite composition on the mechanical properties of a short flax fiber-reinforced polypropylene composite. *Polym Compos* 36(12):2282–2290. <https://doi.org/10.1002/pc.23141>
124. Nalini R, Kristiina O, Nayak SK et al (2016) Effect of long fiber thermoplastic extrusion process on fiber dispersion and mechanical properties of viscose fiber/polypropylene composites. *Polym Adv Technol* 27(5):685–692. <https://doi.org/10.1002/pat.3742>
125. Phelps JH, Abd El-Rahman AI, Kunc V et al (2013) A model for fiber length attrition in injection-molded long-fiber composites. *Compos Part A: Appl Sci Manuf* 51:11–21. <https://doi.org/10.1016/j.compositesa.2013.04.002>
126. Kmetty Á, Bárány T, Karger-Kocsis J (2012) Injection moulded all-polypropylene composites composed of polypropylene fibre and polypropylene based thermoplastic elastomer. *Compos Sci Technol* 73:72–80. <https://doi.org/10.1016/j.compscitech.2012.09.017>
127. Kmetty Á, Tábi T, Kovács JG et al (2013) Development and characterisation of injection moulded, all-polypropylene composites. *Express Polym Lett* 7(2):134–145. <https://doi.org/10.3144/expresspolymlett.2013.13>
128. Karger-Kocsis J, Friedrich K (1989) Effect of skin-core morphology on fatigue crack propagation in injection moulded polypropylene homopolymer. *Int J Fatigue* 11(3):161–168. [https://doi.org/10.1016/0142-1123\(89\)90435-0](https://doi.org/10.1016/0142-1123(89)90435-0)
129. Tadmor Z (1974) Molecular orientation in injection molding. *J Appl Polym Sci* 18(6):1753–1772. <https://doi.org/10.1002/app.1974.070180614>
130. Rose W (1961) Fluid-fluid interfaces in steady motion. *Nature* 191:242. <https://doi.org/10.1038/191242a0>
131. Hegler RP, Mennig G, Schmauch C (1987) Phase separation effects in processing of glass-bead- and glass-fiber-filled thermoplastics by injection molding. *Adv Polym Technol* 7(1):3–20. <https://doi.org/10.1002/adv.1987.060070102>
132. Karger-Kocsis J (1989) Chapter 6—Microstructure and fracture mechanical performance of short-fibre reinforced thermoplastics. In: Friedrich K (ed) *Composite Materials Series*, vol 6. Elsevier, pp 189–247. <https://doi.org/10.1016/b978-0-444-87286-9.50010-3>
133. Karger-Kocsis J, Friedrich K (1988) Fracture behavior of injection-molded short and long glass fiber—polyamide 6.6 composites. *Compos Sci Technol* 32(4):293–325. [https://doi.org/10.1016/0266-3538\(88\)90067-x](https://doi.org/10.1016/0266-3538(88)90067-x)
134. Spahr DE, Friedrich K, Schultz JM et al (1990) Microstructure and fracture behaviour of short and long fibre-reinforced polypropylene composites. *J Mater Sci* 25(10):4427–4439. <https://doi.org/10.1007/bf00581104>
135. Karger-Kocsis J (1995) Microstructural aspects of fracture in polypropylene and in its filled, chopped fiber and fiber mat reinforced composites. In: Karger-Kocsis J (ed) *Polypropylene structure, blends and composites*, vol 3. Springer Netherlands, Dordrecht, pp 142–201. https://doi.org/10.1007/978-94-011-0523-1_4
136. Clegg DW, Collyer AA (eds) (1986) *Mechanical properties of reinforced thermoplastics*. Springer, Netherlands. <https://doi.org/10.1007/978-94-009-4193-9>

137. Garcea SC, Wang Y, Withers PJ (2018) X-ray computed tomography of polymer composites. *Compos Sci Technol* 156:305–319. <https://doi.org/10.1016/j.compscitech.2017.10.023>
138. Köpplmayr T, Milosavljevic I, Aigner M et al (2013) Influence of fiber orientation and length distribution on the rheological characterization of glass-fiber-filled polypropylene. *Polym Test* 32(3):535–544. <https://doi.org/10.1016/j.polymertesting.2013.02.002>
139. Alemdar A, Zhang H, Sain M et al (2008) Determination of fiber size distributions of injection moulded polypropylene/natural fibers using X-ray microtomography. *Adv Eng Mater* 10(1–2):126–130. <https://doi.org/10.1002/adem.200700232>
140. Hanneschläger C, Revol V, Plank B et al (2015) Fibre structure characterisation of injection moulded short fibre-reinforced polymers by X-ray scatter dark field tomography. *Case Stud Nondestr Test Eval* 3:34–41. <https://doi.org/10.1016/j.csdnt.2015.04.001>
141. Fischer G, Eyerer P (1988) Measuring spatial orientation of short fiber reinforced thermoplastics by image analysis. *Polym Compos* 9(4):297–304. <https://doi.org/10.1002/pc.750090409>
142. Hermans PH (1946) Contributions to the physics of cellulose fibres. *J Polym Sci.* (Elsevier, New York). <https://doi.org/10.1002/pol.1947.120020321>
143. Pipes BR, McCullough RL, Taggart DG (1982) Behavior of discontinuous fiber composites: fiber orientation. *Polym Compos* 3(1):34–39. <https://doi.org/10.1002/pc.750030107>
144. Krenchel H (1964) Fibre reinforcement: theoretical and practical investigations of the elasticity and strength of fibre-reinforced materials. Akademisk Forlag, Copenhagen
145. Advani SG, Tucker CL (1987) The use of tensors to describe and predict fiber orientation in short fiber composites. *J Rheol* 31(8):751–784. <https://doi.org/10.1122/1.549945>
146. Friedrich K (1985) Microstructural efficiency and fracture toughness of short fiber/thermoplastic matrix composites. *Compos Sci Technol* 22(1):43–74. [https://doi.org/10.1016/0266-3538\(85\)90090-9](https://doi.org/10.1016/0266-3538(85)90090-9)
147. Hull D (1981) An introduction to composite materials. Cambridge University Press, Cambridge
148. Bader MG, Hill AR (1993) Short fiber composites. In: Chou T-W (ed) *Materials science and technology*. VCH, Weinheim, pp 293–338. <https://doi.org/10.1002/maco.19940450218>
149. Fu S-Y, Lauke B, Mai Y-W (2009) Science and engineering of short fibre reinforced polymer composites. CRC Press
150. Cox HL (1952) The elasticity and strength of paper and other fibrous materials. *Br J Appl Phys* 3(3):72. <https://doi.org/10.1088/0508-3443/3/3/302>
151. Kelly A, Tyson WR (1965) Tensile properties of fibre-reinforced metals: copper/tungsten and copper/molybdenum. *J Mech Phys Solids* 13(6):329–336. [https://doi.org/10.1016/0022-5096\(65\)90035-9](https://doi.org/10.1016/0022-5096(65)90035-9)
152. Thomason JL (1999) Mechanical and thermal properties of long glass fiber reinforced polypropylene. In: Karger-Kocsis J (ed) *Polypropylene: an A-Z reference*, vol 2. Springer Netherlands, Dordrecht, pp 407–414. https://doi.org/10.1007/978-94-011-4421-6_57
153. Bowyer WH, Bader MG (1972) On the re-inforcement of thermoplastics by imperfectly aligned discontinuous fibres. *J Mater Sci* 7(11):1315–1321. <https://doi.org/10.1007/bf00550698>
154. Bowyer WH, Bader MG (1972) Reinforcement of thermoplastics using carbon fibres. *Faraday Special Discuss Chem Soc* 2:165–173. <https://doi.org/10.1039/S19720200165>
155. Affdl JCH, Kardos JL (1976) The Halpin-Tsai equations: a review. *Polym Eng Sci* 16(5):344–352. <https://doi.org/10.1002/pen.760160512>
156. Garesci F, Fliegner S (2013) Young's modulus prediction of long fiber reinforced thermoplastics. *Compos Sci Technol* 85:142–147. <https://doi.org/10.1016/j.compscitech.2013.06.009>
157. Yaghoobi H, Fereidoon A (2018) Modeling and optimization of tensile strength and modulus of polypropylene/kenaf fiber biocomposites using Box-Behnken response surface method. *Polym Compos* 39(S1):E463–E479. <https://doi.org/10.1002/pc.24596>

158. Hoecker F, Karger-Kocsis J (1993) Effects of crystallinity and supermolecular formations on the interfacial shear strength and adhesion in GF/PP composites. *Polym Bull* 31(6):707–714. <https://doi.org/10.1007/BF00300131>
159. Etaati A, Pather S, Cardona F et al (2016) Injection molded noil hemp fiber composites: interfacial shear strength, fiber strength, and aspect ratio. *Polym Compos* 37(1):213–220. <https://doi.org/10.1002/pc.23172>
160. Karger-Kocsis J, Czirágy T (1998) Effects of interphase on the fracture and failure behavior of knitted fabric reinforced composites produced from commingled GF/PP yarn. *Compos Part A: Appl Sci Manuf* 29A:1319–1330. [https://doi.org/10.1016/S1359-835X\(98\)00042-6](https://doi.org/10.1016/S1359-835X(98)00042-6)
161. Wu C-M, Chen M, Karger-Kocsis J (1998) Transcrystallization in syndiotactic polypropylene induced by high-modulus carbon fibers. *Polym Bull* 41(2):239–245. <https://doi.org/10.1007/s002890050357>
162. Sanadi AR, Caulfield DF (2000) Transcrystalline interphases in natural fiber-PP composites: effect of coupling agent. *Compos Interfaces* 7(1):31–43. <https://doi.org/10.1163/156855400300183560>
163. Abraham TN, Wanjale SD, Bárány T et al (2009) Tensile mechanical and perforation impact behavior of all-PP composites containing random PP copolymer as matrix and stretched PP homopolymer as reinforcement: effect of β nucleation of the matrix. *Compos Part A: Appl Sci Manuf* 40(5):662–668. <https://doi.org/10.1016/j.compositesa.2009.03.001>
164. Karger-Kocsis J (2000) Interphase with lamellar interlocking and amorphous adherent—a model to explain effects of transcrystallinity. *Adv Compos Lett* 9(2):225–227
165. Pickering KL, Efendy MGA, Le TM (2016) A review of recent developments in natural fibre composites and their mechanical performance. *Compos Part A: Appl Sci Manuf* 83:98–112. <https://doi.org/10.1016/j.compositesa.2015.08.038>
166. Fu S-Y, Lauke B, Mäder E et al (2001) Hybrid effects on tensile properties of hybrid short-glass-fiber-and short-carbon-fiber-reinforced polypropylene composites. *J Mater Sci* 36(5):1243–1251. <https://doi.org/10.1023/a:1004802530253>
167. Ranganathan N, Oksman K, Nayak SK et al (2015) Regenerated cellulose fibers as impact modifier in long jute fiber reinforced polypropylene composites: effect on mechanical properties, morphology, and fiber breakage. *J Appl Polym Sci* 132(3). <https://doi.org/10.1002/app.41301>
168. Hartl AM, Jerabek M, Lang RW (2015) Anisotropy and compression/tension asymmetry of PP containing soft and hard particles and short glass fibers. *Express Polym Lett* 9(7):658–670. <https://doi.org/10.3144/expresspolymlett.2015.61>
169. Diego P, Alessandro P, Kyriaki K (2015) Synergistic effect of graphite nanoplatelets and glass fibers in polypropylene composites. *J Appl Polym Sci* 132(12). <https://doi.org/10.1002/app.41682>
170. Cui-Cui W, Yue-Ying Z, He-Yi G et al (2018) Enhanced mechanical and thermal properties of short carbon fiber reinforced polypropylene composites by graphene oxide. *Polym Compos* 39(2):405–413. <https://doi.org/10.1002/pc.23950>
171. Atkins AG, Mai YW (1988) Elastic and plastic fracture: metals, polymers, ceramics, composites, biological materials. Ellis Horwood, Chichester
172. Gsellmann W, Seidler S (eds) (2013) Polymer testing, 2nd edn. Hanser Publishers, Munich
173. Karger-Kocsis J (1993) Microstructure-fracture toughness relationship of short fiber-reinforced PP homopolymer and PP/elastomer blends. *J Polym Eng* 12(1–2):77–108. <https://doi.org/10.1515/POLYENG.1993.12.1-2.77>
174. Karger-Kocsis J (1993) Instrumented impact fracture and related failure behavior in short-and long-glass-fiber-reinforced polypropylene. *Compos Sci Technol* 48(1–4):273–283. [https://doi.org/10.1016/0266-3538\(93\)90144-6](https://doi.org/10.1016/0266-3538(93)90144-6)
175. Karger-Kocsis J (1993) Instrumented impact fracture and related failure behavior in short-and long-glass-fiber-reinforced polypropylene. *Compos Sci Technol* 48(1):273–283. [https://doi.org/10.1016/0266-3538\(93\)90144-6](https://doi.org/10.1016/0266-3538(93)90144-6)

176. Nouri H, Meraghni F, Lory P (2009) Fatigue damage model for injection-molded short glass fibre reinforced thermoplastics. *Int J Fatigue* 31(5):934–942. <https://doi.org/10.1016/j.ijfatigue.2008.10.002>
177. Pegoretti A, Ricco T (1999) Fatigue crack propagation in polypropylene reinforced with short glass fibres. *Compos Sci Technol* 59(7):1055–1062. [https://doi.org/10.1016/S0266-3538\(98\)00143-2](https://doi.org/10.1016/S0266-3538(98)00143-2)
178. Karger-Kocsis J, Friedrich K, Bailey RS (1991) Fatigue and failure behavior of short and long glass fiber reinforced injection-molded polypropylene. *Sci Eng Compos Mater* 2(1):49–68. <https://doi.org/10.1515/SECM.1991.2.1.49>
179. Karger-Kocsis J, Friedrich K, Bailey RS (1991) Fatigue crack propagation in short and long glass fiber reinforced injection-molded polypropylene composites. *Adv Compos Mater* 1(2):103–121. <https://doi.org/10.1163/156855191X00225>
180. Pegoretti A, Ricco T (2000) Fatigue fracture of neat and short glass fiber reinforced polypropylene: effect of frequency and material orientation. *J Compos Mater* 34(12):1009–1027. <https://doi.org/10.1177/002199830003401203>
181. Karger-Kocsis J (2004) In: Moore DR (ed) *the application of fracture mechanics to polymers, adhesive and composites* (European Structural Integrity Society), vol 33, 1st edn. Elsevier, Amsterdam, pp 233–239
182. Vas LM, Bakonyi P (2012) Estimating the creep strain to failure of PP at different load levels based on short term tests and Weibull characterization. *Express Polym Lett* 6:987–996. <https://doi.org/10.3144/expresspolymlett.2012.104>
183. Achereiner F, Engelsing K, Bastian M et al (2013) Accelerated creep testing of polymers using the stepped isothermal method. *Polym Test* 32(3):447–454. <https://doi.org/10.1016/j.polymertesting.2013.01.014>
184. Houshyar S, Shanks RA, Hodzic A (2005) Tensile creep behaviour of polypropylene fibre reinforced polypropylene composites. *Polym Test* 24(2):257–264. <https://doi.org/10.1016/j.polymertesting.2004.07.003>
185. Vas LM, Bakonyi P (2013) Creep failure strain estimation of glass fibre/polypropylene composites based on short-term tests and Weibull characterisation. *J Reinf Plast Compos* 32(1):34–41. <https://doi.org/10.1177/0731684412453513>
186. Williams ML, Landel RF, Ferry JD (1955) The temperature dependence of relaxation mechanisms in amorphous polymers and other glass-forming liquids. *J Am Chem Soc* 77(14):3701–3707. <https://doi.org/10.1021/ja01619a008>
187. Karger-Kocsis J (2012) Structure and fracture mechanics of injection-molded composites. In: Nicolais L (ed) *Wiley encyclopedia of composites*. Wiley, New York, pp 2939–2952
188. Wetherhold RC (2012) Short-fiber-reinforced polymeric composites: structure–property relations. In: Nicolais L (ed) *Wiley encyclopedia of composites*. Wiley, pp 1–8. <https://doi.org/10.1002/9781118097298.weoc224>
189. Advani SG (2012) Molding: short-fiber composites, flow processing. In: Nicolais L (ed) *Wiley encyclopedia of composites*. Wiley, New York, pp 1–12. <https://doi.org/10.1002/9781118097298.weoc154>
190. Wang Z, Smith DE (2018) Rheology effects on predicted fiber orientation and elastic properties in large scale polymer composite additive manufacturing. *J Compos Sci* 2(1):18. <https://doi.org/10.3390/jcs2010010>
191. Ausias G, Agassant J-F, Vincent M et al (1992) Rheology of short glass-fiber reinforced polypropylene. *J Rheol* 36(4):525–542. <https://doi.org/10.1122/1.550362>
192. Matsuoka T (1999) Warpage and its prediction in injection-molded parts. In: Karger-Kocsis J (ed) *Polypropylene: an A-Z reference*, vol 2. Springer Netherlands, Dordrecht, pp 859–865. https://doi.org/10.1007/978-94-011-4421-6_117
193. Diez-Pascual AM, Naffakh M (2013) Polypropylene/glass fiber hierarchical composites incorporating inorganic fullerene-like nanoparticles for advanced technological applications. *ACS Appl Mater Interfaces* 5(19):9691–9700. <https://doi.org/10.1021/am402750t>

194. Djamila K, Ahmed K, Ghezalla T et al (2018) Tensile properties, thermal conductivity, and thermal stability of short carbon fiber reinforced polypropylene composites. *Polym Compos* 39(S2):E664–E670. <https://doi.org/10.1002/pc.24093>
195. Chen C-H, Wang Y-C (1996) Effective thermal conductivity of misoriented short-fiber reinforced thermoplastics. *Mech Mater* 23(3):217–228. [https://doi.org/10.1016/0167-6636\(96\)00010-5](https://doi.org/10.1016/0167-6636(96)00010-5)
196. Kumlutas D, Tavman IH (2006) A numerical and experimental study on thermal conductivity of particle filled polymer composites. *J Thermoplast Compos Mater* 19(4):441–455. <https://doi.org/10.1177/0892705706062203>
197. Vuorinen E, Nhlapo N, Mafa T et al (2013) Thermooxidative degradation of LDPE nanocomposites: effect of surface treatments of fumed silica and boehmite alumina. *Polym Degrad Stab* 98(11):2297–2305. <https://doi.org/10.1016/j.polyimdegradstab.2013.08.011>
198. Bellucci F, Camino G (2012) Flammability of polymer composites. In: Nicolais L (ed) *Wiley encyclopedia of composites*. Wiley, New York, p 17. <https://doi.org/10.1002/9781118097298.weoc091>
199. Bourbigot S, Bras ML, Delobel R (1999) Flame-retardant polypropylene compositions. In: Karger-Kocsis J (ed) *Polypropylene: an A-Z reference*, vol 2. Springer Netherlands, Dordrecht, pp 254–263. https://doi.org/10.1007/978-94-011-4421-6_35
200. S-l Du, X-b Lin, R-k Jian et al (2015) Flame-retardant wrapped ramie fibers towards suppressing “candlewick effect” of polypropylene/ramie fiber composites. *Chin J Polym Sci* 33(1):84–94. <https://doi.org/10.1007/s10118-015-1560-z>
201. Vadas D, Kmetty Á, Bárány T et al (2018) Flame retarded self-reinforced polypropylene composites prepared by injection moulding. *Polym Adv Technol* 29(1):433–441. <https://doi.org/10.1002/pat.4132>
202. Yeetsorn R, Fowler MW, Tzoganakis C (2011) A review of thermoplastic composites for bipolar plate materials in PEM fuel cells In: Cuppoletti J (ed) *Nanocomposites with unique properties and applications in medicine and industry*, InTech, pp 317–344. <https://doi.org/10.5772/19262>
203. Hsieh C-T, Pan Y-J, Lin J-H (2017) Polypropylene/high-density polyethylene/carbon fiber composites: manufacturing techniques, mechanical properties, and electromagnetic interference shielding effectiveness. *Fibers Polym* 18(1):155–161. <https://doi.org/10.1007/s12221-017-6371-0>
204. Huang C-L, Lou C-W, Liu C-F et al (2015) Polypropylene/graphene and polypropylene/carbon fiber conductive composites: mechanical, crystallization and electromagnetic properties. *Appl Sci* 5(4):1196–1210. <https://doi.org/10.3390/app5041196>
205. Krause B, Pötschke P (2015) Electrical and thermal conductivity of polypropylene filled with combinations of carbon fillers. In: *Regional Conference Graz 2015—Polymer Processing Society PPS*, Graz, 21–25 September 2015. AIP Conference Proceedings, pp 040003-040001. <https://doi.org/10.1063/1.4965494>
206. Kalay G, Bevis MJ (1999) Application of shear-controlled orientation in injection molding of isotactic polypropylene. In: Karger-Kocsis J (ed) *Polypropylene: an A-Z reference*, vol 2. Springer Netherlands, Dordrecht, pp 38–46. https://doi.org/10.1007/978-94-011-4421-6_6
207. Wang J, Geng C, Luo F et al (2011) Shear induced fiber orientation, fiber breakage and matrix molecular orientation in long glass fiber reinforced polypropylene composites. *Mater Sci Eng, A* 528(7):3169–3176. <https://doi.org/10.1016/j.msea.2010.12.081>
208. Fisa B, Meddad A (1999) Weldlines. In: Karger-Kocsis J (ed) *Polypropylene: an A-Z reference*, vol 2. Springer Netherlands, Dordrecht, pp 874–881. https://doi.org/10.1007/978-94-011-4421-6_119
209. Tomioka M, Ishikawa T, Okuyama K et al (2017) Recycling of carbon-fiber-reinforced polypropylene prepreg waste based on pelletization process. *J Compos Mater* 51(27):3847–3858. <https://doi.org/10.1177/0021998317694423>
210. Meng F, McKechnie J, Pickering SJ (2018) An assessment of financial viability of recycled carbon fibre in automotive applications. *Compos Part A* 109:207–220. <https://doi.org/10.1016/j.compositesa.2018.03.011>

211. Karger-Kocsis J (1999) Glass mat reinforced thermoplastic polypropylene. In: Karger-Kocsis J (ed) *Polypropylene: an A-Z Reference*. Polymer Science and Technology Series, vol 2. Springer Netherlands, pp 284–290. <https://doi.org/10.1007/978-94-011-4421-6>
212. N/A (1968) Carbide, PPG form G.R.T.L. to make thermoplastic sheet. *Chemical & Engineering News* 46:15. <https://doi.org/10.1021/cen-v046n004.p015>
213. Shah DU (2013) Developing plant fibre composites for structural applications by optimising composite parameters: a critical review. *J Mater Sci* 48:6083–6107. <https://doi.org/10.1007/s10853-013-7458-7>
214. Kurcz M, Baser B, Dittmar H et al (2005) A case for replacing steel with glass-mat thermoplastic composites in spare-wheel well application. <https://doi.org/10.4271/2005-01-1678>
215. Schemme M (2008) LFT—development status and perspectives. *Reinf Plast* 52(32–34):36–39. [https://doi.org/10.1016/S0034-3617\(08\)70036-5](https://doi.org/10.1016/S0034-3617(08)70036-5)
216. Okzman K (2000) Mechanical properties of natural fibre mat reinforced thermoplastic. *Appl Compos Mater* 7(5):403–414. <https://doi.org/10.1023/a:1026546426764>
217. Bárány T, Karger-Kocsis J, Czigány T (2006) Development and characterization of self-reinforced poly(propylene) composites: carded mat reinforcement. *Polym Adv Technol* 17:818–824. <https://doi.org/10.1002/pat.813>
218. Bárány T, Izer A, Czigány T (2006) On consolidation of self-reinforced polypropylene composites. *Plast, Rubber Compos* 35(9):375–379
219. Karger-Kocsis J (2000) Swirl mat- and long discontinuous fiber mat-reinforced polypropylene composites—status and future trends. *Polym Compos* 221(4):514–522. <https://doi.org/10.1002/pc.10206>
220. Benevolenski OI, Karger-Kocsis J, Czigány T et al (2003) Mode I fracture resistance of glass fiber mat-reinforced polypropylene composites at various degree of consolidation. *Compos Part A: Appl Sci Manuf* 34(3):267–273. [https://doi.org/10.1016/S1359-835X\(02\)00045-3](https://doi.org/10.1016/S1359-835X(02)00045-3)
221. Raghavendran V, Haque E (2001) Development of low density GMT headliners with improved acoustic performance. In: *Automotive Composites Conference*, Troy, MI, p 7, 19–20 Sept 2001
222. Roch A, Huber T, Henning F et al (2014) LFT foam—lightweight potential for semi-structural components through the use of long-glass-fiber-reinforced thermoplastic foams. In: Altstädt V, Keller J-H, Fathi A (eds) *29th International Conference of the Polymer Processing Society*, Nuremberg, Germany. AIP Publishing LLC, pp 471–476. <https://doi.org/10.1063/1.4873824>
223. Roch A, Menrath A, Huber T et al (2013) Lightweight potential of fiber-reinforced foams. *Cell Polym* 32(4):213–227
224. Bos HL, Müssig J, van den Oevera MJA (2006) Mechanical properties of short-flax-fibre reinforced compounds. *Compos Part A: Appl Sci Manuf* 37:1591–1604. <https://doi.org/10.1016/j.compositesa.2005.10.011>
225. <http://www.hanwhaus.com/html/gmt.html>. Accessed 27 Mar 2018
226. Knox MP (2001) Continuous fiber reinforced thermoplastic composites in the automotive industry. In: *Automotive Composites Conference*, Troy, MI, p 5, 19–21 Sept 2001
227. Caba AC (2005) Characterization of carbon mat thermoplastic composites: flow and mechanical properties. PhD Thesis. Virginia Polytechnic Institute and State University
228. Karger-Kocsis J, Harmia T, Czigány T (1995) Comparison of the fracture and failure behavior of polypropylene composites reinforced by long glass fibers and by glass mats. *Compos Sci Technol* 54(3):287–298. [https://doi.org/10.1016/0266-3538\(95\)00068-2](https://doi.org/10.1016/0266-3538(95)00068-2)
229. Karger-Kocsis J, Fejes-Kozma ZS (1994) Failure mode and damage zone development in a GMT-PP by acoustic emission and thermography. *J Reinf Plast Compos* 13(9):768–792. <https://doi.org/10.1177/073168449401300901>
230. Karger-Kocsis J (1993) Fracture mechanical characterization and damage zone development in glass fiber mat-reinforced thermoplastics. *Polym Bull* 31(2):235–241. <https://doi.org/10.1007/bf00329971>

231. Benevolenski OI, Karger-Kocsis J (2001) Comparative study of the fracture behavior of flow-molded GMT-PP with random and chopped-fiber mats. *Compos Sci Technol* 61 (16):2413–2423. [https://doi.org/10.1016/S0266-3538\(01\)00160-9](https://doi.org/10.1016/S0266-3538(01)00160-9)
232. Bourmaud A, Fazzini M, Renouard N et al (2018) Innovating routes for the reused of PP-flax and PP-glass non woven composites: a comparative study. *Polym Degrad Stab* 152:259–271. <https://doi.org/10.1016/j.polyimdegradstab.2018.05.006>
233. Davies P, Manson J-AE (1993) Rheological properties of stampable thermoplastic composites. *J Thermoplast Compos Mater* 6:239–254. <https://doi.org/10.1177/089270579300600305>
234. Davis SM, Mcalea KP (1990) Stamping rheology of glass mat reinforced thermoplastic composites. *Polym Compos* 11(6):368–378. <https://doi.org/10.1002/pc.750110610>
235. Kotsikos G, Bland JH, Gibson AG (1996) Squeeze flow testing of glass mat thermoplastic material. *Compos Part A* 27 A:1195–1200. [https://doi.org/10.1016/1359-835x\(96\)00077-2](https://doi.org/10.1016/1359-835x(96)00077-2)
236. Kotsikos G, Bland JH, Gibson AG (1999) Rheological characterization of commercial glass mat thermoplastics (GMTs) by squeeze flow testing. *Polym Compos* 20(1):114–123. <https://doi.org/10.1002/pc.10339>
237. Dweib MA, Brádaigh CMÓ (1998) Anisotropic modeling of isothermal squeezing flow of glass-mat reinforced thermoplastics (GMT). *Polym Compos* 19(5):588–599. <https://doi.org/10.1002/pc.10132>
238. Dweib MA, Brádaigh CMÓ (1999) Extensional and shearing flow of a glass-mat-reinforced thermoplastics (GMT) material as a non-Newtonian viscous Fluid. *Compos Sci Technol* 59:1399–1410. [https://doi.org/10.1016/S0266-3538\(98\)00182-1](https://doi.org/10.1016/S0266-3538(98)00182-1)
239. Gibson AG, Kotsikos G, Bland JH et al (1998) Squeeze flow In: Collyer AA, Clegg DW (eds) *Rheological measurement*. Springer, Dordrecht, p 779. <https://doi.org/10.1007/978-94-011-4934-1>
240. Dasappa P, Lee-Sullivan P, Xiao X (2009) Temperature effect on creep behavior of continuous fiber GMT composites. *Compos Part A: Appl Sci Manuf* 40:1071–1081. <https://doi.org/10.1016/j.compositesa.2009.04.026>
241. Czigány T, Marosfalvi J, Karger-Kocsis J (2000) An acoustic emission study of the temperature-dependent fracture behavior of polypropylene composites reinforced by continuous and discontinuous fiber mats. *Compos Sci Technol* 60(8):1203–1212. [https://doi.org/10.1016/S0266-3538\(00\)00059-2](https://doi.org/10.1016/S0266-3538(00)00059-2)
242. Biro DA, Pleizier G, Deslandes Y (1992) Application of the microbond technique. 3. Effects of plasma treatment on the ultra-high modulus polyethylene fiber epoxy interface. *J Mater Sci Lett* 11(10):698–701
243. Vanclooster K, Lomov SV, Vespoest I (2008) Investigation of interply shear in composite forming. In: *The 11th International ESAFORM Conference on Material Forming*, Lyon, France. Springer, Heidelberg, 23–25 April 2008
244. Mitschang P, Blinzler M, Woginger A (2003) Processing technologies for continuous fibre reinforced thermoplastics with novel polymer blends. *Compos Sci Technol* 63:2099–2110. [https://doi.org/10.1016/S0266-3538\(03\)00107-6](https://doi.org/10.1016/S0266-3538(03)00107-6)
245. Hine PJ, Ward IM, Jordan ND et al (2003) The hot compaction behaviour of woven oriented polypropylene fibres and tapes. I. Mechanical properties. *Polymer* 44(4):1117–1131
246. Ward IM, Hine PJ (2004) The science and technology of hot compaction. *Polymer* 45 (5):1413–1427. <https://doi.org/10.1016/j.polymer.2003.11.050>
247. Swolfs Y, Zhang Q, Baets J et al (2014) The influence of process parameters on the properties of hot compacted self-reinforced polypropylene composites. *Compos Pt A-Appl Sci Manuf* 65:38–46. <https://doi.org/10.1016/j.compositesa.2014.05.022>
248. Goodman KE, Loos AC (1990) Thermoplastic prepreg manufacture. *J Thermoplast Compos Mater* 3(1):34–40. <https://doi.org/10.1177/089270579000300104>
249. Turton CN, McAinsh J (1974) Thermoplastic compositions US3785916A Patent US3785916A, 1974-01-15
250. Iyer SR, Drzal LT (1990) Manufacture of powder-impregnated thermoplastic composites. *J Thermoplast Compos Mater* 3:325–355. <https://doi.org/10.1177/089270579000300404>

251. Sharma M, Bijwe J, Mitschang P (2011) Wear performance of PEEK–carbon fabric composites with strengthened fiber–matrix interface. *Wear* 271(9):2261–2268. <https://doi.org/10.1016/j.wear.2010.11.055>
252. Kim JW, Lee JS (2016) The effect of the melt viscosity and impregnation of a film on the mechanical properties of thermoplastic composites. *Materials* 9(6):448. <https://doi.org/10.3390/ma9060448>
253. Gibson AG, Manson J-A (1992) Impregnation technology for thermoplastic matrix composites. *Compos Manuf* 3(4):223–233. [https://doi.org/10.1016/0956-7143\(92\)90110-G](https://doi.org/10.1016/0956-7143(92)90110-G)
254. Hartness T, Husman G, Koenig J et al (2001) The characterization of low cost fiber reinforced thermoplastic composites produced by the DRIFT™ process. *Compos Part A: Appl Sci Manuf* 32(8):1155–1160. [https://doi.org/10.1016/S1359-835X\(01\)00061-6](https://doi.org/10.1016/S1359-835X(01)00061-6)
255. Connor M, Toll S, Manson J-AE et al (1995) A model for the consolidation of aligned thermoplastic powder impregnated composites. *J Thermoplast Compos Mater* 8:138–162. <https://doi.org/10.1177/089270579500800201>
256. Price RV (1970) Production of impregnated rovings. US3742106 Patent US3742106A
257. Astrom BT (1997) Thermoplastic composite sheet forming: materials and manufacturing techniques. In: Bhattacharyya D (ed) *Composite sheet forming*, vol 11. Elsevier, p 530
258. Wong CC, Long AC, Sherburn M et al (2006) Comparisons of novel and efficient approaches for permeability prediction based on the fabric architecture. *Compos Part A: Appl Sci Manuf* 37(6):847–857. <https://doi.org/10.1016/j.compositesa.2005.01.020>
259. Bird RB, Armstrong RC, Hassager O (eds) (1987) *Dynamics of polymeric fluids*, vol 1. Wiley Interscience, New York (Fluid Mechanics)
260. Gutowsky TG, Morigaki T, Cai Z (1987) The consolidation of laminate composites. *J Compos Mater* 21:172–188. <https://doi.org/10.1177/002199838702100207>
261. Wakeman MD, Cain TA, Rudd CD et al (1998) Compression moulding of glass and polypropylene composites for optimised macro- and micro- mechanical properties—I commingled glass and polypropylene. *Compos Sci Technol* 58(12):1879–1898. [https://doi.org/10.1016/S0266-3538\(98\)00011-6](https://doi.org/10.1016/S0266-3538(98)00011-6)
262. Svensson N, Shishoo R, Gilchrist M (1998) Manufacturing of thermoplastic composites from commingled yarns—a review. *J Thermoplast Compos Mater* 11:22–56. <https://doi.org/10.1177/089270579801100102>
263. Mäder E, Rausch J, Schmidt N (2008) Commingled yarns—processing aspects and tailored surfaces of polypropylene/glass composites. *Compos Part A: Appl Sci Manuf* 39(4):612–623. <https://doi.org/10.1016/j.compositesa.2007.07.011>
264. Wiegand N, Mäder E (2017) Commingled yarn spinning for thermoplastic/glass fiber composites. *Fibers* 5(26):1–15. <https://doi.org/10.3390/fib5030026>
265. Akonda MH, Lawrence CA, Weager BM (2012) Recycled carbon fibre-reinforced polypropylene thermoplastic composites. *Compos Part A* 43:79–86. <https://doi.org/10.1016/j.compositesa.2011.09.014>
266. Van West BP, Pipes BR, Keefe M et al (1991) The draping and consolidation of commingled fabrics. *Compos Manuf* 2(1):10–22. [https://doi.org/10.1016/0956-7143\(91\)90154-9](https://doi.org/10.1016/0956-7143(91)90154-9)
267. Van West BP, Pipes BR, Advani SG (1991) The consolidation of commingled thermoplastic fabrics. *Polym Compos* 2(6):417–427. <https://doi.org/10.1002/pc.750120607>
268. Alcock B, Cabrera NO, Barkoula NM et al (2007) The mechanical properties of woven tape all-polypropylene composites. *Compos Pt A-Appl Sci Manuf* 38(1):147–161
269. Peijs T (2003) Composites for recyclability. *Mater Today* 6(4):30–35
270. Grünwald J, Parlevliet P, Altstädt V (2017) Manufacturing of thermoplastic composite sandwich structures: a review of literature. *J Thermoplast Compos Mater* 30(4):437–464. <https://doi.org/10.1177/0892705715604681>
271. Liu D, Ding J, Fan X et al (2014) Non-isothermal forming of glass fiber/polypropylene commingled yarn fabric composites. *Mater Des* 57:608–615. <https://doi.org/10.1016/j.matdes.2014.01.027>

272. Bureau MN, Denault J (2004) Fatigue resistance of continuous glass fiber/polypropylene composites: consolidation dependence. *Compos Sci Technol* 64(12):1785–1794. <https://doi.org/10.1016/j.compscitech.2004.01.016>
273. Bernhardsson J, Shishoo R (2000) Effect of processing parameters on consolidation quality of GF/PP commingled yarn based composites. *J Thermoplast Compos Mater* 13:292–313. <https://doi.org/10.1177/089270570001300403>
274. Youssef Y, Denault J (1998) Thermoformed glass fiber reinforced polypropylene: microstructure, mechanical properties and residual stresses. *Polym Compos* 19(3):301–309. <https://doi.org/10.1002/pc.10103>
275. Trudel-Boucher D, Fisa B, Denault J et al (2006) Experimental investigation of stamp forming of unconsolidated commingled E-glass/polypropylene fabrics. *Compos Sci Technol* 66(3):555–570. <https://doi.org/10.1016/j.compscitech.2005.05.036>
276. Karger-Kocsis J, Czirágy T (1997) Interfacial effects on the dynamic mechanical behavior of weft-knitted glass fiber fabric-reinforced polypropylene composites produced of commingled yarns. Tensile and flexural response. *Appl Compos Mater* 4:209–218. <https://doi.org/10.1007/BF02481390>
277. Zhao N, Rödel H, Herzberg C et al (2009) Stitched glass/PP composite. Part I: tensile and impact properties. *Compos Part A: Appl Sci Manuf* 40(5):635–643. <https://doi.org/10.1016/j.compositesa.2009.02.019>
278. Lu Z, Gu H, Zhen Zhong L (2011) Study on the natural fiber/PP wrap spun yarns reinforced thermoplastic composites. *Adv Mater Res* 194–196:1470–1475. <https://doi.org/10.4028/www.scientific.net/AMR.194-196.1470>
279. Kim JW, Lee JS (2016) Influence of interleaved films on the mechanical properties of carbon fiber fabric/polypropylene thermoplastic composites. *Materials* 9(5):344. <https://doi.org/10.3390/ma9050344>
280. Russo P, Acierno D, Simeoli G et al (2013) Flexural and impact response of woven glass fiber fabric/polypropylene composites. *Compos Part B: Eng* 54:415–421. <https://doi.org/10.1016/j.compositesb.2013.06.016>
281. Scarponi C, Schiavoni E, Sanchez-Saez S et al (2012) Polypropylene/hemp fabric reinforced composites manufacturing and mechanical behavior. *J Biobased Mater Bioenergy* 6(4):361–369. <https://doi.org/10.1166/jbmb.2012.1245>
282. Okumura W, Hasebe H, Kimizu M et al (2013) Development of carbon fiber fabric reinforced polypropylenes. Part 1: effect of content of maleic acid and removal of sizing agent. *Sen'i Gakkaishi* 69(9):177–182. <https://doi.org/10.2115/fiber.69.177>
283. Bárány T, Izer A, Karger-Kocsis J (2009) Impact resistance of all-polypropylene composites composed of alpha and beta modifications. *Polym Test* 28(2):176–182. <https://doi.org/10.1016/j.polymertesting.2008.11.011>
284. Izer A, Bárány T, Varga J (2009) Development of woven fabric reinforced all-polypropylene composites with beta nucleated homo- and copolymer matrices. *Compos Sci Technol* 69(13):2185–2192. <https://doi.org/10.1016/j.compscitech.2009.06.002>
285. TWINTEX® T PP. PP Glass Fabrics. http://www.ocvreinforcements.com/pdf/products/Twintex_TPP_09_2008_Rev0.pdf
286. Brown KA, Brooks R, Warrior NA (2010) The static and high strain rate behaviour of a commingled E-glass/polypropylene woven fabric composite. *Compos Sci Technol* 70(2):272–283. <https://doi.org/10.1016/j.compscitech.2009.10.018>
287. Hufenbach W, Langkamp A, Gude M et al (2013) Characterisation of strain rate dependent material properties of textile reinforced thermoplastics for crash and impact analysis. *Procedia Mater Sci* 2:204–211. <https://doi.org/10.1016/j.mspro.2013.02.025>
288. Han SH, Oh HJ, Kim SS (2014) Evaluation of fiber surface treatment on the interfacial behavior of carbon fiber-reinforced polypropylene composites. *Compos Part B: Eng* 60:98–105. <https://doi.org/10.1016/j.compositesb.2013.12.069>
289. Malkapuram R, Kumar V, Negi YS (2009) Recent development in natural fiber reinforced polypropylene composites. *J Reinf Plast Compos* 28(10):1169–1189. <https://doi.org/10.1177/0731684407087759>

290. Etcheverry M, Barbosa SE (2012) Glass fiber reinforced polypropylene mechanical properties enhancement by adhesion improvement. *Materials* 5:1084–1113. <https://doi.org/10.3390/ma5061084>
291. Simeoli G, Acierno D, Meola C et al (2014) The role of interface strength on the low velocity impact behaviour of PP/glass fibre laminates. *Compos Part B: Eng* 62:88–96. <https://doi.org/10.1016/j.compositesb.2014.02.018>
292. Alcock B, Cabrera NO, Barkoula NM et al (2006) Low velocity impact performance of recyclable all-polypropylene composites. *Compos Sci Technol* 66(11–12):1724–1737
293. Boisse P (2015) Textile composite forming simulation. In: Aliabadi MH (ed) *Computational and experimental methods in structures*, vol 6. Imperial College Press, London, p 241
294. Cherouat A, Borouchaki H, Giraud-Moreau L (2010) Mechanical and geometrical approaches applied to composite fabric forming. *Int J Mater Form* 3(2):1189–1204. <https://doi.org/10.1007/s12289-010-0692-5>
295. Boisse P, Zouari B, Daniel J-L (2006) Importance of in-plane shear rigidity in finite element analyses of woven fabric composite preforming. *Compos Part A: Appl Sci Manuf* 37 (12):2201–2212. <https://doi.org/10.1016/j.compositesa.2005.09.018>
296. Cabrera NO, Reynolds CT, Alcock B et al (2008) Non-isothermal stamp forming of continuous tape reinforced all-polypropylene composite sheet. *Compos Part A: Appl Sci Manuf* 39(9):1455–1466. <https://doi.org/10.1016/j.compositesa.2008.05.014>
297. McGuinness GB, Brádaigh CMÓ (1998) Characterisation of thermoplastic composite melts in rhombus-shear: the picture-frame experiment. *Compos Part A: Appl Sci Manuf* 29 (1):115–132. [https://doi.org/10.1016/S1359-835X\(97\)00061-4](https://doi.org/10.1016/S1359-835X(97)00061-4)
298. Lebrun G, Bureau MN, Denault J (2003) Evaluation of bias-extension and picture-frame test methods for the measurement of intraply shear properties of PP/glass commingled fabrics. *Compos Struct* 61(4):341–352. [https://doi.org/10.1016/S0263-8223\(03\)00057-6](https://doi.org/10.1016/S0263-8223(03)00057-6)
299. Harrison P, Clifford MJ, Long AC (2004) Shear characterisation of viscous woven textile composites: a comparison between picture frame and bias extension experiments. *Compos Sci Technol* 64:1453–1465. <https://doi.org/10.1016/j.compscitech.2003.10.015>
300. Johnson AF, Pickett AK (1996) Numerical simulation of the forming process in long fibre reinforced thermoplastics. In: *CADCOMP '96*, Udine, Italy, pp 233–242, 1–3 July 1996
301. Nishi M, Hirashima T (2013) Approach for dry textile composite forming simulation. In: *The 19th International Conference on Composite Materials-ICCM19*, Montreal, Canada, p 8, 28 July–2 Aug 2013
302. Johnson AF (1995) Rheological model for the forming of fabric-reinforced thermoplastic sheets. *Compos Manuf* 6(3):153–160. [https://doi.org/10.1016/0956-7143\(95\)95006-K](https://doi.org/10.1016/0956-7143(95)95006-K)
303. Boisse P, Hamila N, Helenon B et al (2008) Different approaches for woven composite reinforcement forming simulation. *Int J Mater Form* 1(21–29). <https://doi.org/10.1007/s12289-008-0002-7>
304. Pickett AK, Queckborner T, de Luka P et al (1994) Industrial press forming of continuous fibre reinforced thermoplastic sheets and the development of numerical simulation tools. In: *Flow processes in composite materials 94*, Galway, Republic of Ireland, University College Galway, pp 356–368
305. Rogers TG (1989) Rheological characterization of anisotropic materials. *Composites* 20 (1):21–27. [https://doi.org/10.1016/0010-4361\(89\)90677-0](https://doi.org/10.1016/0010-4361(89)90677-0)
306. Spencer AJM (1972) *Deformation of fibre-reinforced materials*. Oxford University Press, Oxford
307. Spencer AJM (1984) Constitutive theory for strongly anisotropic solids. In: Spencer AJM (ed) *Continuum theory of the mechanics of fibre-reinforced composites*, vol 282. Springer Vienna, Vienna, pp 1–32. https://doi.org/10.1007/978-3-7091-4336-0_1
308. de Luca P, Lefébre P, Pickett AK (1998) Numerical and experimental investigation of some press forming parameters of two fibre reinforced thermoplastics: APC2-AS4 and PEI-CETEX. *Compos Part A: Appl Sci Manuf* 29(1):101–110. [https://doi.org/10.1016/S1359-835X\(97\)00060-2](https://doi.org/10.1016/S1359-835X(97)00060-2)

309. Nishi M, Kaburagi T, Kurose M et al (2014) Forming simulation of thermoplastic pre-impregnated textile composite. *Int J Mater Text Eng* 8:779–787
310. Ivanov I, Tabiei A (2004) Loosely woven fabric model with viscoelastic crimped fibres for ballistic impact simulations. *Int J Numer Methods Eng* 61:1565–1583. <https://doi.org/10.1002/nme.1113>
311. Gong Y, Xu P, Peng X et al (2018) A lamination model for forming simulation of woven fabric reinforced thermoplastic prepregs. *Compos Struct* 196:89–95. <https://doi.org/10.1016/j.compstruct.2018.05.004>
312. Harrison P, Clifford MJ, Long AC et al (2004) A constituent-based predictive approach to modelling the rheology of viscous textile composites. *Compos Part A: Appl Sci Manuf* 35 (7):915–931. <https://doi.org/10.1016/j.compositesa.2004.01.005>
313. Harrison P, Long AC, Yu WR et al (2006) Investigating the performance of two different constitutive models for viscous textile composites In: 8th international conference on textile composites (TEXCOMP), Nottingham, UK, 16–18 October 2006
314. Harrison P, Yu W-R, Long AC (2011) Rate dependent modelling of the forming behaviour of viscous textile composites. *Compos Part A: Appl Sci Manuf* 42(11):1719–1726. <https://doi.org/10.1016/j.compositesa.2011.07.026>
315. Harrison P, Gomes R, Curado-Correia N (2013) Press forming a 0/90 cross-ply advanced thermoplastic composite using the double-dome benchmark geometry. *Compos Part A: Appl Sci Manuf* 54:56–69. <https://doi.org/10.1016/j.compositesa.2013.06.014>
316. Hufenbach WA, Kostka P, Maron B et al (2013) Development and investigation of a textile-reinforced thermoplastic leaf spring with integrated sensor networks. *Procedia Mater Sci* 2:173–180. <https://doi.org/10.1016/j.mspro.2013.02.021>
317. Hufenbach W, Gude M, Böhm R et al (2011) The effect of temperature on mechanical properties and failure behaviour of hybrid yarn textile-reinforced thermoplastics. *Mater Des* 32(8):4278–4288. <https://doi.org/10.1016/j.matdes.2011.04.017>
318. Hufenbach W, Böhm R, Thieme M et al (2011) Polypropylene/glass fibre 3D-textile reinforced composites for automotive applications. *Mater Des* 32(3):1468–1476. <https://doi.org/10.1016/j.matdes.2010.08.049>
319. Gibson AG, Torres MEO, Browne TNA et al (2010) High temperature and fire behaviour of continuous glass fibre/polypropylene laminates. *Compos Part A: Appl Sci Manuf* 41 (9):1219–1231. <https://doi.org/10.1016/j.compositesa.2010.05.004>
320. Bureau MN, Denault J (2004) Fatigue resistance of continuous glass fiber/polypropylene composites: temperature dependence. *Polym Compos* 25(6):622–629. <https://doi.org/10.1002/pc.20057>
321. Bocz K, Bárány T, Toldy A et al (2013) Self-extinguishing polypropylene with a mass fraction of 9% intumescent additive—a new physical way for enhancing the fire retardant efficiency. *Polym Degrad Stab* 98(1):79–86. <https://doi.org/10.1016/j.polymdegradstab.2012.10.029>
322. Bocz K, Igricz T, Domonkos M et al (2013) Self-extinguishing polypropylene with a mass fraction of 9% intumescent additive II—influence of highly oriented fibres. *Polym Degrad Stab* 98:2445–2451. <https://doi.org/10.1016/j.polymdegradstab.2013.06.011>
323. Ferreira JAM, Costa JDM, Reis PNB et al (1999) Analysis of fatigue and damage in glass-fibre-reinforced polypropylene composite materials. *Compos Sci Technol* 59 (10):1461–1467. [https://doi.org/10.1016/S0266-3538\(98\)00185-7](https://doi.org/10.1016/S0266-3538(98)00185-7)
324. Reis PNB, Ferreira JAM, Richardson MOW (2011) Fatigue damage characterization by NDT in polypropylene/glass fibre composites. *Appl Compos Mater* 18(5):409–419. <https://doi.org/10.1007/s10443-010-9172-9>
325. Mathieu R, René R, Brahim B (2010) Environmental effects on glass fiber reinforced polypropylene thermoplastic composite laminate for structural applications. *Polym Compos* 31(4):604–611. <https://doi.org/10.1002/pc.20834>
326. Hufenbach W, Langkamp A, Adam F et al (2011) An integral design and manufacturing concept for crash resistant textile and long-fibre reinforced polypropylene structural components. *Proc Eng* 10:2086–2091. <https://doi.org/10.1016/j.proeng.2011.04.345>

327. Vaidya UK, Samalot F, Pillay S et al (2004) Design and manufacture of woven reinforced glass/polypropylene composites for mass transit floor structure. *J Compos Mater* 38 (21):1949–1971. <https://doi.org/10.1177/0021998304048418>
328. Knox MP (2001) Continuous fiber reinforced thermoplastic composites in the automotive industry. In: *Automotive composites conference*, Troy, Michigan, p 6, 19–20 Sept 2001
329. Ye L, Friedrich K (1995) Processing of thermoplastic composites from powder/sheath-fibre bundles. *J Mater Process Technol* 48(1):317–324. [https://doi.org/10.1016/0924-0136\(94\)01664-M](https://doi.org/10.1016/0924-0136(94)01664-M)
330. Friedrich K, Gogeva T, Fakirov S (1988) Thermoplastic impregnated fiber bundles: manufacturing of laminates and fracture mechanics characterization. *Compos Sci Technol* 33 (2):97–120. [https://doi.org/10.1016/0266-3538\(88\)90013-9](https://doi.org/10.1016/0266-3538(88)90013-9)
331. Maywood W (2003) Thermoplastic pultrusion process unveiled. *Reinf Plast* 47(9):18. [https://doi.org/10.1016/S0034-3617\(03\)00926-3](https://doi.org/10.1016/S0034-3617(03)00926-3)
332. Novo PJ, Silva JF, Nunes JP et al (2016) Pultrusion of fibre reinforced thermoplastic pre-impregnated materials. *Compos Part B: Eng* 89:328–339. <https://doi.org/10.1016/j.compositesb.2015.12.026>
333. COMPTAPE. <http://compositetape.com/>. Accessed 10 June 2018
334. Nunes JP, Silva JF, Santos MS et al (2013) Processing conditions and properties of continuous fiber reinforced GF/PP thermoplastic matrix composites manufactures from different pre-impregnated materials. In: *The 19th international conference on composite materials*, Montreal, Canada, pp 3428–3438, 28 July–2 August 2013
335. Poon WKY, Jin YZ, Li RKY (2001) Pultrusion of glass fibre reinforced/maleated-PP modified/PP matrix composites. In: *13th international conference on composite materials*, Beijing, p 10
336. Novo PJ, Nunes JP, Silva JF et al (2013) Production of thermoplastics matrix preimpregnated materials to manufacture composite pultruded profiles. *Ciência & Tecnologia dos Materiais* 25(2):85–91. <https://doi.org/10.1016/j.ctmat.2014.03.004>
337. Novo P, Silva JF, Nunes JP et al (2012) Development of a new pultrusion equipment to manufacture thermoplastic matrix composite profiles. In: *15th European conference on composite materials*, Venice, Italy, 24–28 June 2012. *European Society for Composite Materials*, pp 1–8
338. Price RV (1973) Production of impregnated rovings. US3742106 Patent 3742106
339. Goud V, Alagirusamy R, Das A et al (2018) Dry electrostatic spray coated towpregs for thermoplastic composites. *Fibers Polym* 19(2):264–374. <https://doi.org/10.1007/s12221-018-7470-7>
340. Silva RF, Silva JF, Nunes JP et al (2008) New powder coating equipment to produce continuous fibre thermoplastic matrix towpregs. *Mater Sci Forum* 587–588:246–250. <https://doi.org/10.4028/www.scientific.net/MSF.587-588.246>
341. Velosa JC, Nunes JP, Silva JF et al (2010) Production of thermoplastic towpregs. *Mat Sci Forum* 636–637:220–225. <https://doi.org/10.4028/www.scientific.net/MSF.636-637.220>
342. Silva JF, Nunes JP, Velosa JC et al (2010) Thermoplastic matrix towpreg production. *Adv Polym Technol* 29(2):80–85. <https://doi.org/10.1002/adv.20174>
343. Padaki S, Drzal LT (1999) A simulation study on the effects of particle size on the consolidation of polymer powder impregnated tapes. *Compos Part A: Appl Sci Manuf* 30 (3):325–337. [https://doi.org/10.1016/S1359-835X\(98\)00115-8](https://doi.org/10.1016/S1359-835X(98)00115-8)
344. Nunes JP, van Hattum FWJ, Bernardo CA et al (2005) Production of thermoplastic Towpregs and Towpreg-based composites. In: Friedrich K, Fakirov S, Zhang Z (eds) *Polymer composites: from nano- to macro-scale*. Springer US, Boston, MA, pp 189–213. https://doi.org/10.1007/0-387-26213-x_11
345. Nunes JP, Silva JF, Marques AT et al (2003) Production of powder-coated towpregs and composites. *J Thermoplast Compos Mater* 16:231–248. <https://doi.org/10.1177/089270503025872>
346. O'Connor JE (1987) Reinforced plastic US4680224 Patent 4,680,224

347. Ho KKC, Shamsuddin S-R, Riaz S et al (2011) Wet impregnation as a route to unidirectional carbon fibre reinforced thermoplastic composites manufacturing. *Plast, Rubber Compos* 40 (2):100–107. <https://doi.org/10.1179/17432891X12988>
348. Vodermayr AM, Kaerger JC, Hinrichsen G (1993) Manufacture of high performance fibre-reinforced thermoplastics by aqueous powder impregnation. *Compos Manuf* 4(3):123–132. [https://doi.org/10.1016/0956-7143\(93\)90096-Q](https://doi.org/10.1016/0956-7143(93)90096-Q)
349. Carlsson A, Astrom BT (1998) Experimental investigation of pultrusion of glass fibre reinforced polypropylene composites. *Compos Part A: Appl Sci Manuf*, 585–593. [https://doi.org/10.1016/S1359-835X\(97\)00115-2](https://doi.org/10.1016/S1359-835X(97)00115-2)
350. Tomas ÅB, Byron PR (1993) A modeling approach to thermoplastic pultrusion. I: Formulation of models. *Polym Compos* 14(3):173–183. <https://doi.org/10.1002/pc.750140302>
351. Angelov I, Wiedmer S, Evstatiev M et al (2007) Pultrusion of a flax/polypropylene yarn. *Compos Part A: Appl Sci Manuf* 38(5):1431–1438. <https://doi.org/10.1016/j.compositesa.2006.01.024>
352. Devlin BJ, Williams MD, Quinn JA et al (1991) Pultrusion of unidirectional composites with thermoplastic matrices. *Compos Manuf* 2(3):203–207. [https://doi.org/10.1016/0956-7143\(91\)90141-3](https://doi.org/10.1016/0956-7143(91)90141-3)
353. Dai S-C, Ye L (2002) GF/PP tape winding with on-line consolidation. *J Reinf Plast Compos* 21(1):71–90. <https://doi.org/10.1106/073168402024283>
354. Schledjewski R, Latrille M (2003) Processing of unidirectional fiber reinforced tapes—fundamentals on the way to a process simulation tool (ProSimFRT). *Compos Sci Technol* 63 (14):2111–2118. [https://doi.org/10.1016/S0266-3538\(03\)00108-8](https://doi.org/10.1016/S0266-3538(03)00108-8)
355. Lionetto F, Dell’Anna R, Montagna F et al (2016) Modeling of continuous ultrasonic impregnation and consolidation of thermoplastic matrix composites. *Compos Part A: Appl Sci Manuf* 82:119–129. <https://doi.org/10.1016/j.compositesa.2015.12.004>
356. Funck R, Neitzel M (1994) Thermoplastic tape winding with high speed and at quasi-axial pattern. In: 3rd International conference on flow processes in composite materials (FPCM-3), Galway, Ireland, pp 237–247, 7–9 July 1994
357. Funck R, Neitzel M (1995) Improved thermoplastic tape winding using laser or direct-flame heating. *Compos Manuf* 6(3):189–192. [https://doi.org/10.1016/0956-7143\(95\)95010-V](https://doi.org/10.1016/0956-7143(95)95010-V)
358. Dobrzanski LA, Domagala J, Silva JF (2007) Application of Taguchi method in the optimisation of filament winding of thermoplastic composites. *Arch Mater Sci Eng* 28 (3):133–140
359. Åstrom BT, Pipes RB (1990) Thermoplastic filament winding with on-line impregnation. *J Thermoplast Compos Mater* 3(4):314–324. <https://doi.org/10.1177/089270579000300403>
360. Henninger F, Friedrich K (2002) Thermoplastic filament winding with online-impregnation. Part A: Process technology and operating efficiency. *Compos Part A: Appl Sci Manuf* 33 (11):1479–1486. [https://doi.org/10.1016/S1359-835X\(02\)00135-5](https://doi.org/10.1016/S1359-835X(02)00135-5)
361. Henninger F, Hoffmann J, Friedrich K (2002) Thermoplastic filament winding with online-impregnation. Part B. Experimental study of processing parameters. *Compos Part A: Appl Sci Manuf* 33(12):1684–1695. [https://doi.org/10.1016/S1359-835X\(02\)00136-7](https://doi.org/10.1016/S1359-835X(02)00136-7)
362. Kim HJ, Kim SK, Lee WI (1996) A study on heat transfer during thermoplastic composite tape lay-up process. *Exp Therm Fluid Sci* 13(4):408–418. [https://doi.org/10.1016/S0894-1777\(96\)00095-7](https://doi.org/10.1016/S0894-1777(96)00095-7)
363. Maurer D, Mitschang P (2015) Laser-powered tape placement process—simulation and optimization. *Adv Manuf Polym Compos Sci* 1(3):129–137. <https://doi.org/10.1179/2055035915Y.0000000005>
364. Brecher C, Stimpfl J, Dubratz M et al (2011) Innovative manufacturing of 3D-lightweight components. *Micro Mater Process* 8(5):36–40. <https://doi.org/10.1002/latj.201190057>
365. Brecher C, Emonts M, Stimpfl J et al (2014) Production of customized hybrid fiber-reinforced thermoplastic composite components using laser-assisted tape placement. In: Denkena B (ed) *New production technologies in aerospace industry. Lecture Notes in Production Engineering*. Springer, Cham, Switzerland, pp 123–129. https://doi.org/10.1008/978-3-319-01964-2_17

366. Parandoush P, Tucker L, Zhou C et al (2017) Laser assisted additive manufacturing of continuous fiber reinforced thermoplastic composites. *Mater Des* 131:186–195. <https://doi.org/10.1016/j.matdes.2017.06.013>
367. Brecher C, Werner D, Emonts M (2015) Multi-material-head. One tool for 3 technologies: laser-assisted thermoplast-tape placement, thermoset-prepreg-placement and dry-fiber-placement. In: 20th international conference on composite materials, Copenhagen, 19–24 July 2015
368. Kukla C, Peters T, Janssen H et al (2017) Joining of thermoplastic tapes with metal alloys utilizing novel laser sources and enhanced process control in a tape placement process. *Proc CIRP* 66:85–90. <https://doi.org/10.1016/j.procir.2017.03.307>
369. Janssen H, Peters T, Brecher C (2017) Efficient production of tailored structural thermoplastic composite parts by combining tape placement and 3D printing. *Proc CIRP* 66:91–95. <https://doi.org/10.1016/j.procir.2017.02.022>
370. Rijdsdijk HA, Contant M, Peijs AAJM (1993) Continuous-glass-fibre-reinforced polypropylene composites: I. Influence of maleic-anhydride-modified polypropylene on mechanical properties. *Compos Sci Technol* 48(1):161–172. [https://doi.org/10.1016/0266-3538\(93\)90132-z](https://doi.org/10.1016/0266-3538(93)90132-z)
371. Hamada H, Fujihara K, Harada A (2000) The influence of sizing conditions on bending properties of continuous glass fiber reinforced polypropylene composites. *Compos Part A: Appl Sci Manuf* 31(9):979–990. [https://doi.org/10.1016/S1359-835X\(00\)00010-5](https://doi.org/10.1016/S1359-835X(00)00010-5)
372. Rausch J, Zhuang RC, Mader E (2010) Systematically varied interfaces of continuously reinforced glass fibre/polypropylene composites: comparative evaluations of relevant interfacial aspects. *Express Polym Lett* 4(8):576–588. <https://doi.org/10.3144/expresspolymlett.2010.72>
373. Yashas Gowda TG, Sanjay MR, Subrahmanya Bhat K et al (2018) Polymer matrix-natural fiber composites: an overview. *Cogent Eng* 5:13. <https://doi.org/10.1080/23311916.2018.1446667>
374. Lariviere D, Krawczak P, Tiberi C et al (2004) Interfacial properties in commingled yarn thermoplastic composites. Part I: characterization of the fiber/matrix adhesion. *Polym Compos* 25(6):577–588. <https://doi.org/10.1002/pc.20052>
375. Liu CR (1998) A step-by-step method of rule-of-mixture of fiber- and particle-reinforced composite materials. *Compos Struct* 40:313–322. [https://doi.org/10.1016/S0263-8223\(98\)00033-6](https://doi.org/10.1016/S0263-8223(98)00033-6)
376. Van de Velde K, Kiekens P (2001) Thermoplastic pultrusion of natural fibre reinforced composites. *Compos Struct* 54(2):355–360. [https://doi.org/10.1016/S0263-8223\(01\)00110-6](https://doi.org/10.1016/S0263-8223(01)00110-6)
377. Van de Velde K, Kiekens P (2003) Effect of material and process parameters on the mechanical properties of unidirectional and multidirectional flax/polypropylene composites. *Compos Struct* 62(3):443–448. <https://doi.org/10.1016/j.compstruct.2003.09.018>
378. Lee S, Shi SQ, Groom LH et al (2010) Properties of unidirectional kenaf fiber–polyolefin laminates. *Polym Compos* 31(6):1067–1074. <https://doi.org/10.1002/pc.20893>
379. Tholibon D, Tharazi I, Bakar A et al (2016) Tensile properties of unidirectional kenaf fiber polypropylene composite. *Jurnal Teknologi (Sci Eng)* 78:101–106. <https://doi.org/10.11113/jt.v78.9153>
380. Okereke MI (2016) Flexural response of polypropylene/E-glass fibre reinforced unidirectional composites. *Compos Part B: Eng* 89:388–396. <https://doi.org/10.1016/j.compositesb.2016.01.007>
381. Zushi H, Ohsawa I, Kanai M et al (2005) Fatigue behaviour of unidirectional carbon fiber reinforced polypropylene. In: The 9th Japan international SAMPE symposium, Tokyo, 29 Nov–2 Dec 2005, pp 26–31
382. Ashton JE, Whitney JM (1970) Theory of laminated plates. In: *Progress in Material Science*, vol 4. Technomic, Stamford, Conn
383. Herakovich CT (1998) *Mechanics of fibrous composites*. Wiley, New York
384. Orifici AC, Herszberg I, Thomson RS (2008) Review of methodologies for composite material modelling incorporating failure. *Compos Struct* 86(1):194–210. <https://doi.org/10.1016/j.compstruct.2008.03.007>

385. Boudenne A, Tlili R, Certes YC (2012) Thermophysical and thermal expansion properties. In: Nicolais L, Borzacchiello A (eds) Wiley Encyclopedia of Composites. Wiley, New York
386. Progelhof RC, Throne JL, Ruetsch RR (1976) Methods for predicting the thermal conductivity of composite systems: a review. *Polym Eng Sci* 16(9):615–625. <https://doi.org/10.1002/pen.760160905>
387. Cho YJ, Youn JR, Kang TJ et al (2005) Prediction of thermal conductivities of fibre reinforced composites using a thermal-electrical analogy. *Polym Polym Compos* 13(6):637–644
388. Talreja R (1981) Fatigue of composite materials: damage mechanisms and fatigue-life diagrams. *Proc R Soc Lond Ser A Math Phys Sci* 378(1775):461–475. <https://doi.org/10.1098/rspa.1981.0163>
389. van den Oever M, Peijs T (1998) Continuous-glass-fibre-reinforced polypropylene composites II. Influence of maleic-anhydride modified polypropylene on fatigue behaviour. *Compos Part A: Appl Sci Manuf* 29(3):227–239. [https://doi.org/10.1016/s1359-835x\(97\)00089-4](https://doi.org/10.1016/s1359-835x(97)00089-4)
390. Gamstedt EK, Berglund LA, Peijs T (1999) Fatigue mechanisms in unidirectional glass-fibre-reinforced polypropylene. *Compos Sci Technol* 59(5):759–768. [https://doi.org/10.1016/S0266-3538\(98\)00119-5](https://doi.org/10.1016/S0266-3538(98)00119-5)
391. Joo S-J, Yu M-H, Kim WS et al (2018) Damage detection and self-healing of carbon fiber polypropylene (CFPP)/carbon nanotube (CNT) nano-composite via addressable conducting network. *Compos Sci Technol* 167:62–70. <https://doi.org/10.1016/j.compscitech.2018.07.035>